Tropical tropospheric water vapor budget, maintenance of the lapse rate, and distribution of the extratropical tropospheric temperature and wind

by

De-Zheng Sun

M.S. in Physical Oceanography
Graduate School of Academia Sinica, China
(1987)

Submitted to the Center for Meteorology and Oceanography
Department of Earth, Atmospheric and Planetary Sciences
in partial fulfillment of the requirements for the degree of

Doctor of Philosophy in Meteorology

at the

MASSACHUSETTS INSTITUTE OF TECHNOLOGY

February 1993

Author .....
Center for Meteorology and Oceanography
Department of Earth, Atmospheric and Planetary Sciences
September, 1992

Certified by .....
Richard S. Lindzen
Sloan Professor in Meteorology
Thesis Supervisor

Accepted by .....
Thomas H. Jordan
Chairman, Departmental Committee on Graduate Students

Tropical tropospheric water vapor budget, maintenance of the lapse rate, and distribution of the extratropical tropospheric temperature and wind

by

De-Zheng Sun

Submitted to the Center for Meteorology and Oceanography
Department of Earth, Atmospheric and Planetary Sciences
on September, 1992, in partial fulfillment of the
requirements for the degree of
Doctor of Philosophy in Meteorology

Abstract

The first goal of this thesis research is to assess the nature of water vapor feedback in climate change. Utilizing observational data and conceptual models, we examined the tropical tropospheric water vapor budget and the maintenance of the lapse rate. In light of the mountain-snow line record for the last glaciation, we investigated the nature of water vapor feedback in climate change. The chief finding is that water vapor in the tropical free troposphere may play a stablizing role in climate change through a coupling with the tropical tropospheric lapse rate.

Based on the observed vertical structure of tropical convection, we first formulated a model for the vertical distribution of tropical tropospheric temperature. In the model, heating from deep convection is parameterized as subsidence heating and the magnitude of the subsidence is determined through the surface moisture budget. The radiative-convective equilibrium profiles predicted by the model successfully depict the observed characteristics. The model lapse rate in the free troposphere is related to the speed at which air outside of deep clouds subsides and the radiative cooling rate it suffers in the course of subsiding.

We then examined the tropical tropospheric water vapor budget. We found that the evaporation of the hydrometeors pumped into the upper troposphere by deep convective towers appears to be the major moisturizer for the large-scale subsiding flow. Using the large-scale subsidence deduced from the energy budget and a simple parameterization for the moistening from the evaporation of hydrometeors, we are able to simulate the observed distribution of water vapor in the context of a simple conceptual model.

The role of water vapor and lapse rate in different climate regimes was examined in light of the mountain-snow line record for the last glaciation. Together with CLIMAP data for the surface temperature estimate, the mountain snowline record suggests that the mean lapse rate in the low tropical troposphere during the last glaciation

was about 20% larger than at present. Using the model for the tropical tropospheric temperature, we studied the dependence of the lapse rate on the relative humidity in the middle and upper troposphere. Under the assumption that the vertical structure of the averaged convective mass flux is not subject to change, we find that only a significant increase of relative humidity in the middle and upper troposphere (20-40% percent greater than at present) can lead to the 20% increase of the lapse rate. This conclusion remains unchanged even when a substantial decrease in the surface and low level relative humidity is assumed to accompany the surface cooling. It is noted that the profiles observed in CLIMAP have much more convective available potential energy (CAPE) than present profiles, which can lead to enhanced production of hydrometeors in the middle and the upper troposphere whose reevaporation can moisturize the free troposphere. It is shown that the water vapor change leads to an extremely strong negative feedback which would greatly reduce the response of the tropical atmosphere to a doubling of CO_2. It is also found that the lapse rate feedback is also negative and can contribute as much as the water vapor feedback in reducing the tropical climate sensitivity to the increase of CO_2. We stressed that results of the present analyses should be taken with caution since observations of the current climate and more sophisticated modeling do not support the idea that the tropical tropospheric temperature can deviate considerably from a moist adiabatic profile.

The second goal of the thesis research is to obtain the zonal mean temperature and wind distribution of an extratropical troposphere with zero gradient of potential vorticity (PV) along isentropic surfaces and estimate the tropical impact on the extratropical troposphere in this extreme case of PV mixing. We found that for a fixed meridional distribution of surface temperature and a tropical lapse rate which are the same as the observed, the extratropical troposphere with constant PV along isentropic surfaces has a considerably colder upper troposphere near the jet and a stronger jet than the observed. Nevertheless, the overall structure is quite similar to the observed including the width of the jet. The presence of a planetary vorticity gradient limits the meridional extent of tropical impact on the extratropical temperature and wind distribution. However, to a greater or lesser degree, the temperature and wind distribution in the extratropical troposphere is found to be sensitive to the vertical distribution of PV and the position of the edge of the Hadley circulation. We examined the mutual dependence between temperature, wind and PV, and highlighted the role of the stratospheric PV and its meridional gradient in affecting the zonal wind. Though the temperature and wind distribution cannot be accurately determined without the reference to the global momentum balance, the meridional distribution of wind has negligible effects on the temperature structure. We also showed how the thermal structure within the surface boundary layer may affect a large portion of the zonal mean temperature and wind distribution. The sensitivity of the temperature and wind distribution to the PV gradient along isentropic surfaces is also examined. For a fixed meridional distribution of surface temperature, we found that the larger the gradient along isentropic surfaces, the warmer the upper troposphere and the weaker the jet.

Thesis Supervisor: Richard S. Lindzen
Title: Sloan Professor in Meteorology

Acknowledgments

I am deeply grateful to my advisor Professor Richard S. Lindzen, for his invaluable guidance and encouragement during the last four years. I am also very grateful to Professor Kerry A. Emanuel, Alan Plumb, Ronald Prinn, Peter Stone and Earle Williams for their teaching and advice in many stimulating discussions. Professor Emanuel has been particularly helpful in the part of research concerning moist convection. Assistances in using the radiative code from Dr. Ming-Dah Chou and Dr. Arthur Hou of Goddard Space Flight Center at Greenbelt, Maryland are also greatly appreciated.

I wish to thank Diana Spiegel for her assistance with computers, and Jane MacNabb, Joan wood, Joel Sloaman and Tracey Stanelun for their help with administrative details. The helpful discussions with my colleagues Roger Atkinson, Robert Boldi, Barry Klinger, Michael Morgan, Nilton Renno, James Risbey, Lars Schade, and Chun-Chieh Wu are also greatly appreciated. In particular, I would like to thank Roger, Barry, Michael, James and Robert for helping me to transform my writing into correct English. In addition, I would like to thank the K. C. Wang Education Foundation at Hong Kong for awarding me the scholarship for graduate study abroad, which expedited my trip to America.

Finally, I wish to thank my wife Hong for her love and support, and my parents for their continuing encouragement from afar.

Contents

List of Figures

List of Tables

Chapter 1

Introduction.

1.1 Motivation

Chief among the green-house gases in the atmosphere is water vapor. Whether the increase of CO_2 in the atmosphere can cause global warming is crucially dependent on whether water vapor enhances the warming or not.

The current global circulation models (GCMs) predict that there will be 2-4 K increase in the global mean temperature if the CO_2 content of the atmosphere is doubled. Roughly half of this warming is due to the positive feedback of water vapor in the models (Schlesinger 1988, Houghton et al. 1990). However, dealing with the transport of water vapor is among the weakest aspects of GCMs. The source of water vapor in the atmosphere is the Earth's surface, and the vertical transport of water vapor is predominantly fulfilled by convective-scale motions. Convective-scale motions are subgrid-scale motions in GCMs and cannot be explicitly calculated. Instead, their effects in transporting water vapor are dealt with through the use of parameterization schemes which express the collective effects of convective-scale motions in transporting heat and water vapor in terms of large-scale variables. These schemes in the current models have serious problems (Lindzen 1990a). Some important physical processes are either completely ignored or inadequately treated in these schemes; indeed, the very nature of the water vapor feedback in global climate change is uncertain (Lindzen 1990b, Betts 1990).

The greenhouse effect is also crucially dependent on the vertical distribution of temperature. An extreme example is that the greenhouse effect will be zero for a vertically isothermal atmosphere regardless of the amount of green-house gases present. Numerical models for climate studies have found that the lapse rate feedback is potentially as important as the feedback from water vapor (Cess 1991, Cess et al 1990). Just as in the case of the water vapor distribution, the maintenance of the tropospheric lapse rate has not been well understood. The treatment of the lapse rate in climate models is either completely empirical or based on very crude assumptions about the role of dynamical transports. Notable examples are the constant lapse rate adjustment and the moist adiabatic adjustment for the entire troposphere. Based on paleoclimate records, it has been suggested that the tropical tropospheric lapse rate during the last glaciation was 20% steeper than at present (Broecker and Denton 1989). This lapse rate behavior is inconsistent with both the notion of the constant lapse rate adjustment and the notion of moist adiabatic adjustment.

The distribution of water vapor and the distribution of temperature are expected to be mutually dependent on each other. The distribution of temperature is the product of radiative forcing and dynamic transport associated with circulations which are driven by radiative forcing. Water vapor is the major contributor to the radiation field in the Earth's troposphere in both the infrared and solar bands (Goody and Yung 1989). The temperature distribution in return determines the driving force for moist convection, which is the chief agent in distributing the sinks and sources for water vapor. Observations have shown that the ability of tropical cloud systems to transport water vertically is crucially dependent on the environmental convective available potential energy, which is a function of vertical distribution of temperature (Williams et al. 1992). Therefore it is expected that the nature of water vapor feedback cannot be well understood without some understanding of the nature of the lapse rate feedback, and vice versa. The investigation of the maintenance of the vertical distribution of temperature is the second objective of this thesis, and the mutual dependence between the distribution of water vapor and the distribution of temperature will be the focus of this investigation.

In addition to the study of the maintenance of the water vapor and the temperature distribution in the tropical troposphere and their impact on the tropical climate sensitivity in response to radiative perturbations, the maintenance of the zonal mean temperature and wind structure in the extratropical troposphere is also studied. In this thesis the tropics are defined as the domain of the Hadley circulation.

The temperature and wind distribution of the zonal mean flow in the extratropical troposphere is dependent on the property of baroclinic eddies in transporting potential vorticity. It is the distribution of the potential vorticity that defines the stability of the zonal mean flow. Also, the temperature and wind are both accurately related to the potential vorticity by a single elliptical operator. However, few efforts have been made to document the dependence of the temperature and wind distribution of the zonal mean flow on the distribution of potential vorticity, particular the dependence on the gradient of potential vorticity along isentropic surfaces. Theoretical and observational analysis have not been made to establish a clear casual relationship between the diabatic and frictional processes, dynamical transport and the global distribution of potential vorticity, though efforts are currently being made (Haynes and McIntyre 1990, Hoskins 1991)

As highlighted by Charney's model and Eady's model, the two most crucial parameters which determine the instability of extratropical large-scale flow are the gradient of potential vorticity along isentropic surfaces (or the pseudo-potential vorticity along isobaric surfaces) and the height of the tropopause. In the study of instability of the large-scale extratropical flow, these two parameters have been largely treated as given. Little attention has been paid to the fact that they are also a result of the instability. Very recently, it has been conjectured that the large-scale extratropical tropospheric flow may largely behave as an Eady model, in the sense that the potential vorticity gradient along isentropic surfaces between the tropopause and the ground level tends to vanish and the tropopause height is such that it is neutral for the longest waves (Lindzen 1992). This hypothesis offers a completely new perspective from which to look at the extratropical climate. In the second part of the thesis, we investigate the maintenance of the extratropical zonal mean temperature and wind in light of this

hypothesis. In the context of the balanced dynamics, we investigate the dependence of the temperature and wind on the gradient of PV along isentropic surfaces and show what an efficient PV mixing by baroclinic eddies implies for the tropical impact on the extratropics.

1.2 Synopsis of the thesis

The thesis is divided into two parts. The first part, Chapter 2 to Chapter 7 focuses on the distributions of tropical tropospheric temperature and water vapor, their interdependence and nature of feedback in the global warming. It consists of 6 chapters. The second part deals with the distribution of temperature and wind in the extratropical troposphere from the point of view of instability and the transport of potential vorticity, in particular the dependence of temperature and wind in the extratropical troposphere on the gradient of PV along isentropes and how they are possibly connected with the tropics. The second part consists of Chapter 8 alone.

In the first part, we begin with a review of the previous studies on the distribution of water vapor and temperature in the tropical troposphere from both the observational and theoretical aspects. The purpose is to provide the necessary background to sharpen the questions we are going to address in detail, and sort out the useful tools which we will adopt immediately or with modifications. The concern that the feedback of water vapor and lapse rate may play a subtle, but vitally important role in the climate change is a very recent concern and the studies which directly address this issue are scarce. Consequently, the tools applicable to further investigations are primitive. Nevertheless, some ideas in treating convective transport are germane to the atmospheric flow and are both stimulating and insightful. Examples are Ooyama and Arakawa's formulations of the heat and water vapor budget equations for the large-scale atmospheric flow in which convective-scale motions are treated as spatially isolated and distinguishable elements, Lindzen's schemes which demonstrates the importance of the convective boundary layer, and Emanuel's schemes which reveals the potential importance of microphysics. Chapter 3 outlines the observed characteristics

of tropical convection and the general features in the large-scale distribution of water vapor and temperature, which will be given a coherent account later on. Chapter 4 presents the mathematical aspects of the problem and gives the derivation of the heat and water vapor budget equations of a large-scale flow embedding moist convection. In Chapter 5, we show how the mean vertical structure of the tropical tropospheric temperature can be adequately described by a historical picture for the tropical convection and its associated circulations. A radiative-convective model is presented in this Chapter, which shows the role of radiative cooling and the presence of the convective boundary layer in maintaining the vertical thermal structure of the tropical troposphere. In Chapter 6, we make an effort to describe both the characteristics of tropical convection and the observed large-scale distribution of water vapor in a coherent manner. The purpose is to outline and highlight the important physical processes in maintaining the tropical tropospheric water vapor budget. We will show that the evaporation of hydrometeors[1] falling from the upper level clouds acts as the chief moisturizer for the large-scale subsiding motion. In Chapter 7, we investigate the nature of the feedback of water vapor and lapse rate in light of the mountain-snow line record for the last glaciation, and estimate the feedback of both water vapor and lapse rate in affecting the sensitivity of the tropical climate in response to the increase of CO_2.

In the second part (Chapter 8), we begin with the spatial distribution of the Ertel potential vorticity for the observed time and zonal mean flow over four seasons. We then obtain the temperature and wind distribution of a troposphere with well mixed potential vorticity along isentropic surfaces. Sensitivities to the tropical lapse rate and to the position of the edge of the Hadley circulation are then studied. Finally, we investigate the quantitative dependence of the temperature and wind on the gradient of potential vorticity along isentropic surfaces.

The last chapter (Chapter 9) summarizes the important findings of the present study and outlines future research.

[1]Hydrometeors throughout this thesis refer to the liquid or ice particles that exist outside of saturated cumulus updrafts.

Chapter 2

Background

2.1 Observations

Despite the uniquely important role of water vapor in the global circulation, water vapor appears to be among the worst observed quantities. This is particularly true for water vapor in the upper troposphere. This is partially due to the instrumental difficulty in measuring water vapor at low temperatures and partially due to a lack of appreciation of the role that water vapor in the upper troposphere plays in the global circulation.

The most widely used instrument in measuring the tropospheric water vapor is the borne carbon hygristor, which has problems at low temperatures and low relative humidity. As a result, compilations of conventional sounding data usually end below 400 mb (Peixoto 1958, Newell et al 1972, Oort 1983). Before satellites and other remote sensing techniques were introduced, data for the upper tropospheric water vapor were taken largely by air craft measurements and therefore only for a few places over the earth. Even more unfortunate, the objective of these early air craft measurements was not to investigate the upper tropospheric water vapor budget, but rather to find the origin of stratospheric water vapor. Deep cumulus convection was suspected to be the major player in the exchange of air between the troposphere and the stratosphere (Danielson, 1982) and naturally almost all the available measurements were taken over the most convective regions.

The earlist reliable measurements of the upper tropospheric water vapor of the tropical troposphere were perhaps those made by Mastenbrook over Trinidad in 1968. The instrument used was the frost point hygrometer. The measurements showed that the upper tropospheric water vapor content has profound seasonal changes and detailed vertical structures. The bulk upper troposphere is in general as subsaturated as the middle troposphere. However, the relative humidity near the tropopause is frequently found near 100%. These observations all suggest the essential role of deep convection in the tropospheric water vapor budget. The most recent air craft measurements were made over Indonesia and Panama through the Stratosphere and Troposphere Exchange Program. As the earliest measurements of 1968, the bulk troposphere was frequently found to be subsaturated even though clouds were frequently present (Kelly et al 1987)

An overall picture of the tropical tropospheric water vapor was not available until satellites were employed to take the measurements (Rind et al 1991). The advantage of the satellite measurements is their good spatial coverage. The drawback of the satellite measurements is that the satellite can only take measurements in clear sky conditions. Nevertheless, since satellite data is the only available data set for the upper troposphere and gives good spatial cover, it will be the basis of the present analysis in conjunction with the available conventional data.

At first sight, it seems to be surprising that more efforts were made in measuring stratospheric water vapor than in measuring the water vapor in the upper troposphere. This is perhaps related to the widely accepted assumption that the water vapor content throughout the troposphere is strictly controlled by temperature through the classical Clausius-Clapeyron equation. And indeed, the lack of the seasonal change of relative humidity in the low troposphere supports this assumption. The assumption that the tropospheric water vapor content is controlled by a fixed relative humidity has been used in studying climate sensitivity (Manabe et al. 1965). A seemingly trivial but important fact in the distribution of tropospheric water vapor is that it is subsaturated. Therefore thermo-dynamic process cannot be the only process at work. More importantly, a small change in the relative humidity can greatly affect

the climate sensitivity, not only because of the important role of water vapor itself in the earth's radiative budget, but also because of its close relationship with the cloud field and temperature distribution. As we will show later, they are so closed related to each other that one cannot be well understood without understanding the other.

The apparent lack of understanding of the tropospheric water vapor distribution and the ignorance of the need to understand it are also reflected in the theoretical efforts in dealing with the convective transport of water vapor, as we will see in the following section.

2.2 Parameterization schemes

The chief agent that transports water vapor vertically is convective-scale motion. This is particularly true in the tropics. The convective-scale motions are subgrid-scale motions in GCMs for weather forecasting and climate modeling. Their effects are dealt with by so-called parameterization schemes. Underlying these parameterization schemes is the hope that the collective effects of the subgrid-scale motions on the large scale flow are determined by the large scale variables. In the following, we briefly review the past efforts in constructing parameterization schemes. The intent is neither to have an exhaustive description nor to provide a detailed critique, but to provide the essential background and isolate the ideas behind these schemes which have physical significance.

2.2.1 Past efforts

Parameterization schemes used in large-scale models may be divided into two groups. Schemes in the first group are semi-empirical adjustment schemes, such as the dry adjustment scheme and the moist adjustment scheme (Manabe and Strickler 1964, Manabe et al. 1965, Krishnamurti and Moxim 1971, Krishnamurti et al. 1980). In the adjustment schemes, the atmosphere is always adjusted to a specified moisture and temperature structure. In the dry adjustment scheme, the specific humidity is arbitrarily specified and in the moist adjustment the air is always saturated. Due

to the lack of physics and predictability, these schemes are certainly not qualified for studying how the atmosphere behaves when it is perturbed, for example by an increase in the CO_2 concentration. It is interesting to note that there are continuing efforts devoted to this line of research (Betts 1986, Betts and Miller 1986).

Parameterization schemes in the second group have some physics and predictability, though the physics is quite crude and consequently the predictability is questionable. These schemes were mostly designed to represent the role of convective-scale heating in the development of synoptic scale disturbances (Charney and Eliassen 1964; Kuo 1965, 1974; Ooyama 1971; Arakawa and Schubert 1974). Naturally, the effect of convective scale transports on the mean state is not a direct concern in these studies. Furthermore, the emphasis of these early attempts was the transport of heat rather than the transport of water vapor.

Schemes in the second group may be further divided into two types according to the way clouds are represented and the way the large-scale flow is idealized. In the schemes of the first type, clouds are not treated as distinguishable elements from their environment. (Charney and Eliassen 1964; Kuo 1965, 1974).

In Charney and Eliassen's scheme, the convective heating was related to the low level moisture convergence, but specific humidity of the environment was arbitrarily specified. In Kuo's approach, the low level moisture convergence and conditionally unstable stratification were used as two indicators to determine whether convection could set in. Clouds were assumed to be mixed into the environment immediately after their formation. Convection heats and moistens the environment through mixing. The cloudy air may not be warmer than the environment at all when it detrains into the environment, and the environment is unlikely to get more moist and finally reach saturation as convection goes on, the way the clouds in this scheme modify the environment is in question. Though Kuo used the total moisture converged by the large scale flow as a constraint to the total cumulus heating and moistening, the scheme is unlikely to give a correct vertical distribution of the modified specific humidity and temperature field, which is extremely important in the interaction between convective heating and radiation transfer.

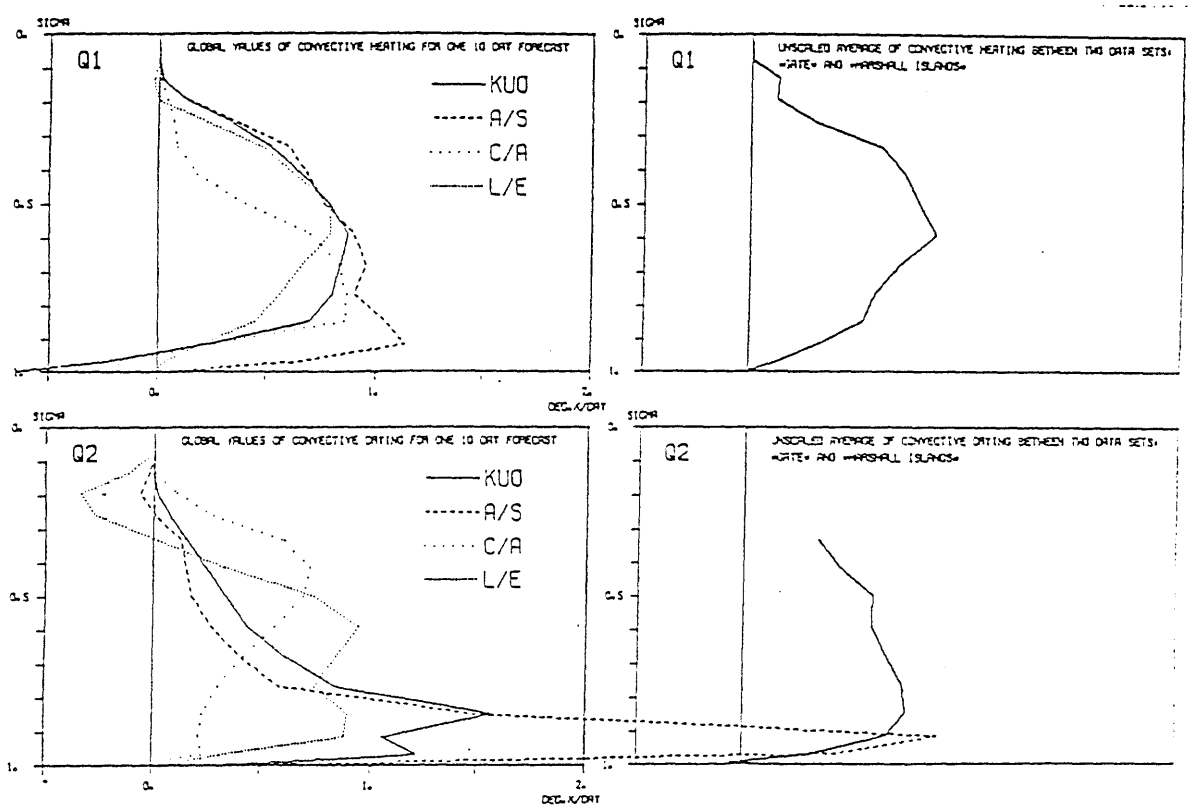

Figure 2-1: An observational verification of various Schemes. Presented are vertical profiles for the cumulus heating Q_1 and cumulus drying Q_2, globally averaged over one-ten day forecast at the European Center for Medium-Range Weather Forecasting for four convection schemes (Kuo, Arakawa-Schubert, convective adjustment, and Lindzen-ECMWF). On the right are the unscaled averages of the same profiles obtained from the Gate and Marshall Islands experiments by Thompson et al. (1979). From Geleyn et al., 1982.

An observational verification of this scheme was given by Geleyn (1982) (see Figure 2-1). Plotted in 2-1 are the tendency of the temperature change caused by the transport of heat by clouds and the tendency of the water vapor change (multiplied by the latent heat) due to the transport of water vapor by clouds. These two quantities have been termed cumulus heating Q_1 and cumulus drying Q_2 respectively. As expected, the verification showed that there were considerable discrepancies between the observed water vapor transported by cumulus and the corresponding model result of Kuo's.

Schemes of the second type treat clouds as distinguishable elements (Ooyama 1971, Arakawa and Schubert 1974). This type of approach is also termed as mass flux formulation. In this formulation, the large scale flow is divided into two regions, the moist convection region and its environment. The budget equations are formulated for the environment. Because the fractional cover of clouds is small, the budget equations for the environment are also approximately the area averaged budget equations. In Ooyama's work, he assumed that cumulus convection could be represented by individual buoyant elements and adopted a bubble cloud model to represent these buoyant elements. While these buoyant elements arise through their environment, they entrain environmental air and also detrain cloud air back to the environment. He then reduced the parameterization to a determination of a so called "dispatcher function" which is defined as the rate of the generation of the buoyant elements. He also argued that this "dispatcher function" may mainly depend on the low level structure of the large scale flow where cloud air originates. This result is very suggestive in the sense that a successful parameterization may mainly depend on the way cumulus clouds release the energy concentrated in the low level atmosphere–the convective boundary layer. Ooyama left his scheme unclosed due to the lack of understanding of the generation of cloud bubbles in the low atmosphere.

Arakawa's complex scheme is quite similar to Ooyama's except that an entraining plume in a laminar environment was used to represent a cloud and the introduction of the concept of the quasi-equilibrium between clouds and their environment by which he closed his scheme.

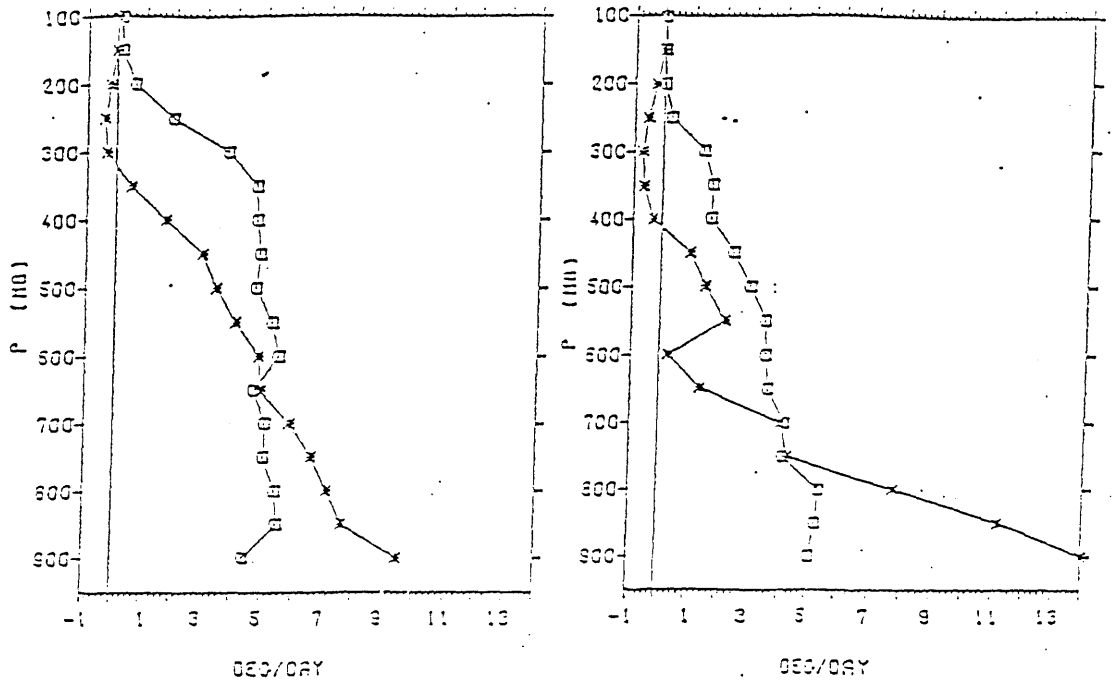

Figure 2-2: An observational verification of Arakawa and Schubert's scheme. The left is the cumulus heating (Q_1) and the right is the cumulus drying (Q_2). Stars represent the model predictions and squares are for the observation. From Lord, 1978.

The quasi-equilibrium assumption is the most distinguishing feature of Arakawa's scheme. Though he showed some observational evidence for this assumption, it is not very clear how general this assumption is. This assumption is not expected to work well for parameterizing tropical convection subjected to a strong diurnal cycle. The destabilizing forces are certainly not always in balance with the stablizing forces. Rather they tend to achieve dominance in different periods. This is at least true for the deep convection over land. The processes which accumulate convective available energy are in general a much slower processes than the processes which release it. The time mean feedback of convection to the mean flow is dependent on both the time-scale of the accumulating CAPE and the time-scale of the releasing CAPE.

The observational verifications to Arakawa's scheme were made by Lord (1978) and Geleyn et al (1982). Considerable discrepancies between the observed cumulus drying and the model predictions occur in the low atmosphere. (see Figure 2-1 and Figure 2-2). The discrepancies have been generally attributed to the plume model used in representing tropical convection (Lord 1978, Emanuel 1991).

Observations show that cloud compositions are spatially inhomogeneous (Stommel 1947, Malkus 1954, Warner 1955 and Warner and Squires 1958). This suggests that the plume model is inadequate in representing the real clouds. Warner (1970) further noted that an entraining plume model could not simultaneously predict the cloud top height and liquid water content correctly.

Squires (1958) noted that mixing at the cloud top could lead to penetrative downdrafts. Emanuel (1981) further calculated the vertical velocity of these penetrative downdrafts and found that they could be as strong as convective updrafts. It was further noted that some discrepancies between the observed clouds and those modeled as plumes could be better explained if the mixing by penetrative downdrafts was taken into account (Warner 1970, Telford 1975, and Raymond 1979).

Direct observational evidence for the presence of subcloud scale downdrafts was offered by Paluch' analyses (Paluch 1979). His results suggested that entrainment of air into the clouds may primarily occur at the cloud top. His finding was supported by the subsequent analyses by Boatman and Auer (1983) and Jansen et al (1985). However, Blyth et al (1988), Raga et al. (1990) and Talor and Baker (1991) found that the lateral entrainment of the environmental air into clouds is also important. Based on these observations, a conceptual model for clouds gradually took shape, which was termed the " buoyancy sorting model " (Talor and Baker 1991). This model evolved from the earlier work by Telford (1975).

Based on these observational works and theoretical considerations about clouds, Emanuel modified the representation of clouds in Arakawa's approach (Emanuel 1991). In his formulation, the moist convection is constituted by sub-cloud scale downdrafts and updrafts. The model is based on the " buoyancy sorting " model. In this scheme, mass flux associated with downdrafts is related to the mass flux associated with updrafts, which is determined by the "quasi-equilibrium" assumption. The radiative-convective equilibrium experiments with this scheme produce realistic profiles for both the temperature and relative humidity (Emanuel 1991). In addition, this scheme revealed the potential importance of the details of the micro-physical processes in determining the large-scale distribution of water vapor. Renno (1992)

further demonstrated that this scheme performs better than those schemes which have been used in GCMs.

Despite the complexity of the tropical convection, its overall vertical structure appears quite simple. Tropical convection tends to be bimodal. Shallow convection is largely restricted to below 2-3 km and forms a well defined convective boundary layer. The convective boundary layer supplies the fuel for deep convection. Realizing that the boundary layer may play a dominant role in determining the overall convective activity, Lindzen proposed a new closure for determining the total mass flux of deep convection: the moisture budget of the boundary layer was used to determine the total cloud mass flux (Lindzen, 1981, 1988). This scheme was carried out by the European Center for Middle Range Weather Forecasting and the agreement with observation is better than for any other existing schemes in predicting the cumulus heating and drying (Figure 2-1, Geleyn et al 1982). The success of this formulation suggests the important role of the presence of a well defined convective boundary layer.

2.2.2 Concluding remarks

Moist convective motion (turbulence) is usually confined to small regions and that moist convection transports mass primarily vertically. Ooyama and Arakawa's formulations in which clouds are treated as distinguishable elements are more appropriate to atmospheric flows with scales much larger than the scale of moist convection (i.e., synoptic disturbances, the Hadley circulation, etc.). However, the models adopted for the clouds by Ooyama and Arakawa were over simplified and the way the moist convection interacts with its environment is probably too limited to accurately describe the real atmospheric situation. This will be seen more clearly when the observed characteristics of the tropical convection are discussed in the following chapter.

By definition, parameterization schemes are scale dependent and necessarily involve empirical elements. Schemes which are good for weather forecasting may not be good for climate prediction. Yet none of the past schemes have been tested against the climatological distribution of water vapor and temperature. The traditional quantities tested against the observation are cumulus drying and heating (usually termed

as Q_1 and Q_2) . As pointed out by Emanuel and Raymond (1991), Q_1 and Q_2 are insufficient tests of cumulus parameterizations. The actual tendencies of temperature and water vapor represent very small differences between Q_1 and Q_2 and the tendencies produced by large-scale processes such as advection and radiation. Thus relatively small differences between correct and incorrect values would lead to large errors in prediction.

Chapter 3

Observation

The purpose of this chapter is to outline what is known about moist convection in the tropics, as well as the large-scale distributions of temperature and water vapor, mostly from the observational point of view. We focus on the characteristics which we will either explore further theoretically in the subsequent chapters or use as a basis in idealizing the heat and moisture transfer in the tropical atmosphere.

3.1 Tropical convection

The overall vertical structure for the tropical convection may be schematically illustrated by Figure 3-1. A free troposphere with isolated deep convective towers sits on a well defined convective boundary layer containing shallow clouds.

The well defined convective boundary layer is found over bulk of the tropical ocean (Augstein 1973, 1974). The top of this layer is characterized by the trade inversion, a sharp decrease of water vapor and an increase of temperature (Figure 3-2). Water vapor mixing ratio and potential temperature within the convective boundary layer tend to be nearly homogeneous, though more detailed structures exist as can be see in Figure 3-3. The feature of trade inversion is most profound in the region undisturbed by deep convection. In the disturbed region where there is much deep convection, the trade inversion tends to disappear in the monthly mean soundings, but to appear in daily sounding maps (Reihl 1979).

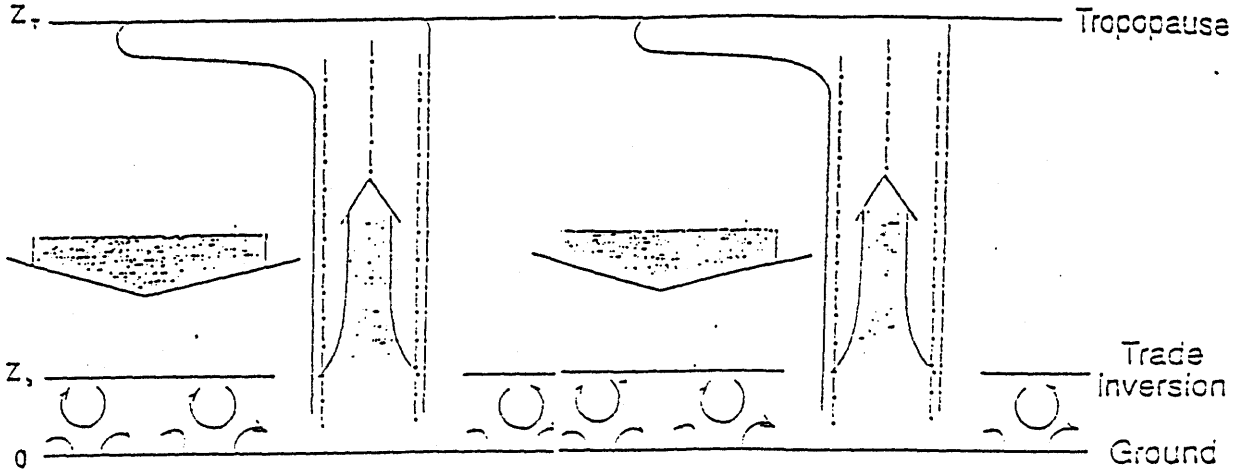

Figure 3-1: A schematic illustration of the historical picture of tropical convection and its associated circulation.

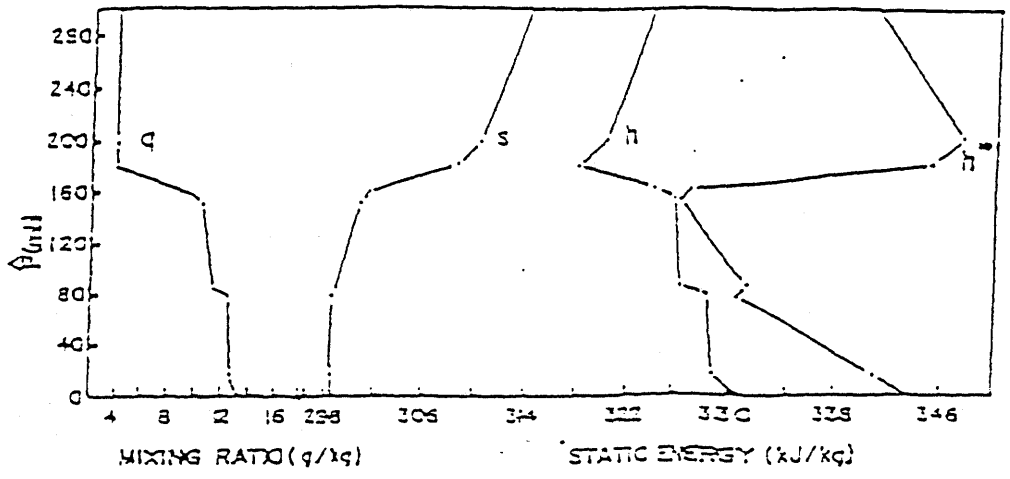

Figure 3-2: Vertical profiles of water vapor mixing ratio, q, dry enthalpy s, moist enthalpy of h, and saturation moist enthalpy h^* in the tropical low atmosphere, for the ship Planet, February, 7-12, 1969. From Augstein et al., 1974.

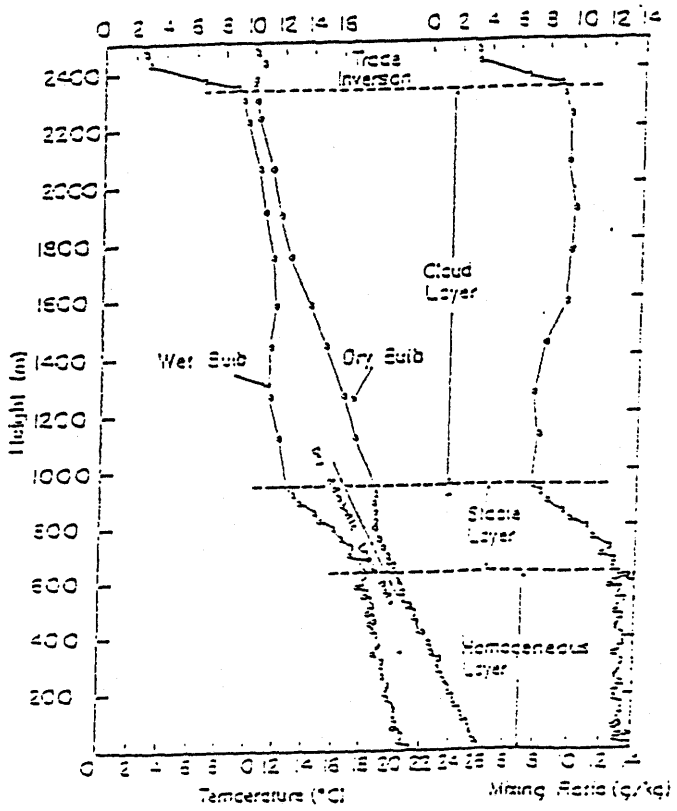

Figure 3-3: Vertical temperature and moisture profiles of the undisturbed low tropical atmosphere. From Garstrang and Betts, 1974.

The shallow clouds contained within the convective boundary layer hardly precipitate. Their major role is to moisten the convective boundary layer against the erosion by the large-scale subsidence from the top and supply moisture for the deep convection (Betts 1978)

The air parcels participating in the deep convective towers are primarily from the boundary layer. The moisture and temperature within the boundary layer and boundary layer thickness are strongly influenced by the deep convection (Reihl 1979). The height of inversion and the jump across the inversion oscillate with the birth and decay of the deep convection (Figure 3-4). Consequently, the feature of inversion is usually smoothed out in the mean sounding maps.

The existence of the trade wind inversion in nature has been shown by observations and theoretical models to be due to penetrative convection (Ball 1964, Tennekes 1973, Sarachik 1978). When a stably stratified flow is heated from below, a convective turbulent boundary layer develops and is capped by an inversion of temperature. In

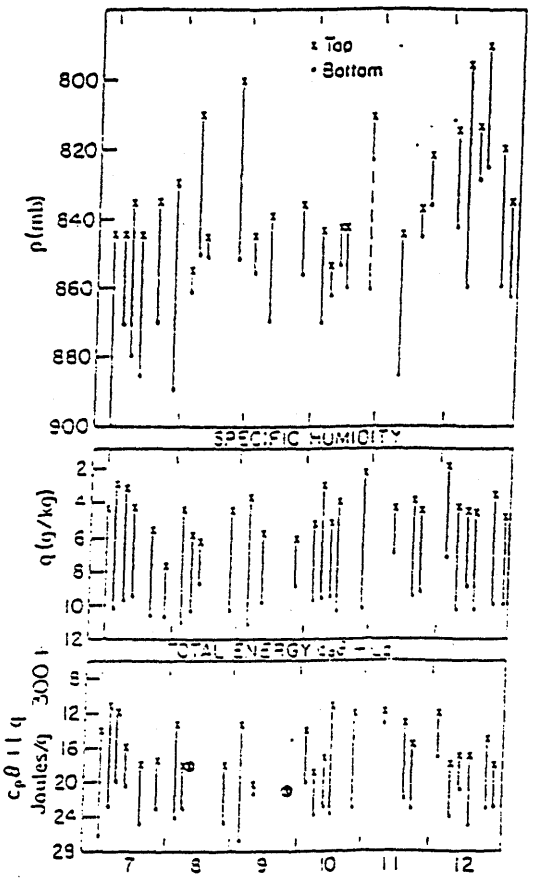

Figure 3-4: Upper: Pressure of top and bottom of trade inversion at the German ship Planet for all soundings 6-12 February 1969; Center: specific humidity at top and bottom; lower: total static energy at top and bottom (Partly dashed line in upper diagram indicates double inversion). From Riehl, 1979.

the tropical troposphere, the large-scale subsidence associated with deep convection tends to maintain a stable stratification and a dry free troposphere. The surface evaporation and sensible heat flux render the low atmosphere moist and unstable. Consequently, a convective boundary layer develops. The turbulent flow in the convective boundary layer, including the shallow clouds, transports water vapor upwards efficiently to balance the drying from the large-scale subsidence and maintain a moist boundary layer (Betts 1978).

The earliest observational study of the properties of deep convection was motivated by the need to explain the energy budget of the tropics. The value of moist enthalpy decreases from the surface to a certain height (roughly 600mb for a typical tropical sounding) , then begins to increase all the way to the tropopause (see Figure 3-5). To investigate the means that fulfills the vertical energy transfer to balance the radiative cooling and the loss of heat to the higher latitude in the upper tropical troposphere, Riehl and Malkus (1958, 1979) carried out detailed energy budget analyses and his results show that tropical deep convection must be dominated by "Hot Tower" type (undiluted ascent), otherwise the feature of the vertical structure of moist enthalpy can not be maintained. Recent observations on the tropical convection from the Gate experiments also showed the validity of the "Hot Tower" concept for tropical deep convection. It was found that there is a considerable departure from saturation even in the trough region where the heaviest rainfall is observed. Consistently in the divergence field, there is a sharp peak around the height of 175mb which corresponds to the neutral buoyancy level of the undiluted ascent originating from the surface level (Reed and Recker 1971, Thompson et al 1978).

More details about the deep convection were revealed in the Gate experiment . It was found that deep convection tends to be organized into mesoscale structures (Houze and Betts 1981, Houze 1989). A typical tropical rain fall system is schematically illustrated in Figure 3-6. It includes two regions. One is covered by deep convective towers and the other by the wider stratiform clouds. The deep and nearly undiluted towers in the convective region detrain a significant amount of hydrometeors into the upper troposphere which feed the wide spread upper level clouds. The

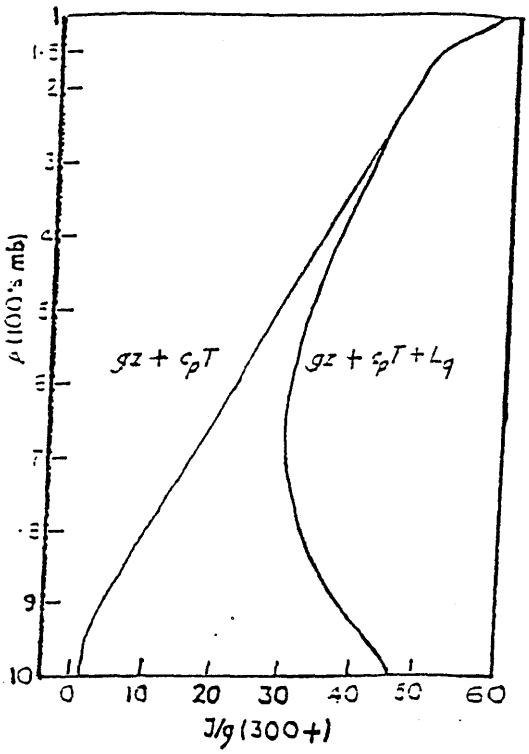

Figure 3-5: A typical vertical thermal structure of the troposphere in the deep tropics as shown by the dry enthalpy and moist enthalpy. From Riehl, 1979

role of upper level clouds in the tropical tropospheric water vapor budget has not attracted much attention. We will show in this thesis that the upper level clouds and precipitation associated with them appears to be the chief moisturizer of the large-scale subsiding motion which covers most of the tropics.

Shallow clouds in conjunction with the dry surface level turbulence moisten the convective boundary layer, which supplies the moisture for the deep convection. The deep convection induces large-scale subsidence, which suppresses the shallow convection. Thus the two kinds of convection form a coherent picture. Schneider (1977) used this picture to estimate the mean stability of the mean thermal structure of the whole Hadley domain and Sarachik (1978) used it as a basis to form a one dimensional coupled ocean-atmosphere model. In Chapter 5, we will show that in the context of radiative convective equilibrium, this simple picture is able to depict the main characteristics of the vertical structure of tropical tropospheric temperature. However, to describe the water vapor budget, the presence of upper level clouds has

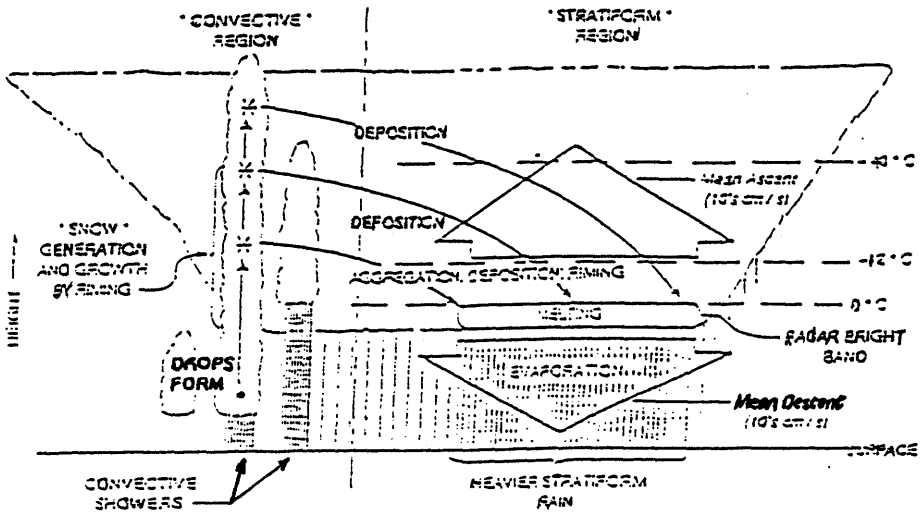

Figure 3-6: Schematic illustration of the structure of a typical tropical cloud system. Solid arrows indicate particle trajectories. From Houze, 1989.

to be considered.

3.2 Distributions of water vapor and temperature

Figures 3-7 and 3-8 present the observed vertical distribution of relative humidity averaged for the Hadley circulation domain for both January and July. In Figure 3-7, the relative humidity is with respect to water saturation while in Figure 3-8 the relative humidity above the height of the melting level is with respect to ice saturation. Conventional sounding data (Oort 1983) and recent satellite data for the clear sky (SAGE II data for the year 1987, see Rind et al 1991) are both presented. Conventional sounding of water vapor ends around 300 mb and satellite measurements cannot probe the low troposphere frequently enough to form a representative sample. In the region where both overlap, the satellite data reveals a much drier troposphere than the sounding data. Though it is expected that clear sky conditions should be drier than

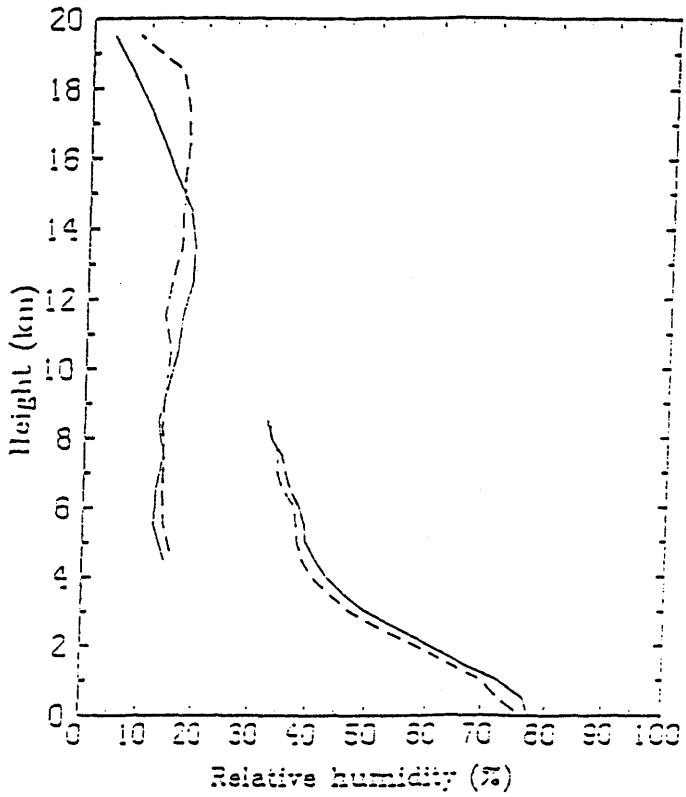

Figure 3-7: The vertical structure of the observed water vapor distribution averaged over the domain of the Hadley circulation. Relative humidity is with respect to liquid water. The satellite data and conventional data are both presented. The solid line is for the month of January and the dashed line is for the month of July (The region over which data was averaged was 15 S to 25 N for January and 25 S to 15 N for July.). Averaged relative humidity was obtained through the averaged water vapor mixing ratio and the averaged temperature. The satellite data for water vapor mixing ratio is from the SAGE II measurements. The conventional data for water vapor mixing ratio and temperature (used to obtain relative humidity) are from Oort (1983).

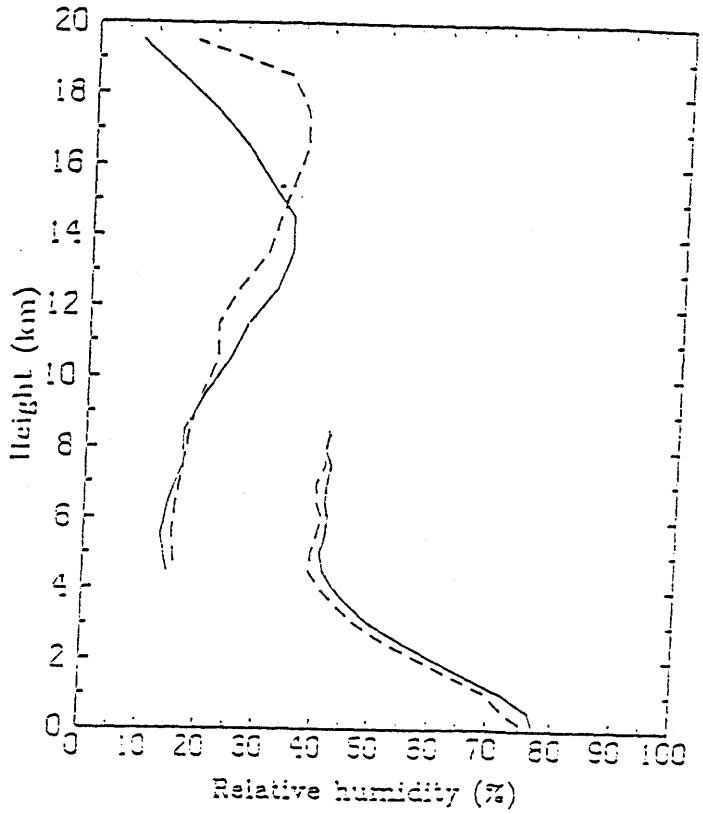

Figure 3-8: Same as Figure 3-7, but above the melting level the relative humidity is with respect to ice saturation.

average (including both cloudy sky and clear sky), the difference is still striking. As discussed in Rind et al (1990), the water vapor distribution obtained by SAGE II has been validated by comparison with radiosonde data, frost point hygrometer, Lyman-α and LIMS satellite observations, and have been shown to produce realistic values with an estimated accuracy of about 10 percent. Though there is still uncertainties in SAGE II data, it is also possible that the conventional sounding data may exaggerate the actual water vapor content of the air. Conventional radiosonde generally fails to report when the relative humidity is below 20 percent (Starr and Melfi 1990). Also, since the water vapor content decreases with height exponentially with a scale height of about 2-3 km, the sond may report an exaggerated relative humidity due to contamination. It is worth noting that some detailed soundings in the trade wind regime, do show the relative humidity immediately above the trade inversion falling to 20 percent (Riehl 1979). We here assume that the two data sets give bounds on the actual water vapor content for average conditions.

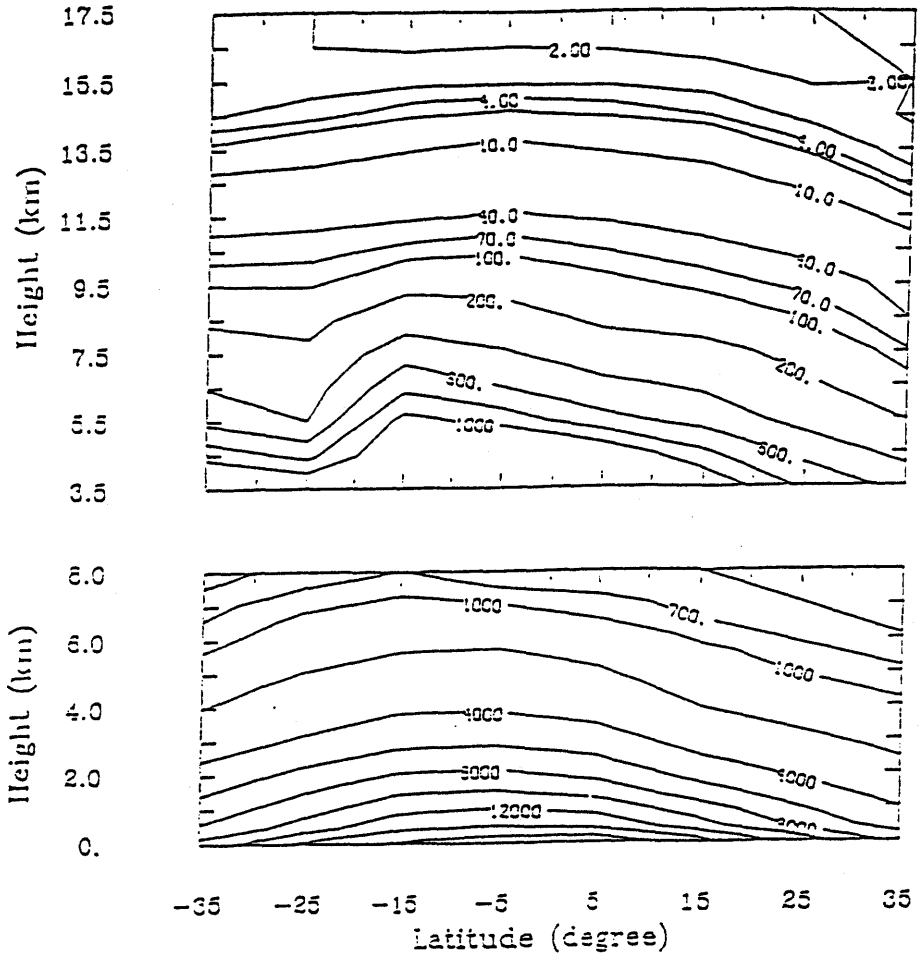

Figure 3-9: Meridional distribution of tropical tropospheric water vapor mixing ratio in January (in units of 10^{-3} g/kg). Upper panel: satellite data. Lower panel: conventional data.

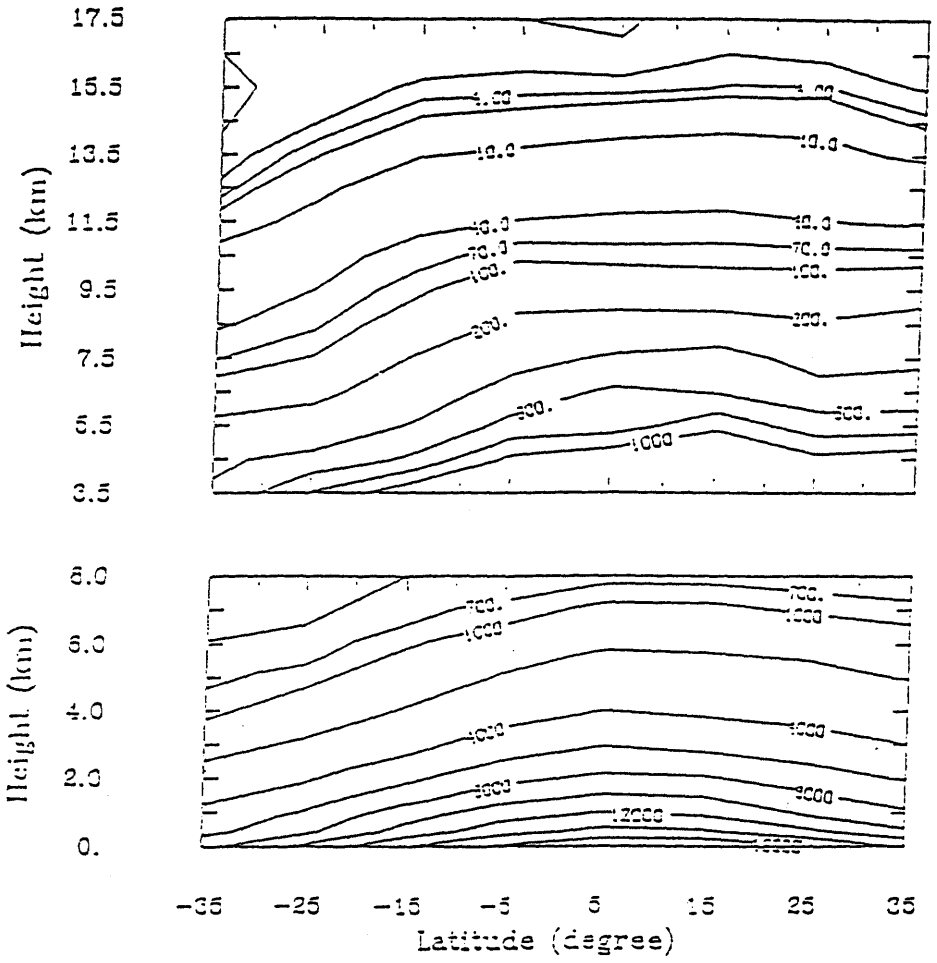

Figure 3-10: Meridional distribution of tropical tropospheric water vapor mixing ratio in July (in units of 10^{-3} g/kg). Upper panel: satellite data. Lower panel: conventional data.

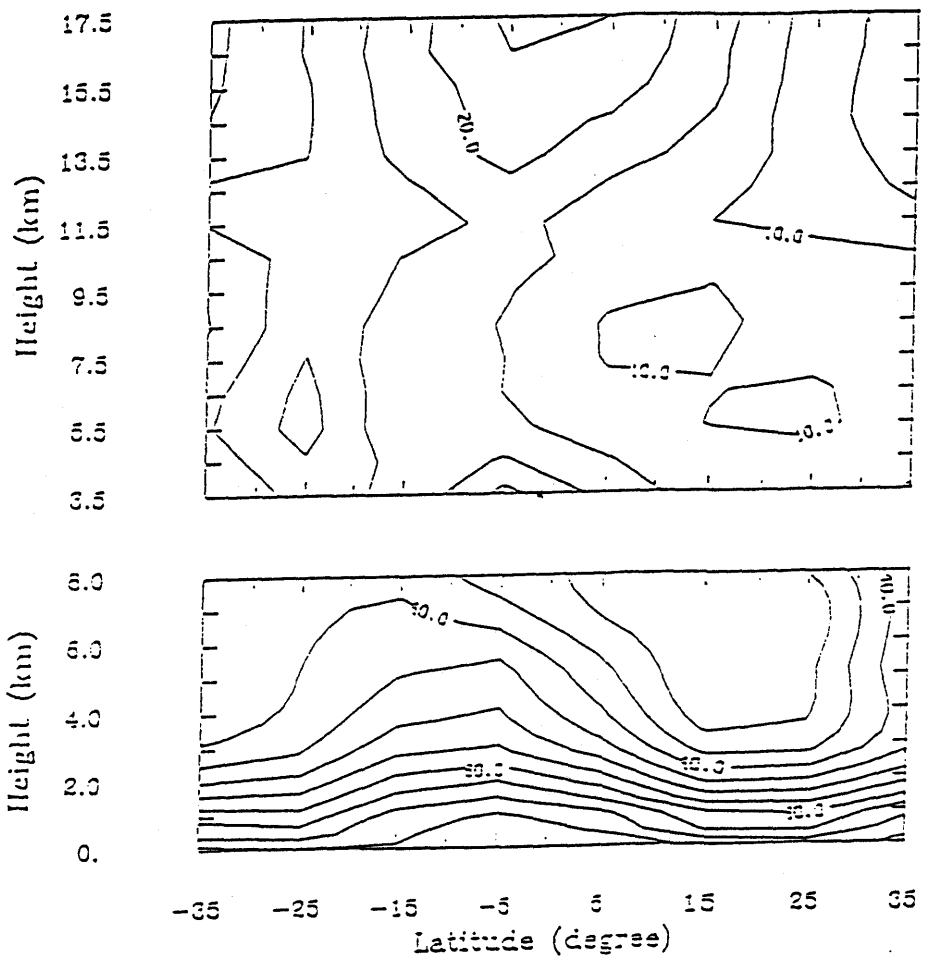

Figure 3-11: Meridional distribution of tropical tropospheric relative humidity(with respect to liquid water) in January. Upper panel: satellite data. Lower panel: conventional data.

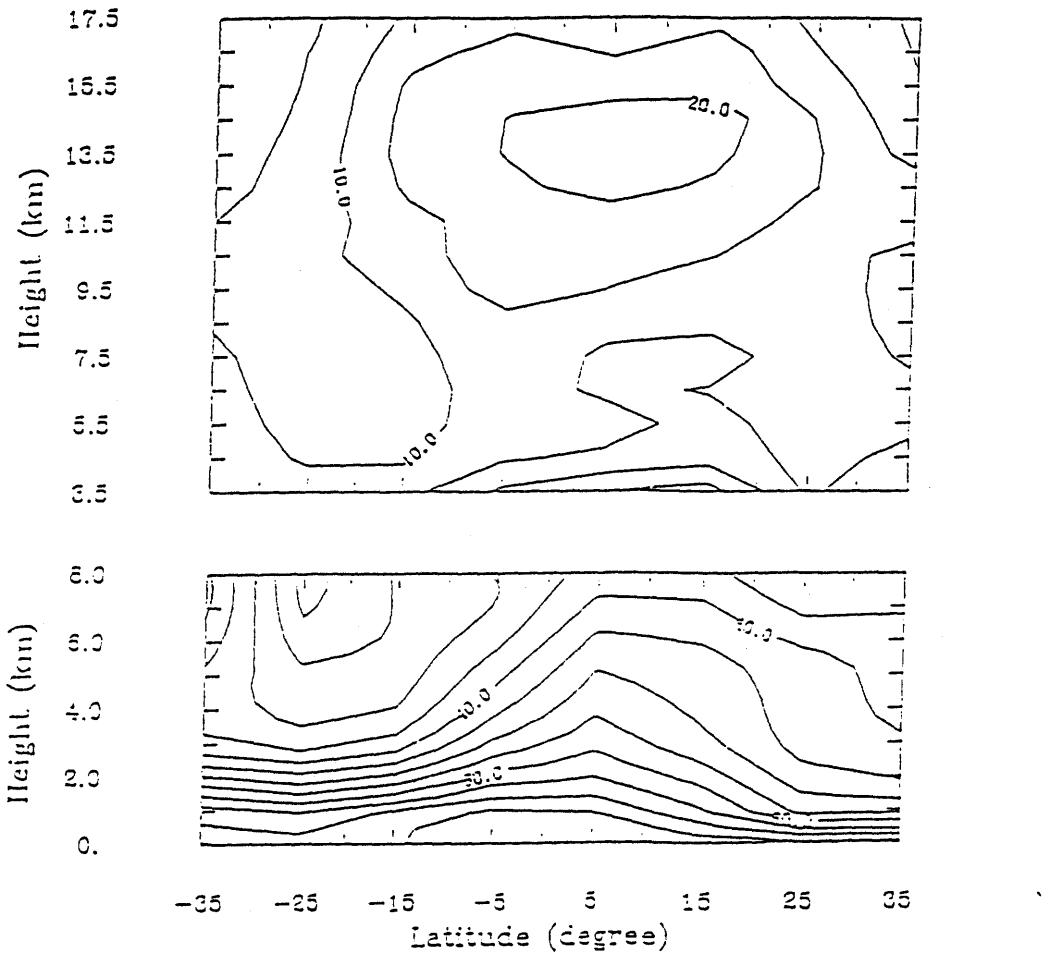

Figure 3-12: Meridional distribution of tropical tropospheric relative humidity (with respect to liquid water) in July. Upper panel: satellite data. Lower panel: conventional data.

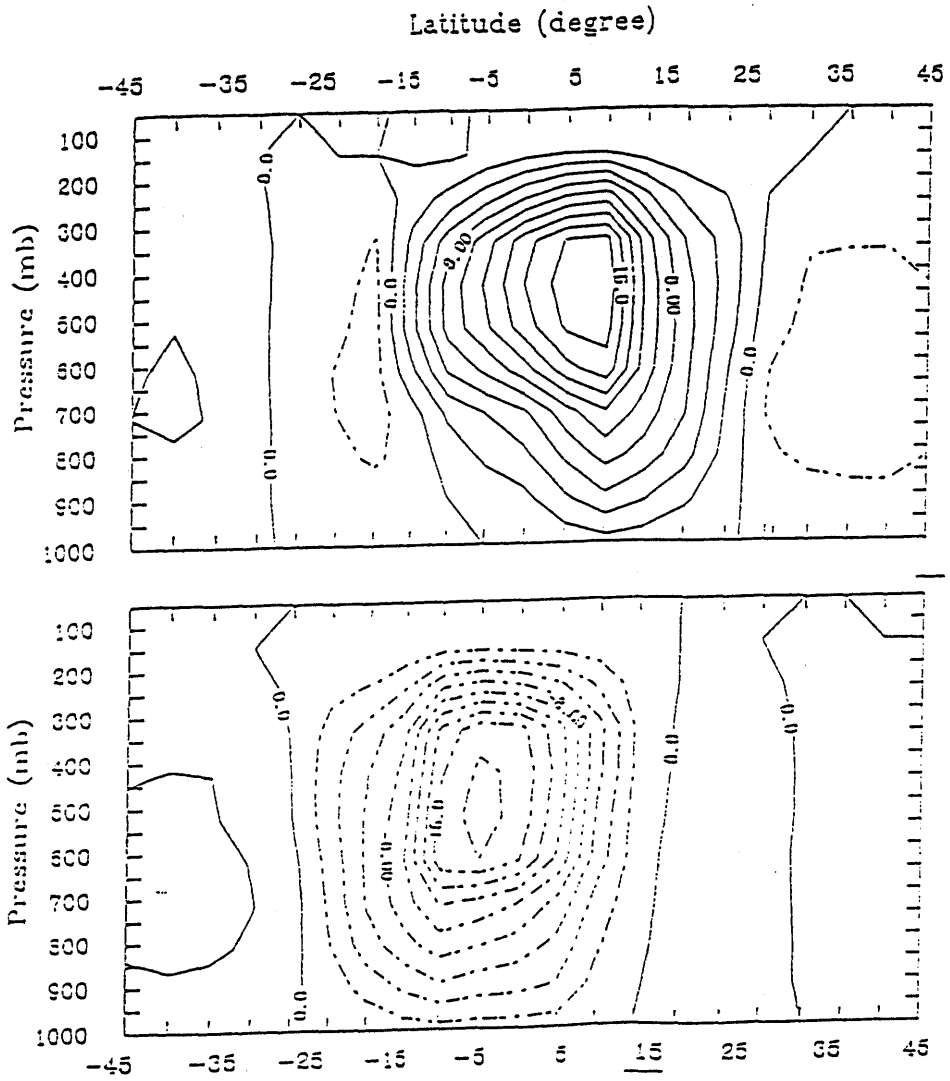

Figure 3-13: Stream lines of the Hadley circulation (in units of $10^{10} kg/s$). Data is from Oort (1983). Upper panel: January. Lower panel: July. The direction of the circulation is indicated by different line types. Solid line: clockwise. Dashed line: counterclockwise.

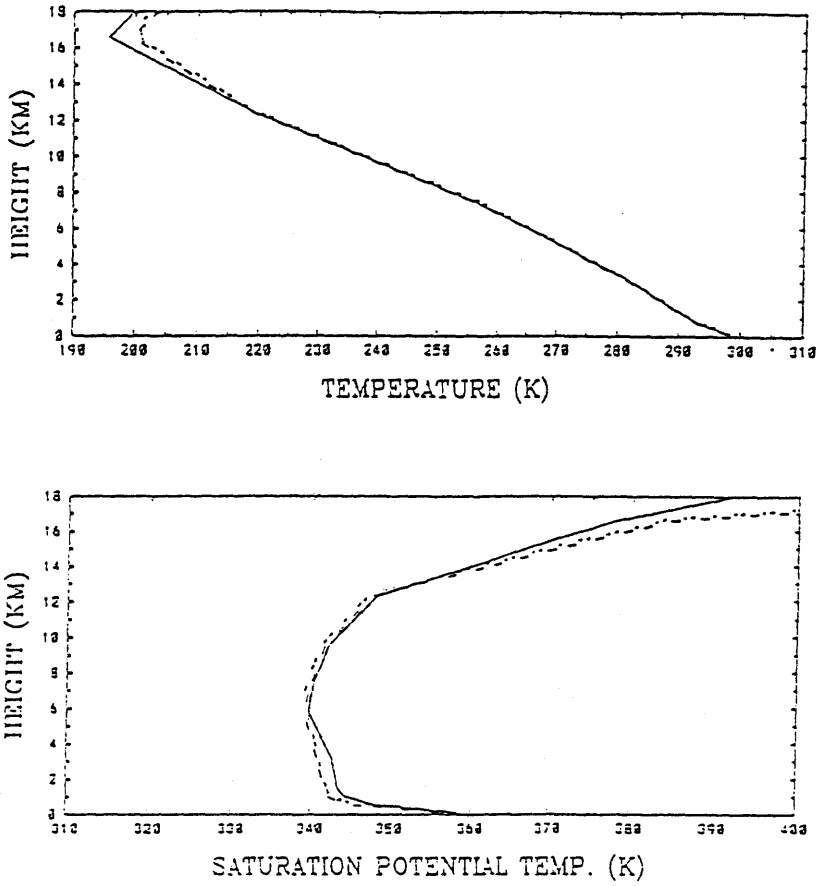

Figure 3-14: The vertical thermal structure of the troposphere horizontally averaged over the domain of the Hadley circulation. Upper: temperature. Lower: saturation equivalent potential temperature. Solid line: January; Dashed line: July.

Figure 3-9 to Figure 3-12 show the zonally averaged specific humidity and relative humidity fields for July and January. Though the satellite data (SAGE II data for the year 1987 (Rind et al 1991)) reveal a much drier middle troposphere than the conventional data (Oort 1983), they both show the distribution of water vapor to be strongly modulated by the zonal mean meridional circulation. Figure 3-13 shows the zonal mean meridional circulation for July and January. The air in the descending portion of the Hadley circulation is much drier than the air in the ascending portion.

The temperature distribution averaged over the domain of the Hadley circulation is presented in Figure 3-14 together with the saturation equivalent potential temperature. The vertical distribution of the saturation potential temperature deviates from a vertically uniform profile, which indicates that the temperature structure deviates from a moist-adiabatic profile. Another feature in the vertical distribution of

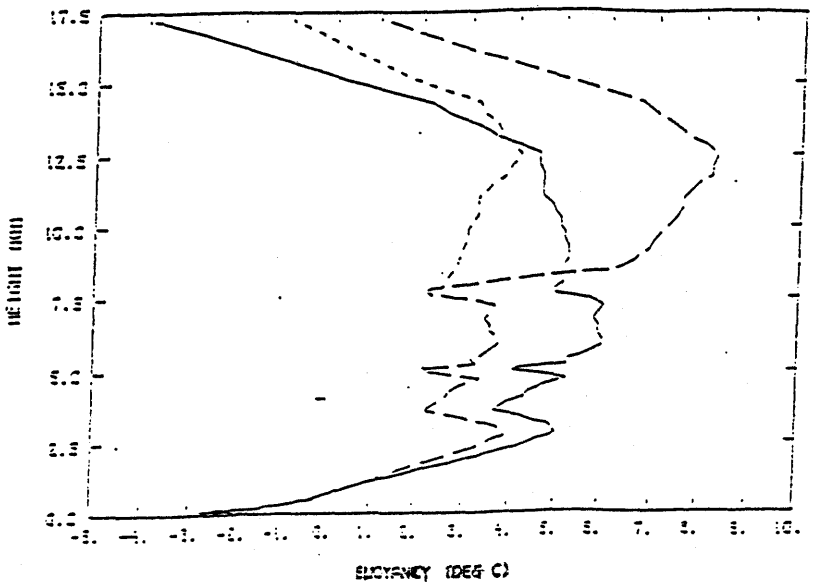

Figure 3-15: Parcel buoyancy versus height for three thermodynamic processes: pseudo-adiabatic (solid line), reversible without freezing (short-dashed line), and reversible with freezing all liquid water at -10°C (long dashed line). The sounding was from a ship measurement north of Australia. From Renno (1992)

temperature which can not be accounted for by a single moist-adiabatic profile is the structure of the trade inversion which is smoothed out in this averaged profile.

Though the overall thermal structure appears to deviate considerably from a single moist-adiabatic profile , whether the tropical troposphere has a significant amount of potential available energy (CAPE) has been in debate (Xu and Emanuel 1988). The controversy arose from the uncertain details about the micro-physical processes accompany the ascending of a moist air parcel. Figure 3-15 presents a recent analysis by Renno (1992), which supports the traditional notion that the tropical troposphere has a considerable amount of CAPE.

The meridional distribution of temperature within the domain of the Hadley circulation is presented in Figure 3-16. The horizontal distribution is rather homogeneous. The dynamics pertinent to the tropics do not allow considerable temperature gradients to develop in the horizontal direction. Note that the width and position of the region in which temperature is almost horizontally uniform correspond with the width and position of the Hadley circulation very well. The lack of inhomogeneity in the temperature fields is also accompanied by negligible horizontal heat transport

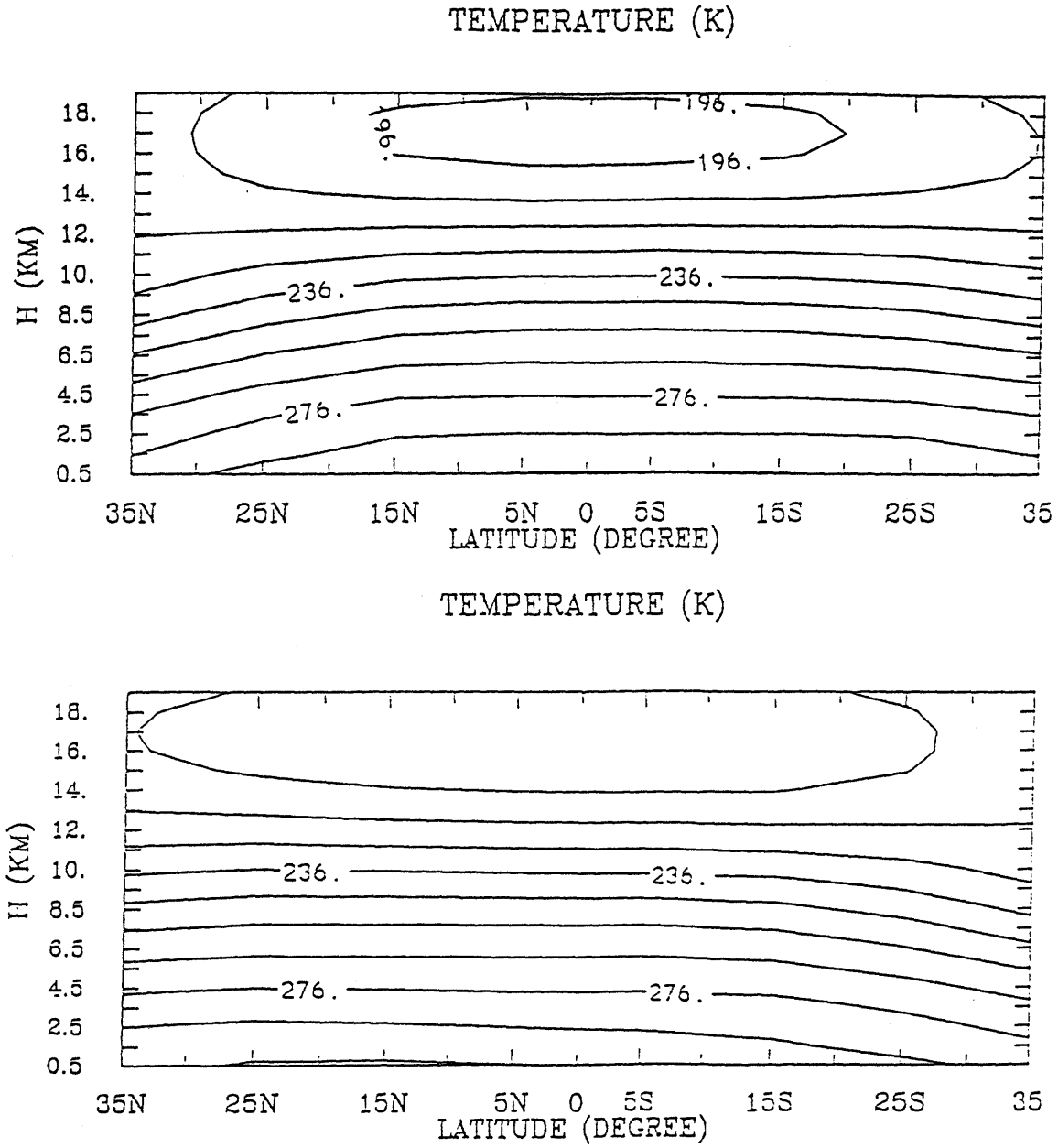

Figure 3-16: The meridional distribution of temperature in the tropical troposphere. Upper: January, Lower: July

by the mean meridional circulation and eddies (Newell et al 1982). These allow simplification of the three dimensional heat transfer problem to a one dimensional heat transfer problem if the transport along the vertical direction is the primary concern.

Chapter 4

Formulation of the water vapor and heat budget equations

Having discussed some ideas about the characteristics of moist convection and the large-scale distribution of temperature and water vapor, in this Chapter we introduce the mathematical aspects of the problem: the formulation of the budget equations for both water vapor and heat.

4.1 Idealization of the large-scale atmospheric flow

As we discussed in some detail in Chapter 1, moist convective motion (turbulence) is usually confined to small regions which are spatially isolated. The physical properties within the small-scale convective regions differ distinctly from the surrounding environmental flow. Thus it seems necessary to treat moist convection as distinguishable elements embedded in the large-scale flow. In this respect, Arakawa and Schubert's formulation is more appropriate to atmospheric flows with scales much larger than the scale of moist convection (i.e., synoptic disturbances, the Hadley circulation, etc.). However, in Arakawa and Schubert's formulation, a steady plume model for moist convection is assumed and the way the moist convection interacts with its environ-

ment is probably too limited to accurately describe the real atmospheric situation.

A straightforward generalization of Arakawa and Schubert's formulation is to replace the steady plume model by moist drafts (up and down) with a finite life cycle. By moist drafts here, we refer to small scale structures associated with moist convection. They are spatially isolated and are distinguished from their environment by differences in density, vertical velocity, water content, and temperature. That is to say, they are out of equilibrium with their environment. These various differences between the small-scale structures and their environment do not always coexist. Here, we focus on the difference in density, (i.e., the buoyancy force) since our primary concern is water vapor and heat.

4.2 Derivation of the heat and water vapor budget equations

We consider a large scale flow with horizontal velocity $\vec{V}_h$ and density ρ. Small scale moist drafts associated with moist convection are embedded in the flow (Figure 4-1 presents a schematic illustration.). Let E_{ci} represent the mass lost from the i^{th} draft to its large scale environment and E_e represent the mass lost from the environment to the moist drafts over a unit volume and time; we then have the following water vapor budget for the environment:

$$\frac{\partial}{\partial t}((1-\sigma)\rho q_e) = -\frac{\partial}{\partial z}((1-\sigma)\rho w_e q_e) - \nabla_2 \cdot (\vec{V}_h \rho q_e) - E_e q_e + \sum_i E_{ci} q_{mi} + E_d \quad (4.1)$$

where q_e is the water vapor mixing ratio of the environment, q_{mi} is the mixing ratio of water vapor of the air flowing out of the i^{th} moist draft, $\vec{V}_h$ is the horizontal flow, $\nabla_2 \cdot$ is the horizontal divergence,w_e is the vertical velocity in the environment, σ is the fractional area covered by the moist drafts and E_d is evaporation of the ice or liquid water detrained into the environment from the moist drafts. The sum $\sum_i$ is over all the moist drafts contained in a unit area. Neither condensation nor sublimation is assumed to occur in the environment. The physical meaning of other terms in the

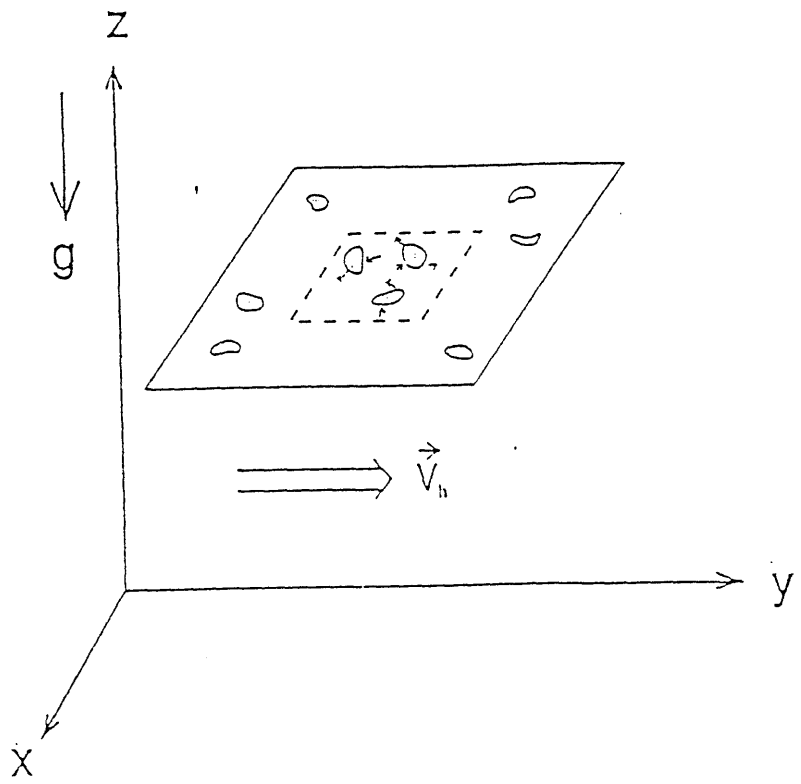

Figure 4-1: A schematic illustration of a large scale flow containing moist drafts (shaded regions) associated with moist convection.

above equation should be self-evident. The mass budget equations within the moist drafts and the environment are respectively

$$\frac{\partial}{\partial t}((1-\sigma)\rho) = -\frac{\partial}{\partial z}((1-\sigma)\rho w_e) - \nabla_2 \cdot (\vec{V}_h \rho) - E_e + \sum_i E_{ci} \tag{4.2}$$

$$\frac{\partial}{\partial t}(\sigma\rho) = -\frac{\partial}{\partial z}\left(\rho \sum_i \sigma_i w_{ci}\right) + E_e - \sum_i E_{ci} \tag{4.3}$$

The density difference between the air within the moist drafts and the environmental air is neglected in the above equations. σ_i is the fractional area covered by the i^{th} draft and $\sigma = \sum \sigma_i$. Using 4.2 and assuming $\frac{\partial \rho}{\partial t} = 0$, equation 4.1 can be re-written as

$$\begin{aligned}(1-\sigma)\rho\frac{\partial q_e}{\partial t} &= -\frac{\partial}{\partial z}((1-\sigma)\rho w_e q_e) - \nabla_2(\vec{V}_h \rho q_e) - q_e \frac{\partial}{\partial z}(\sum \sigma_i \rho w_{ci}) + \\ &\quad \sum_i E_{ci}(q_{mi} - q_e) + E_d \end{aligned} \tag{4.4}$$

Defining a mean vertical velocity by $w = (1-\sigma)w_e + \sum_i \sigma_i w_{ci}$, and replacing $(1-\sigma)w_e$ in equation 4.4, we have

$$(1-\sigma)\rho\frac{\partial q_e}{\partial t} = -\frac{\partial}{\partial z}(\rho w q_e) - \nabla_2 \cdot (\vec{V}_h \rho q_e) + \sum_i \rho\sigma_i w_{ci}\frac{\partial q_e}{\partial z} + \sum_i E_{ci}(q_{mi} - q_e) + E_d \quad (4.5)$$

Using the mass conservation equation in the Boussinesq form, we get

$$\frac{\partial(\rho w)}{\partial z} + \nabla_2 \cdot (\vec{V}_h \rho) = 0. \quad (4.6)$$

Then, we further have

$$(1-\sigma)\rho\frac{\partial q_e}{\partial t} + \rho w\frac{\partial q_e}{\partial z} + \rho\vec{V}_h \cdot \nabla_2(q_e) = \sum_i \sigma_i \rho w_{ci}\frac{\partial q_e}{\partial z} + \sum_i E_{ci}(q_{mi} - q_e) + E_d \quad (4.7)$$

In the case $\sigma \ll 1$, $q = (1-\sigma)q_e + \sum \sigma_i q_{mi} \sim q_e$. After introducing a variable $M_c = \sum_i \rho\sigma_i w_{ci}$, we obtain

$$\rho\frac{\partial q}{\partial t} + \rho w\frac{\partial q}{\partial z} + \rho\vec{V}_h \cdot \nabla_2(q) = M_c\frac{\partial q}{\partial z} + \sum_i E_{ci}(q_{mi} - q) + E_d \quad (4.8)$$

Further parameterization of the last two terms in equation 4.7 will be discussed in Chapter 6 when we apply the above equations to the tropical situations. Here we mainly point out the obvious problems in Arakawa and Schubert's parameterization, which has been widely used in GCM simulations.

In Arakawa and Schubert's scheme, the moistening term was written as $\sum_i E_{ci}(q_{mi} - q) + E_d = \sum_i E_{ci}(q_{ci} + l_i^* - q)$. q_{ci} is the mixing ratio of water vapor and l_i^* is the water in liquid and solid form carried into the environment with the detrained air from the updraft. The problems with this treatment are the following: First, the evaporation of the detrained water will likely generate downdrafts. The downdrafts may penetrate a considerable distance until they reach a new neutral buoyancy level. Therefore, the detrained water substance from the updraft is not used to moisten the environmental air at the top of the updraft but at lower levels. Second, the detrained ice from deep convective towers may primarily take the form

of upper level clouds, which also do not immediately mix into the large-scale environment. This situation is typical of tropical deep convection (Houze 1989). Third, the idea that moist drafts (up or down) moisten their environment through detrainment at their tops is only valid when a steady plume model is applicable. The convective updrafts or downdrafts involved in moist convection have a very transient nature. In light of the starting plume model, the moist draft moistens the environment only when it begins to dissipate (Turner 1979, Turner 1962) which suggests that the air within the drafts detrains at every altitude of the moist draft.

By the same procedure used to derive the water vapor budget, we can obtain the heat budget

$$\rho\frac{\partial s}{\partial t}+\rho w\frac{\partial s}{\partial z}+\rho\vec{V}_h\cdot\nabla_2(s)=M_c\frac{\partial s}{\partial z}+\sum_i E_{ci}(s_{mi}-s)-LE_d \qquad (4.9)$$

where s is the dry enthalpy of the large scale flow, s_{mi} is the dry enthalpy of the air lost from a moist draft to the environmental flow, E_d is the evaporation of liquid water and ice deposited from the moist drafts into the environment, and L is the latent heat. The sum is over all the moist drafts. The air from the moist draft will have the ambient density when it merges with its environment. This implies $s_{mi}\sim s$ and the heating or cooling associated with their difference can be neglected since the density difference is primarily caused by the temperature difference. The term LE_d is the part of evaporative cooling which does not lead to downdrafts and it is expected to be small in the tropical troposphere. There are two reasons for this. First, when there is deep convection, the environmental temperature is close to neutral for moist-adiabatic ascent or descent. Second, the evaporation of detrained ice and liquid water is a much faster processes than the lateral dissipation (We will discuss this more later on). Thus, it is reasonable to assume that the convective heating due to moist convection is primarily realized by re-distributing mass; i.e., by inducing subsidence in its environment. With this assumption and for a flow subject to radiative cooling,

Equation 4.8 should be

$$\rho\frac{\partial s}{\partial t}+\rho w\frac{\partial s}{\partial z}+\rho\vec{V}_h\cdot\nabla_2(s)=M_c\frac{\partial s}{\partial z}-R_c \tag{4.10}$$

where R_c represents the net radiative cooling.

4.3 Budget equations for the time mean Hadley circulation

Replacing the sum of last two terms in equation 4.7 by E and performing time and zonal averaging, the water vapor and heat budget equation for the monthly mean Hadley circulation is obtained

$$\begin{aligned}\rho\frac{\partial[\bar{q}]}{\partial t}+\rho[\bar{w}]\frac{\partial[\bar{q}]}{\partial z}+\rho[\bar{v}]\frac{\partial[\bar{q}]}{\partial y} &= [\bar{E}]+[\bar{M}_c]\frac{\partial[\bar{q}]}{\partial z}-[\overline{q'\frac{\partial M_c{}'}{\partial z}}]-[\bar{q}^*\frac{\partial \bar{M}_c{}^*}{\partial z}]-\\ &\quad \frac{\partial\rho[\overline{v'q'}]}{\partial y}-\frac{\partial\rho[\bar{v}^*\bar{q}^*]}{\partial y}-\\ &\quad \frac{\partial\rho[\overline{w_e{}'q'}]}{\partial z}-\frac{\partial\rho[\bar{w}_e{}^*\bar{q}^*]}{\partial z}\end{aligned} \tag{4.11}$$

Performing time and zonal averaging on equation 4.10, we obtain the heat budget for Hadley circulation.

$$\begin{aligned}\rho\frac{\partial[\bar{S}]}{\partial t}+\rho[\bar{w}]\frac{\partial[\bar{S}]}{\partial z}+\rho[\bar{v}]\frac{\partial[\bar{S}]}{\partial y} &= [\bar{E}]+[\bar{M}_c]\frac{\partial[\bar{S}]}{\partial z}-[\overline{S'\frac{\partial M_c{}'}{\partial z}}]-[\bar{S}^*\frac{\partial \bar{M}_c{}^*}{\partial z}]-\\ &\quad \frac{\partial\rho[\overline{v'S'}]}{\partial y}-\frac{\partial\rho[\bar{v}^*\bar{S}^*]}{\partial y}-\\ &\quad \frac{\partial\rho[\overline{w_e{}'S'}]}{\partial z}-\frac{\partial\rho[\bar{w}_e{}^*\bar{S}^*]}{\partial z}\end{aligned} \tag{4.12}$$

Within the domain of the Hadley circulation, the horizontal transport by eddies (both transient and steady) is negligible compared with the horizontal advection by the mean (temporally and zonally-averaged) circulation (Newell et al 1982). The last two terms represent the vertical eddy transport in the environment of moist convection,

which we may also assume negligible compared with the vertical transport by moist convection (or the vertical advection by the mean circulation). Above the convective boundary layer and away from the immediate region of the tropopause , the vertical variation of M_c is much smaller than the vertical variation of q (Ogura and Cho 1973). Therefore, we may further neglect the eddy transport of water vapor associated with the vertical variation of M_c.

Ignoring the monthly mean tendency, equation 4.10 is simplified to

$$0 = -(\rho[\bar{w}]\frac{\partial[\bar{q}]}{\partial z} + \rho[\bar{v}]\frac{\partial[\bar{q}]}{\partial y}) + [\bar{M}_c]\frac{\partial[\bar{q}]}{\partial z} + [\bar{E}] \tag{4.13}$$

Similar approximation may be made to the heat budget equation, which results

$$0 = -(\rho[\bar{w}]\frac{\partial[\bar{S}]}{\partial z} + \rho[\bar{v}]\frac{\partial[\bar{S}]}{\partial y}) + [\bar{M}_c]\frac{\partial[\bar{S}]}{\partial z} + [\bar{E}] \tag{4.14}$$

The form of equation 4.13 and 4.14 shows that the approximations used to obtain 4.13 and 4.14 from equation 4.11 and 4.12 are equivalent to approximating the Hadley circulation by a laminar two dimensional flow embedding moist convection.

4.4 Budget equations averaged over the domain of the Hadley circulation

Further performing horizontal averaging to equation 4.13 and 4.14, we have

$$0 = -\rho < [\bar{w}_e] > \frac{\partial < [\bar{q}] >}{\partial z} + < [\bar{E}] > \tag{4.15}$$

$$0 = -\rho < [\bar{w}_e] > \frac{\partial < [\bar{S}] >}{\partial z} - < [\bar{R}_c] > \tag{4.16}$$

The horizontal deviation from the mean is assumed to be negligible compared with the mean in deriving the above two equations. <> represents the horizontal average and w_e is the environmental subsidence. By mass continuity, $\frac{\partial \rho < [\bar{w}_e] >}{\partial z} = 0$. Therefore $\rho < [\bar{w}_e] >= - < [\bar{M}_c] >$. This average approach was first proposed by Schneider

(1977) (see also Sarachik 1978). Its corresponding physical picture is the Figure 3-1.

Chapter 5

A model for the tropical tropospheric temperature

In this Chapter, we investigate the maintenance of the mean vertical structure of the tropical tropospheric temperature. We will show, in a context of radiative equilibrium, that the historical picture shown in Chapter 3 is adequate to describe the leading characteristics of the observed temperature distribution. This Chapter contains two sections. The first section presents the mathematical formulation and the second section presents the equilibrium solutions for the temperature distribution.

5.1 Model formulation

The model vertical structure is schematically illustrated in Figure 5-1. It is characterized by a convective boundary layer, a free troposphere containing deep convection and the atmosphere above. This picture corresponds to an horizontally averaged Hadley circulation (Lindzen 1991b).

In light of the formulation presented in Chapter 4, the thermal energy equation for an averaged radiative-convective equilibrium is

$$M_c \frac{ds}{dz} - R_e = 0 \tag{5.1}$$

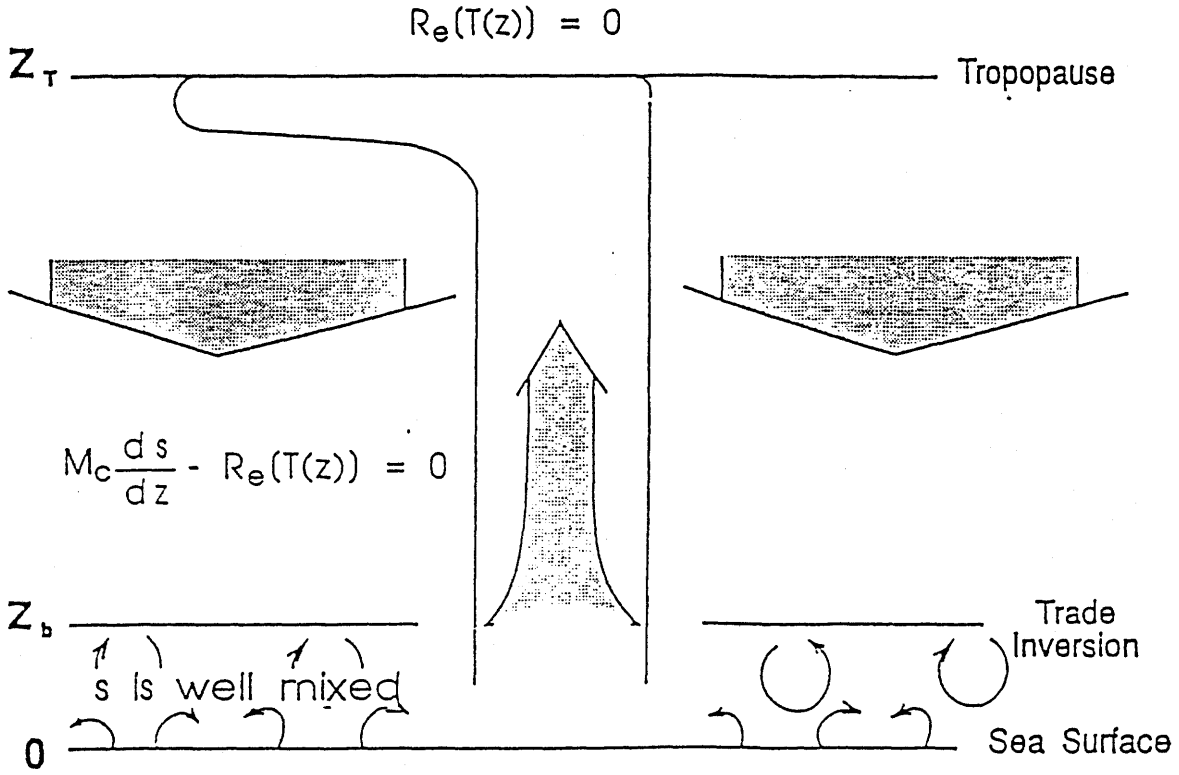

Figure 5-1: A schematic illustration of the model structure. z is the height, T is the temperature, R_e is the net radiative cooling, s is the dry enthalpy (static energy), M_c is the cloud induced subsidence, z_t is the height of the tropopause and z_b is the height of the convective boundary layer.

for $z_b < z < z_t$. M_c is the cloud induced subsidence, s is the dry enthalpy (static energy), R_e is the radiative cooling rate, z_b is the height of the top of the boundary layer and z_t is the height at which the convective heating ends — essentially the tropopause. Values of all quantities are horizontally averaged over the domain of the Hadley circulation. For the sake of brevity, bars and brackets are omitted.

Convective heating ends at the tropopause level; thus, in a radiative -convective equilibrium, the net radiative flux across the top of the tropopause and the top of the atmosphere are both zero. The integral form of the thermal energy equation for the free troposphere can be written as

$$\int_{z_b}^{z_t} M_c \frac{ds}{dz} dz = S\downarrow_b - F\uparrow_b. \tag{5.2}$$

$S\downarrow_b$ and $F\uparrow_b$ are the net solar flux and the net infrared flux across the top of the convective boundary layer.

Within the convective boundary layer, the dry enthalpy is assumed to be well mixed. A finite jump of temperature across the top of the boundary layer is allowed and it is related to the surface water vapor flux by

$$M_c \Delta s = \alpha L E_s. \tag{5.3}$$

L is the latent heat, E_s is the surface water vapor flux and α is the entrainment ratio (Sarachik,1985).

The integral form of the heat budget of the boundary layer is

$$M_c \Delta s + F_s = (S\downarrow_0 - F\uparrow_0) - (S\downarrow_b - F\uparrow_b). \tag{5.4}$$

F_s is the sensible heat flux from the surface; $S\downarrow_0$ and $F\uparrow_0$ are the net solar flux and infrared flux across the surface.

The surface heat budget is

$$S\downarrow_0 - F\uparrow_0 = LE_s + F_s. \tag{5.5}$$

From Equations 5.2, 5.3, 5.4 and 5.5, we obtain

$$\int_{z_b}^{z_t} M_c \frac{ds}{dz} dz + M_c \Delta s = LE_s. \tag{5.6}$$

Following Lindzen et al (1982), the tropopause height z_t is given by the neutral buoyancy level:

$$s(0) + rh_s Lq^*(0) = s(z_t) \tag{5.7}$$

where $s(0)$ is the dry enthalpy of surface air, $s(z_t)$ the dry enthalpy at the tropopause level, $q^*(0)$ the saturation water vapor mixing ratio of surface air, L the latent heat and rh_s the relative humidity of surface air participating in deep convection. The last quantity may not be the same as, and is likely larger than the mean surface relative humidity. Calculations showed that when rh_s is assumed to be 1, there is a better correlation between the tropopause potential temperature and the left side of Equation 5.7 (Chimonas and Rossi, 1987). Here we assume rh_s equals 1 for simplicity. Note that Equation 5.7 is only approximate. Such factors as the detrained humidity have been neglected since their contribution to buoyancy is negligible.

Budgets studies show that above the convective boundary layer, M_c is roughly constant with height up to 300 mb and then sharply decreases to zero (Ogura and Cho, 1973, Cheng et al, 1980). To first order, we may take M_c to be constant with height in the free troposphere. From Equations 5.6 and 5.7, we have the following equation for M_c,

$$M_c = \frac{E_s}{rh_s q^*(0)}. \tag{5.8}$$

The air–sea temperature difference is assumed to be 1 K, close to the climatological mean value. There are good reasons to believe this difference cannot be large since the heat capacity of air is very small. Note that no explicit formula for surface flux is needed after the air–sea temperature difference is specified. When the aerodynamic formula is employed, the air–sea temperature difference can be calculated. However, the drag coefficient may have to be adjusted to give a reasonable air–sea temperature difference.

The radiative code we use is one designed by M.D. Chou . It is a band model including water vapor, CO_2, O_3, CH_4 and N_2O. No aerosol is taken into account. The performance of this code in calculating the cooling and heating rates has been compared with other radiation codes frequently used in climate sensitivity studies, and also with the most sophisticated line by line calculations (Chou, 1986; Chou, et al, 1991). In dealing with water vapor, this code is found to give excellent agreement with the results obtained by the line by line calculations.

5.2 Equilibrium solutions

Figure 5-2 presents two equilibrium solutions for the temperature distribution[1]. One is with fixed specific humidity, the other is with fixed relative humidity. CO_2 and other chemical species are specified at their present values. In the calculation, no clouds are explicitly included. The solar insolation is adjusted to give the surface air temperature, 300 K; this implicitly accounts for effects of clouds on albedo and heat flux out of the tropics.

The model profile is very close to the observed as far as gross features are concerned. The tropopause level determined by the neutral buoyancy assumption is 180 mb and 160 mb respectively for the two states (160 mb for fixed relative humidity and 180 mb for fixed specific humidity). This level should be interpreted as the mean level at which deep clouds detrain when compared to observations (The observed mean detrainment level of deep clouds is about 200 mb). The observed tropopause level is somewhat higher because it is determined by the tallest clouds which originate at the hottest spots in the tropics (note that dynamics, by smoothing horizontal temperature gradients, establishes the tropopause throughout the tropics).

The temperature around the tropopause level is slightly higher than observed, primarily because the tropopause height is underestimated. Additionally, the profile of humidity used in the calculations in the upper troposphere may be inaccurate. The

[1] All our calculations of temperature have used a vertical resolution of 20 mb up to the level of 20 mb. Above 20 mb, there are only three additional levels: 10 mb, 1 mb, and 0.1 mb.

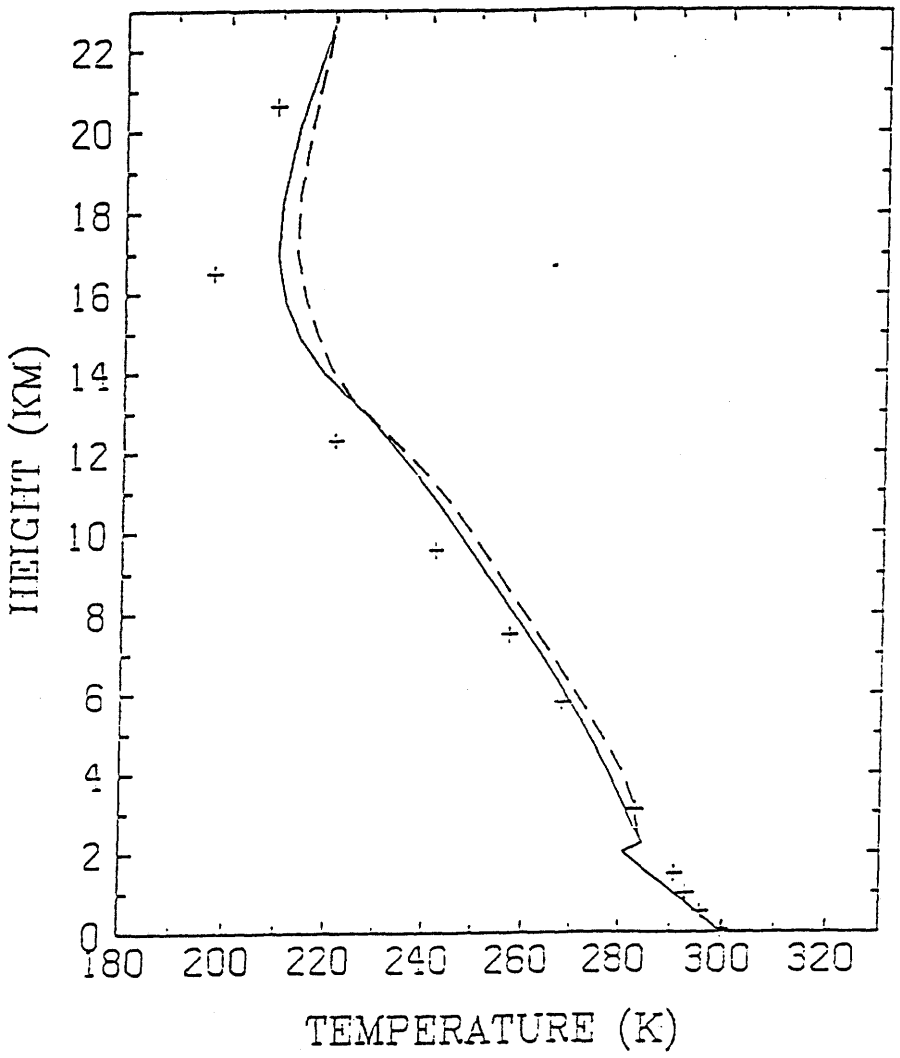

Figure 5-2: Equilibrium temperature. Solid line: fixed relative humidity. Dashed line: fixed specific humidity. The relative humidity is specified as $rh(p) = 0.8^{\frac{(p/1000)-0.02}{(1-0.02)}}$; p is the pressure. The minimum mixing ratio of water vapor is set to be 0.003 g/Kg. The specific humidity profile is from the standard tropical troposphere (McClatchey et al. 1972). +'s indicate the observed temperature averaged over the domain of the Hadley circulation in January. The data is from Oort (1983)

tropopause height and temperature are found to depend on the humidity in the upper troposphere and stratosphere, but there are no adequate observations of water vapor there. Further, assuming M_c is constant with height up to the tropopause is not very realistic. Finally, the effect of upper level clouds on the infrared radiative cooling rate is not included in the radiative code. By adjusting the water vapor profile in the upper troposphere and stratosphere or by choosing a profile for M_c in the upper troposphere which decreases to zero over a finite depth (say from 300 mb to the tropopause), one can indeed get a better fit with observations. However this is not our main purpose and it would be inappropriate to focus on such a level of detail given the simplicity of the present model. What's important here is that the model is able to grasp the main features of the tropical troposphere in an energetically consistent (potentially unstable) way. It also gives a simple interactive picture of how the tropical tropospheric temperature is maintained. Figure 3 shows the vertical structure of the saturation equivalent potential temperature for the two equilibrium states. We see from this figure that the equilibrium profile is potentially unstable. Above the boundary layer, the saturated equivalent potential temperature is almost constant with height, which indicates the temperature profile is close to moist-adiabatic. The minimum of θ_e^* occurs at the top of the convective boundary layer. The observed profile of θ_e^* is smoother than the model profile. In reality the height of the boundary layer oscillates and shallow clouds are not strictly restricted below the climatological mean height for the convective boundary layer (refer to Chapter 3). Nevertheless, it is the presence of the boundary layer that maintains a potentially buoyant tropical troposphere. The model is designed to reflect this as simply as possible.

Very recently, using the same radiative code, Renno showed that a one-dimensional radiative-convective model with Emanuel's scheme also gave an equilibrium profile which was very close to the observed. The profile also implies a certain amount of buoyancy.

It should be emphasized that for present calculations, the calculated profile is close to the moist-adiabatic, as is evident in Figures 5-2 and 5-3. This is hardly surprising given that the surface air temperature, $T(0)$, and the tropopause temperature lie on

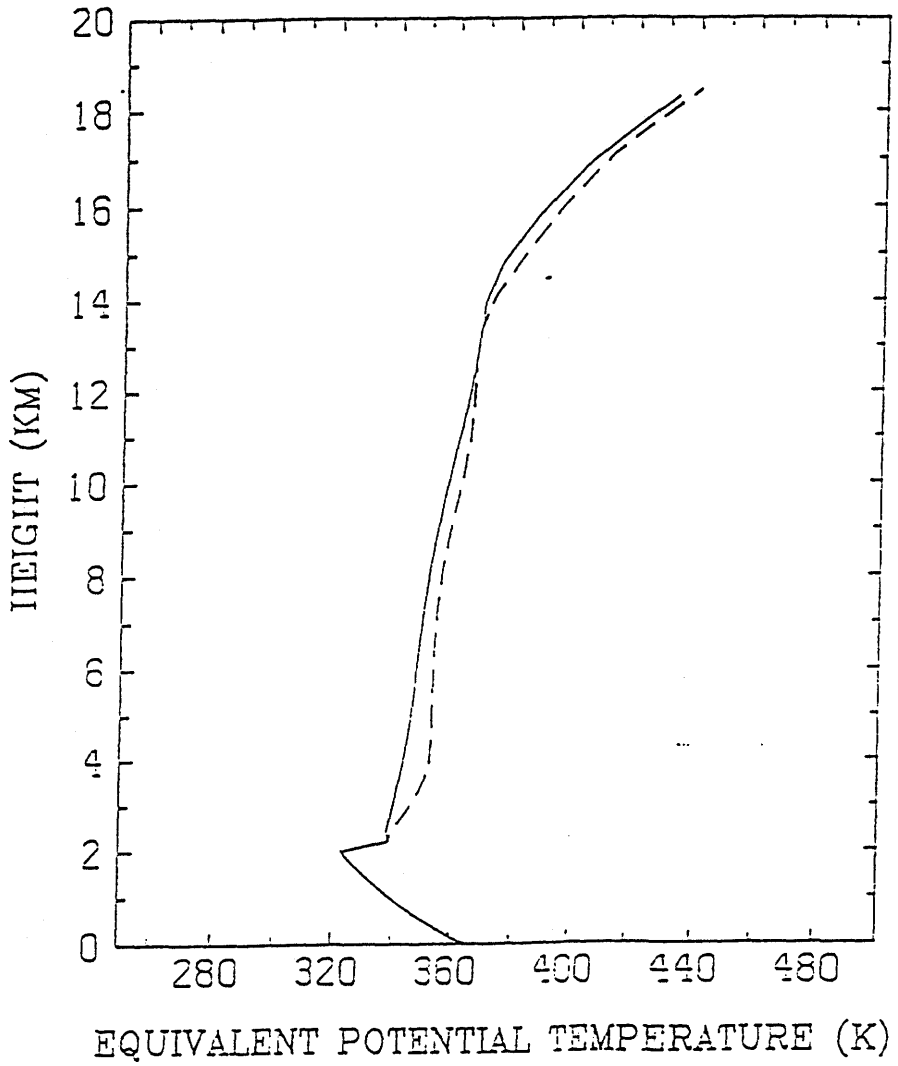

Figure 5-3: Equilibrium saturation equivalent potential temperature θ_e^*. Solid line: fixed relative humidity; dashed line: fixed specific humidity

the same moist-adiabat (Equation 5.7). However, local (in height) deviations are allowed in our model. The deviations are dependent on the radiative cooling rate and the magnitude of M_c. This feature is crucial for dealing with implications of the depressed snowline during the last glaciation. The snow-line record for the last glaciation (18 Kyr BP) indicated that the lapse rate in the low tropical troposphere was about 20% steeper than the present. If M_c did not change, the deepening of the lapse rate requires a reduction of radiative cooling rate in the low atmosphere (equation 5.1). This turns out to have important implications for the water vapor behavior in different climate regimes. We will elaborate on this in Chapter 7. To prepare to fully understand results given in Chapter 7, we investigate the tropical tropospheric water vapor budget in the following chapter.

Chapter 6

Maintenance of the tropical tropospheric water vapor distribution

6.1 Introduction

The large scale distribution of water vapor is dependent on the properties of moist convection. Though we still do not have an adequate understanding of the anatomy of moist convection and how it interacts with the large scale flow, we do have much relevant information, especially through the GATE experiment (Houze and Betts 1981). In this Chapter, we attempt to describe in a coherent manner the observed distribution of water vapor as well as our conceptual understanding of moist convection and its interplay with the large scale circulation. We wish to identify the most important physical processes and their roles in maintaining the large scale water vapor distribution.

Using a conceptual model, we first describe the roles of deep cloud induced subsidence and of evaporation of hydrometeors in maintaining the vertical distribution of water vapor (Section 2). We then discuss the meridional variation and the role of the Hadley circulation (Section 3) In Section 4, we present a one dimensional (horizontally averaged) model which simulates the observed vertical structure of tropical

tropospheric water vapor. In section 6, we discuss in detail the physical processes involved in the moistening of the large-scale subsiding flow. In Section 7, we present a two-dimensional model which explains the meridional variation of the relative humidity throughout the free troposphere (the troposphere above the convective boundary layer). Section 8 provides a summary.

6.2 The vertical distribution and the role of evaporation of hydrometeors

6.2.1 Some general remarks

To form a framework for understanding the observed water vapor distribution, we again start from the heuristic model for the vertical structure of the tropical convection (Figure 3-1).

As mentioned in chapter 2, this picture was first envisioned by Riehl in studying the energy budget of the tropical convergence zone and the trade wind regime (Riehl et al 1957, Riehl and Malkus 1958, 1979), and has been the basis of other studies of the maintenance of the thermal structure in the tropical troposphere (Schneider 1977; Sarachik 1978; Betts and Ridgway 1989). In chapter 5, we further showed how this picture can depict the major characteristics in the vertical thermal structure of the tropical troposphere.

The above-mentioned works were concerned with the energy budget rather than the determination of humidity. Little attention has been paid to the evaporation of hydrometeors and to the precipitation efficiency of individual clouds. This is also reflected in a mechanism of water vapor feedback proposed by Lindzen (1990a). In this paper, it was assumed that all condensed water vapor in deep clouds falls to the ground as rain and that the water vapor source for the free tropospheric air is the detrainment of saturated air from the deep cloud top. This assumption has been questioned by Betts (1990). He points out that the ice detrained into the upper troposphere by deep convection may be a significant source for moistening the large-

scale flow. The importance of evaporation of hydrometeors in maintaining the mean tropospheric water vapor distribution was also noted by Emanuel (1991). Based on a one dimensional radiative-convective model with his parameterization scheme, he showed that the equilibrium profile for the relative humidity was strongly dependent on the precipitation efficiency of cumulus convection. When the parcel precipitation efficiency in his model is specified as 100%, the resulting equilibrium profile for the relative humidity is much drier than the observed profile in the low troposphere.

The non-negligible role of detrained water in the water vapor budget of tropical wave disturbances was noted much earlier (Yanai, 1973, Nitta 1975, Johnson 1980). Using the 1956 Marshall Islands data and assuming clouds can be represented by plumes, Yanai et al (1973) derived the average cloud cluster properties and heat and moisture balance of the environment. His results suggested that detrained liquid water from clouds, especially from the shallow clouds in the lower troposphere contributed considerably to the moistening of the subsiding air. Using the same methods as used by Yanai, Nitta (1975) further obtained the average properties of clouds over the tropical Atlantic ocean during the BOMEX phase 3. His results were mainly about shallow trade cumuli. He also found that the detrained liquid water was non-negligible in the moisture budget of wave disturbances. Since an entraining plume is a very poor model for the real cloud (Emanuel 1991), the importance of Yanai et al and Nitta's analyses were limited. A refined work in the same context was given by Johnson (1980). In his analysis, convective-scale and meso-scale drafts were regarded as the primary components of the tropical cloud cluster. Using data obtained from the GATE, he showed that convective-scale and meso-scale precipitation downdrafts were important contributors to the heat and moisture budgets of the composite wave.

In this chapter, based on the recent available water vapor data for the upper troposphere (Rind et al 1991) and the moisture budget analysis for the tropical meso-scale system (Gamache and Houze 1983), we will see more clearly that the evaporation of hydrometeors associated with upper level precipitation has to be taken into account in order to properly deal with the mean vertical distribution of water vapor.

There are two features in the vertical distribution of tropical tropospheric water

vapor to be noted. First, throughout the troposphere, the air is subsaturated. Second, the relative humidity with respect to ice in the upper troposphere is low and does not drop much between there and the lower troposphere (the relative humidity with respect to water saturation remains fairly constant or increases with the decrease of height). In the absence of any macroscale circulation, the atmosphere would eventually saturate due to molecular diffusion. The first feature indicates the importance of macroscale circulations. The second feature illustrates the importance of the the evaporation of hydrometeors

The mean detrainment level for the cumulonimbus towers is about 200 mb where the water vapor a unit mass of air can hold will be less than 0.1 g/kg (the saturation water mixing ratio with respect to ice). Note that the upward diffusive transport of water vapor is largely restricted to below the trade inversion (the discontinuity in both the water vapor and temperature distribution across its top suggests that the water vapor above the trade inversion is unlikely to be diffused from below). Therefore, if in the process of the air going poleward and subsiding, it does not get more water vapor from any other source, the observed vertical structure over the tropics will be characterized by a constant mixing ratio of 0.1 g/kg from 200 mb to the height of the trade inversion. This also means an exponential decrease of relative humidity away from the tropopause to the low atmosphere with a scale height of about 3 km. The observed profile is far different from this and suggests the presence of a water vapor source in the course of subsiding.

Considering the fact that deep convection in the tropics generates wide-spread upper level clouds and these upper level clouds generate precipitation which falls through a subsaturated environment (Houze and Betts 1981), the leading candidate for moistening the subsiding air seems to be the evaporation of precipitation generated by upper level clouds.

The low value of relative humidity near the tropopause further implies some mechanism is needed to dry out the outflow of deep convective towers. This mechanism is likely provided by the formation of upper level clouds. The upper level clouds generate precipitation which falls out of the outflow, and generate regions with subsiding

motion. Subsaturation can occur in the region of the subsiding motion.

The formation and the life cycle of the upper level clouds have not been well understood, but it is worth noting the role of radiation. As discussed by Danielsen (1982), the difference of the radiative cooling rate between the cloud top and bottom helps to maintain the convective overturning within the clouds and generate more precipitating particles. This mechanism was originally proposed to explain the dryness of the lower stratospheric air.

In the following section, we will present a budget study which further suggests that evaporation of precipitation from upper level clouds is the major moisture source of the large-scale subsiding motion.

6.2.2 A budget study for the free tropospheric water vapor

The tropical rainfall is mostly provided by the meso-scale rain systems described by Houze (1989). The budget study of the meso-scale rain system shows that the amount of water substance carried out of the meso-scale cloud cluster (the edge of the anvil) by the outflow is about 12 percent of the total rainfall produced by the whole meso-scale system (Gamache and Houze 1983). For the month of January, the rain averaged over the whole Hadley cell (say from $15°S$ to $25°N$) is estimated to be about 4.8×10^{-5} kg/(m^{2}s) (Riehl 1979). Therefore, averaged over the month of January and over the Hadley cell, the deposit of moisture in the troposphere through the outflow of the meso-scale system occurs at a rate of about 5.8×10^{-6} kg/(m^{2}s).

The sink of water vapor of the large scale flow is the downward advection by deep cloud induced subsidence. The magnitude of the subsidence can be estimated by the energy budget of the sinking region wherein the subsidence heating is primarily balanced by radiative cooling. At 4.5 km, for example, the corresponding subsidence is estimated to be about 2.0×10^{-3} kg/(m^{2}s) (the radiative cooling rate is taken from Dopplick (1972)). The removal of water vapor by the subsidence from the troposphere above 4.5 km is about 5.2×10^{-6} kg/(m^{2}s) or 2.2×10^{-6} kg/(m^{2}s) depending on if the satellite data or the conventional sounding data is used. These numbers suggest that the moisture carried out of the anvil is sufficient to keep the air as moist as observed

to below 4.5 km.

The other source of water vapor is the mixing associated with the dissipation of deep convective towers. This source for water vapor may be estimated as follows. Suppose the deep convective tower is active for a characteristic time τ and then begins to dissipate, the moisture source per unit area it provides is $\frac{\sigma}{\tau}\int \rho(q^* + l^* - q_m)dz$. q^* is the water vapor mixing ratio of cloud air, l^* is the cloud water content in the dissipating stage, q_m is the water vapor mixing ratio of the surrounding air where the deep convective towers are generated and σ is the fractional area covered by active clouds. The integration is carried out over the region of interest. $\sigma \sim 10^{-3}$ (note velocity within the deep convective tower is about 3 orders of magnitude larger than the mean subsidence over the Hadley circulation), τ is about an hour and l^* is about 0.2 g/kg (Braham 1952). Taking the region between the tropopause and 4.5 km and assuming q_m can be replaced by the mixing ratio of the mean flow over the scale of the Hadley circulation, the rate of moisture input through dissipation of deep clouds is estimated to be between 2.0×10^{-6} kg/$(m^2 s)$ and 2.5×10^{-6} kg/$(m^2 s)$ depending on whether the conventional data or the satellite data is used. It should be noted that q_m can be much larger than the mixing ratio of the mean flow over the scale of the Hadley circulation. Furthermore, the dissipating stage of deep clouds is usually accompanied by cloud-scale downdrafts which may act to effectively remove the water substance within the clouds. The above numbers may greatly overestimate the contribution to the large scale humidity from the dissipation of deep convective towers. Nevertheless, this effect may not be completely negligible in view of Braham's budget study and Emanuel's scheme for cumulus parameterization (Braham 1952, Emanuel 1991).

Dissipation of clouds including deep convective towers and upper level clouds is accompanied by evaporation of hydrometeors. Evaporation of hydrometeors occurs at the edge of clouds. Observations of tropical rain systems further show that dissipation of clouds is characterized by a gradual elevation of the cloud base. While their bases are rising, clouds continue to generate precipitation which falls into the subsaturated air below the cloud base and evaporates (Johnson and Young 1983). The role of the evaporation of hydrometeors is the focus of this chapter.

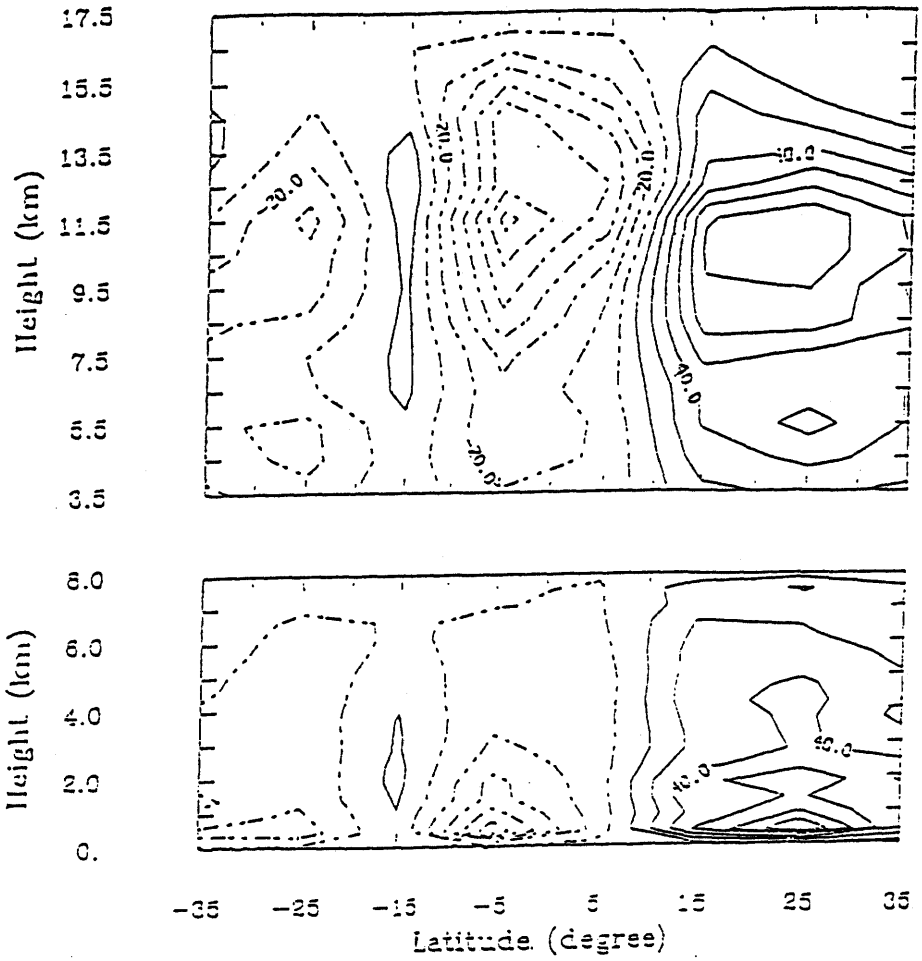

Figure 6-1: $([\bar{w}]\frac{\partial[\bar{q}]}{\partial z} + [\bar{v}]\frac{\partial[\bar{q}]}{\partial y})/[\bar{q}]$ for January ($year^{-1}$). Data for the meridional circulation is from Oort (1983). Upper panel: satellite data. Lower panel: conventional data.

Before we further quantify the above processes, we turn to the meridional distribution of water vapor over the whole Hadley domain. Features in the horizontal variation offer further information about the distributions of sinks and sources of water vapor.

6.3 The meridional variation and the role of the Hadley circulation

The sum of the meridional and vertical advection by the Hadley circulation is shown in Figure 6-1. Monthly mean data were used in the calculation. Due to the much larger vertical gradient of the water vapor mixing ratio, the meridional transport is an

is an order of magnitude smaller than the vertical transport in most regions of the Hadley circulation. Therefore, zonal mean circulation alone generates an excess of water vapor within the rising branch and a deficit of water vapor within the subsiding branch. The budget equation for water vapor is given by equation 4.12 in Chapter 4. By equation 4.12, it is evident that the moist convection acts as a sink in the upward portion and a source term in the region of downward motion. In the ITCZ (upward portion) where moist convection is concentrated, E is positive and significant. Therefore M_c must be larger than w there (note $\rho[\bar{w}]\frac{\partial[\bar{q}]}{\partial z} >> \rho[\bar{v}]\frac{\partial[\bar{q}]}{\partial y}$). What this means is that a percentage of the air pumped into the upper troposphere by deep convection subsides within the ITCZ. Gray (1974) reached the same conclusion in analyzing the water vapor budget of a cloud cluster region. Our picture of the ITCZ results from a spatial average over a scale much larger than the scale of deep convective clouds. In between these deep convective towers is subsiding motion. The concentration of deep convection, itself, is controlled by the sea surface temperature distribution (Lindzen and Nigam 1987).

In the subtropics (the subsiding branch of the Hadley circulation), large scale subsidence prevails, and deep convection is largely suppressed. But, there is still a considerable amount of deep convection in the subtropics as indicated by the upper-level cloud cover (Barton 1983).

In the following section, we will try to quantify the discussed processes and formulate a mathematical model in order to further assess the role of convection in maintaining the observed distribution, especially the interplay between the subsidence drying and the moistening from the evaporation of hydrometeors.

6.4 A model for the mean vertical structure of the tropical tropospheric water vapor

The model structure is schematically shown in Figure 6-2. In the vertical, the troposphere is divided into three different regions, characterized by the physical processes involved in the water vapor budget: the convective boundary layer, the outflow region

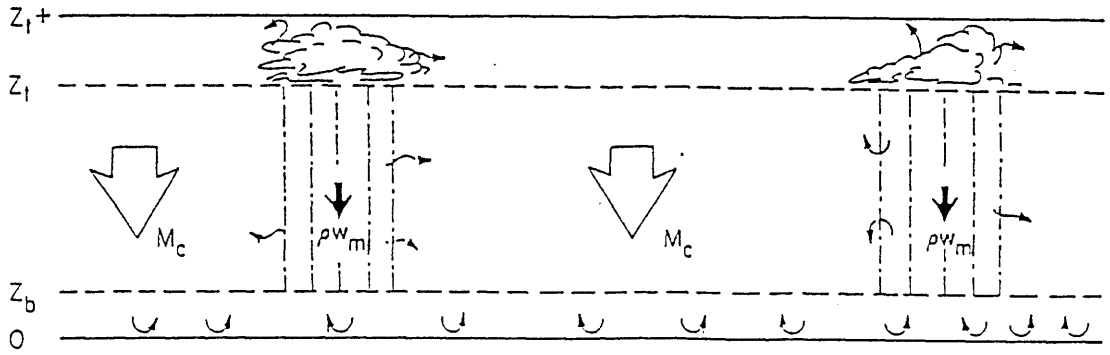

Figure 6-2: A schematic illustration of the model structure. For clarity, the deep convective tower is not drawn. z_{t*} is the tropopause height, z_t is the base height of the outflow and z_b is the height of the convective boundary layer. M_c is the downward mass flux in clear sky and ρw_m is the downward mass flux within the area covered by precipitation

of deep convective towers and the region in between (the free troposphere). Deep convective towers take up the moist air within the convective boundary layer and generate hydrometeors. Some of the hydrometeors fall within the convective towers and some of them are carried to the upper-troposphere leading to the formation of wide-spread upper level clouds. Upper level clouds continue to generate precipitation which falls into the subsaturated free troposphere and evaporates (For clarity of discussion, we temporarily neglect the contribution from the dissipation of deep convective towers. As we will see later, this effect can be easily incorporated). If a first order description cannot be obtained using this idealized picture, we may conclude that there are some things fundamentally wrong with the idealization. However, if this picture can grasp the main features of the observed vertical structure, it may serve as a basis for a more complete representation. We will begin with the formulation of the equations for the water vapor budget and then discuss the parameterization of the moistening from the evaporation of hydrometeors.

6.4.1 Equations for the water vapor budget

Within the upper boundary layer which is the outflow region of the deep convective towers, the supply of moisture is from the detrainment from these towers. The primary sink of moisture is the formation of upper level clouds and the associated precipitation. The moisture budget of the outflow may be written as

$$M_{dc} q_{z_t} + R_{z_t} = S_{dc} \tag{6.1}$$

in which $S_{dc} = \int_{z_t}^{z_t^+} -\frac{dM_{dc}}{dz}(q^* + l^*)dz$; z_t^+ and z_t are the top height and base height of the outflow. M_{dc} is the convective mass flux within the deep convective tower, q^* is the saturation mixing ratio and l^* is the ice water content of the air detrained from the deep convective towers. S_{dc} is thus the total moisture input from the deep convective towers. ρR_{z_t} is the precipitation flux at the base of the outflow; q_{z_t} is the area mean water vapor mixing ratio, and $M_{dc} q_{z_t}$ is the water vapor flux at the base of the outflow. It is believed that l^* can be orders of magnitude larger than q^* in the upper troposphere. Therefore equation 6.1 suggests that a significant precipitation flux is needed to keep the outflow subsaturated.

We further divide the outflow into two regions: the upper-level clouds, and their clear air environment. The water vapor budget for the clear air environment can be written as

$$\rho E_{uc} + \rho E_{dc} + M_c \frac{dq}{dz} = 0 \tag{6.2}$$

M_c is the net large scale subsidence in the clear air environment (Since the model here is one-D (averaged over the Hadley domain), M_c is also the net convective mass flux), q is the water vapor mixing ratio in the clear environment, ρE_{uc} is the moistening from the upper level clouds, and ρE_{dc} is the moistening from the deep convective towers.

We assume that all the detrained water substance from the deep convective towers is directly used to feed the upper level clouds. Then $E_{dc} = 0$ (Note that the dissipation

of deep convective towers is temporarily ignored). Equation 6.2 is simplified as

$$\rho E_{uc} + M_c \frac{dq}{dz} = 0 \tag{6.3}$$

In the free troposphere, the source of water vapor is from the evaporation of the precipitation. Since the precipitation from upper level clouds is a cloud or mesoscale phenomena, it is expected to generate entities which are distinct from the large scale mean flow in terms of vertical velocity, density and water content. Therefore, we have to distinguish the region covered by precipitation from the region free of precipitation (we will discuss some details of the relevant physical processes later on). Let M_c denote the net large scale subsidence in the clear air and E_r the moisture input from the region covered by precipitation; then we have

$$M_c \frac{dq}{dz} + \rho E_r = 0. \tag{6.4}$$

for

$$z_t > z > z_b$$

where z_t is the effective base height of the outflow of deep convective towers, z_b is the height of the surface convective boundary layer, q is the water vapor mixing ratio in the clear air environment, and E_r is the moistening supplied by the evaporation of precipitation.

When the fractional cover of the clouds is very small, the above equations can also be regarded as the area mean budget equation (see the appendix).

Since shallow convection within the convective boundary layer may be regarded as the natural extension of the turbulence driven by surface fluxes, further detailed separation between the dry boundary layer and the cloudy boundary layer will not add physical significance to our discussion. Furthermore, shallow clouds within the convective boundary layer (i.e. below the trade inversion) hardly precipitate. Therefore, to first order their effect in transporting water vapor may be parameterized as downgradient diffusion. In such a treatment, we need not distinguish the shallow non-

precipitating clouds from their clear air environment. Let M_c denote the subsidence within the boundary layer, then the water vapor budget may be written as

$$M_c \frac{dq}{dz} + \frac{d}{dz}(K\rho \frac{dq}{dz}) = 0 \tag{6.5}$$

for

$$z \leq z_b$$

where z_b is the height of the convective boundary layer, and K is the diffusion coefficient.

If one's aim is to produce a realistic vertical structure of the water vapor mixing ratio, the surface value may be chosen as the observed value. Then the boundary conditions for the water vapor equations 6.3, 6.4 and 6.5 may be written

$$q \mid_{z=0} = q_0 \tag{6.6}$$

$$q \mid_{z=z_t^+} = q_t \tag{6.7}$$

q_0 and q_t are the water vapor mixing ratio at the surface level and the tropopause level.

When the value of surface air mixing ratio is also a variable to be predicted, the surface boundary condition may be formulated as follows:

$$M_c(q_0 - q(z_b)) = c_d U \rho (q^*(T_s) - q_0), \tag{6.8}$$

which is a statement of the moisture budget of the convective boundary layer. The left side of this equation is the net loss of water vapor due to dynamic transport, and the right side is a parameterization of surface evaporation based on bulk aerodynamic formulas. c_d is the aerodynamic drag coefficient and U is the frictional velocity.

There are two other implicit boundary conditions, which are the continuity of water vapor content across both the interface between the outflow region and the free troposphere, and the interface between the free troposphere and the convective

boundary layer.

The division into three regions may not be as clear in reality as in our model. The height of the convective boundary layer varies within the tropics and is not well defined in the ITCZ. Averaged over the whole tropics, the height of the convective boundary layer may be chosen as 2 km (Betts and Ridgway 1989). The mean thickness of the outflow of the deep convective tower is less well documented. The base height for cirrus clouds may give a useful indication. Based on London (1957), the base height for cirrus clouds is about 10 km. Therefore, the region in between the convective boundary layer and the outflow of deep convective tower occupies the bulk of the troposphere, which is our focus here.

6.4.2 Determination of the large scale subsidence induced by deep convection

An estimate of M_c can be obtained by considering the energy budget of the large-scale subsidence. Away from the trade wind boundary layer (where turbulent mixing may supply considerable sensible heat) the energy budget may be written as

$$M_c \frac{ds}{dz} - R_c = 0. \tag{6.9}$$

where s is the dry enthalpy, and R_c is the net radiative cooling (infrared cooling plus solar heating). The lateral transfer of heat from deep convection to the subsiding air in the clear environment is assumed to be negligible (Further discussions and a more rigorous derivation are presented in the Appendix.).

Figure 6-3 shows the M_c profile in January deduced from equation 6.9. The temperature profile is from Oort (1983). Radiative cooling is taken from Dopplick (1972). In the boundary layer, M_c unexpectedly increases downward, which may suggest that sensible heating cannot be neglected there. Since there is no reliable data for the sensible heating in the boundary layer, we assume that M_c remains constant with height within the convective boundary layer.

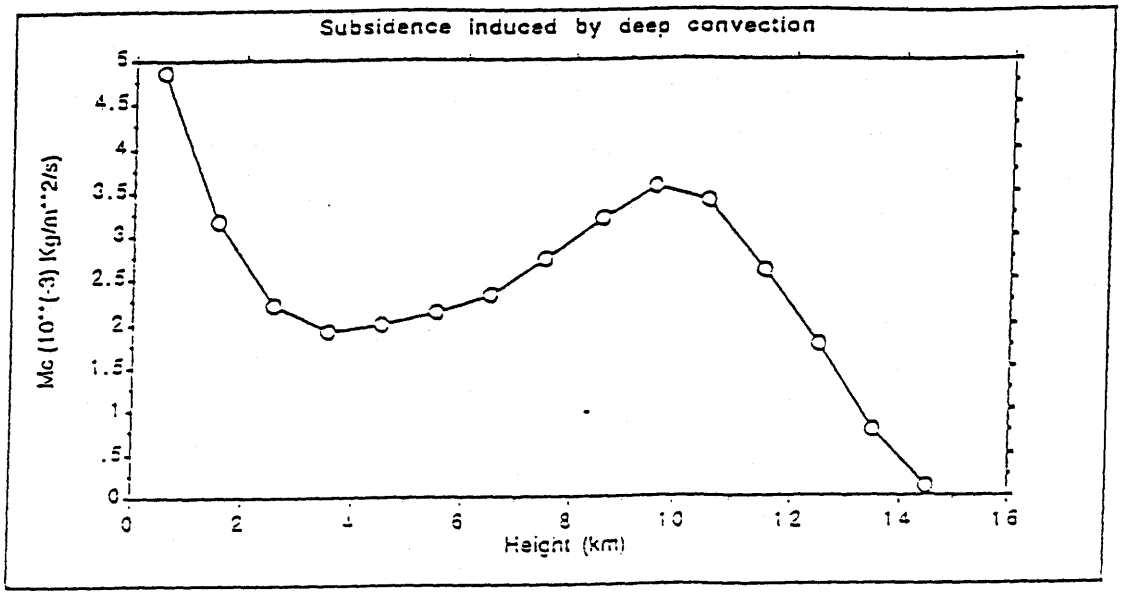

Figure 6-3: Deep cloud induced subsidence deduced from the energy budget (in units of 10^{-3} kg/$(m^2 s)$)

6.4.3 A simple parameterization of the moistening from the upper level clouds and their precipitation

Upper level clouds moisten their environment through evaporation of cloud water and mixing of the saturated cloud air into the environment. The bulk effect of this moistening is to bring the atmosphere to saturation. So is the bulk effect of the evaporation of hydrometeors falling from the base of upper level clouds. Therefore, a simple, straightforward way to parameterize E_{uc} and E_r is through linear approximations,

$$E_{uc} = \alpha_c(q^* - q) \tag{6.10}$$

$$E_r = \alpha(q^* - q) \tag{6.11}$$

where q^* is the saturation value of water vapor mixing ratio (with respect to ice above the melting level), and q is the water vapor mixing ratio. α_c^{-1} is the time scale of moistening for upper level clouds and α^{-1} is the time scale of moistening due to

evaporation of precipitation. α and α_c are related to the total moisture input into the upper level clouds by deep convective towers (S_{dc}) and the precipitation flux at the base level of upper level clouds ($R(z_t)$ by:

$$\alpha_c = \frac{S_{dc} - R_{z_t}}{\int_{z_t}^{z_t^-} \rho(q^* - q)dz} \tag{6.12}$$

and

$$\alpha = \frac{R(z_t)}{\int_{z_b}^{z_t} \rho(q^* - q)dz} \tag{6.13}$$

where ρ is the air's density. It is assumed that precipitation flux at the level of z_b, R_{z_b}, can be ignored compared with R_{z_t}.

This simple parameterization straightforwardly relates the moistening by the upper level clouds and the precipitation they generate to the amount of upper level clouds (i.e. the total moisture input from deep convective towers to the upper boundary layer) and the amount of precipitation generated by upper level clouds. The parameterization is closed either by coupling a deep cloud model which gives S_{dc} and a model for upper level clouds which gives R_{z_t} or with specified S_{dc} and R_{z_t}. Another advantage of this parameterization is that all parameters involved can be directly verified by observations. In the following section, we check this parameterization by estimating the observed vertical distribution of water vapor.

6.4.4 Simulation of the observed vertical distribution of water vapor

A simulation of the vertical distribution of water vapor is presented in Figure 6-4. In our simulation, S_{dc} and R_{z_t} are specified. This is equivalent to specifying α and α_c (equation 6.12 6.13). This is sufficient for our present purpose in estimating the observed distribution. Between z_t and z_{t+}, equation 6.3 is used for the water vapor budget. q_0 and q_t are fixed at the observed values. In general, a simulation with realistic features is obtained. This supports our interpretation for the observed tropical tropospheric water vapor distribution at least as concerns gross behavior. Some

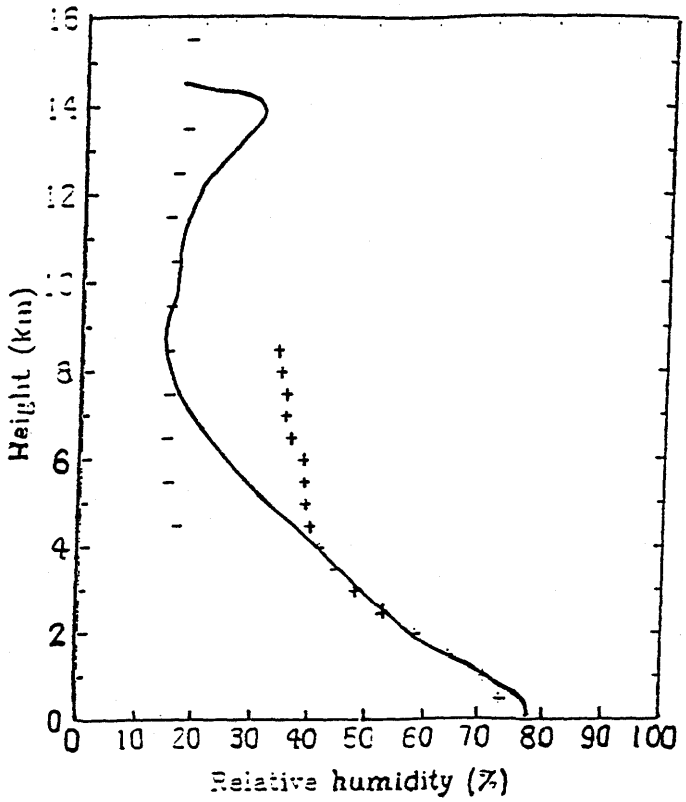

Figure 6-4: The simulated vertical structure of the tropical tropospheric relative humidity in January. Relative humidity is with respect to liquid water. The solid curve is the model simulation. '+' and '-' represent the conventional and satellite data respectively. The temperature profile used in this simulation is also from Oort (1983). Parameters are: $z_{t+} = 14.5\,km$, $z_t = 9.7\,\mathrm{km}$, $z_b = 2.0\,\mathrm{km}$, $K = 3.4m^2/s$

Some discrepancy with observational data is expected, given the simplicity of parameterization and the uncertainties in the observational data. Figure 6-5 shows the parametric dependence of tropical tropospheric relative humidity as depicted by this model. Note that above the boundary layer the effect of increasing α is equivalent to decreasing M_c. Figure 6-5 demonstrates that the relative humidity is related to the circulation and the microphysics of precipitation and can change if the processes change (In these sensitivity studies, α_c is assumed to be proportional to α as it should because R_{z_t} is expected to be proportional to S_{dc}. α_c is assumed to be larger than α considering that the precipitation downdrafts may be subsaturated but upper level clouds consist in saturated updrafts and downdrafts. The physical meaning of these two parameters will be discussed further in the following section).

This model supplies a quantitative context for evaluating the roles of the relevant

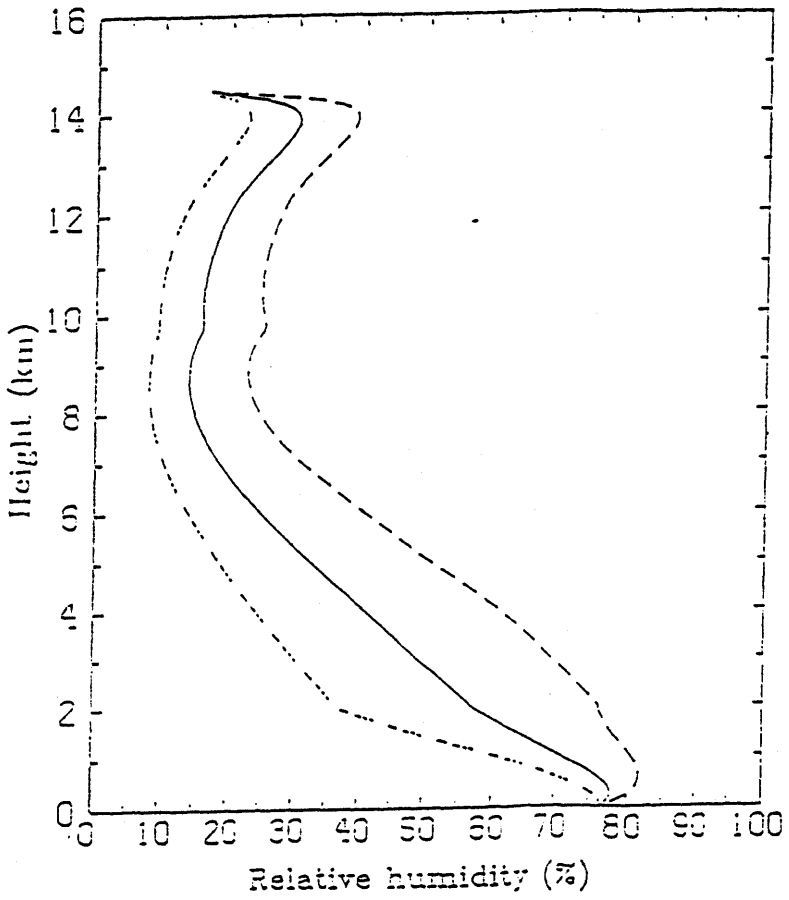

Figure 6-5: The sensitivity of the simulated vertical structure of the tropical tropospheric relative humidity to changes in α and α_c. Relative humidity is with respect to liquid water. Solid line: $\alpha^{-1} = 14$ days and ${\alpha_c}^{-1} = 7$ days. The corresponding S_{dc}=1.24 kg/m^2/day and R_{z_t}=1.21 kg/m^2/day. Long-dashed line: $\alpha^{-1} = 7$ days, ${\alpha_c}^{-1} = 3.5$ days. The corresponding S_{dc}=1.68 kg/m^2/day and R_{z_t}=1.62 kg/m^2/day. Short-dashed line: $\alpha^{-1} = 28$ days and ${\alpha_c}^{-1} = 14$ days. The corresponding S_{dc}=0.796 kg/m^2/day $R_{z_t} = 0.775$ kg/m^2/day Other parameters are: $z_{t+} = 14.5$ km, $z_t = 9.7$ km, $z_b = 2$ km, $K = 3.4 m^2/s$

physical processes as highlighted by observations. However, the physical processes associated with moistening by the upper level clouds and their precipitation are buried in the constant coefficients, α^{-1} and ${\alpha_c}^{-1}$, the time scales for moistening. We will discuss these physical processes below.

6.5 The physical processes of moistening

6.5.1 Precipitation downdrafts and their life cycle

Precipitation processes in the tropics are largely cloud scale and meso-scale phenomena. When the lateral dissipation is a much slower process than the evaporation of hydrometeors, the evaporation of precipitation may establish a considerably moister local environment and the cooling associated with evaporation and precipitation loading will generate negatively buoyant currents. This seems to be true in the tropical atmosphere. Let p, T and RH represent respectively the pressure, temperature and relative humidity of the environment in which an ice crystal with a radius r evaporates, and let τ represent the time it takes for the ice crystal to completely evaporate. The following numbers may serve as a quick reference: for p =600 mb, T =273.15 K, RH=90% and r=0.1 mm, τ = 14 minutes; for p =200 mb, T =233.00 K, RH=90% and r=0.1 mm, τ=137 minutes. The lateral diffusion has the time scale of L^2/D, where L is the horizontal scale of the area covered by the precipitation, and D is the diffusion coefficient. For L= 10 km, and D as large as 5.0 m^2/s (which may be regarded as a characteristic value for boundary layer turbulence), $L^2/D \sim 3.4 \times 10^5$ minutes. This will no doubt enhance the ability of precipitation to survive in a subsaturated mean environment. Here it is worth recalling Braham's observation (Braham and Duran 1967) that ice crystals falling from cirrus can survive 15,000 feet (from 250 mb to 600 mb) in a mean environment with a relative humidity less than 30 percent (given by the sounding data). To parameterize the moisturization from the precipitation falling in a subsaturated environment, one has to take into account the fact that the precipitation flux generates small-scale precipitation downdrafts.

It should also be noted that precipitation downdrafts appear to moisten the environment mainly when they dissipate. When the precipitation penetrates downward, the exchange between the downdrafts and the mean environment is limited in view of the unusual survival ability of the precipitation as observed by Braham and Duran (1967). This may also be shown by the following estimates. For a downdraft with a moderate vertical velocity, 0.05 m/s, the time for an air parcel in the downdraft to descend 10 km is 2.0×10^5 s. The lateral dissipation time scale is $2.0 \times 10^7 s$ for a turbulent downdraft with a half-width 10^4m. Thus, the life cycle of precipitation downdrafts need also be explicitly taken into account in paramterizing their moistening to the large-scale flow.

6.5.2 Representation of the moistening effect of the precipitation downdrafts

In view of the above, we may represent precipitation downdrafts as isolated columns of moist air embedded in the large-scale subsiding motion. These columns of moist air have a characteristic water vapor mixing ratio q_m and a life span of τ. Its life span here is defined as the time the moist air takes to completely merge into the surrounding large-scale subsiding motion. The rate they supply water vapor to the large scale flow may be written as

$$E_r = \frac{\sigma}{\tau}(q_m - q) \tag{6.14}$$

σ represents the fractional area of dissipating downdrafts and q is the water vapor mixing ratio of the large scale flow. For a steady situation, $\frac{\sigma}{\tau}$ may be regarded as the rate of the generation of precipitation downdrafts. A reasonable assumption for q_m is that it lies in between q^* and q. A linear approximation may be written as $q_m = (1-c)q^* + cq$, with moistening written as $E_r = c\frac{\sigma}{\tau}(q^* - q)$. Thus $\alpha = \frac{\sigma}{\tau}c$. Thus this picture is cosistent with our bulk treatment in the above section.

When the downdraft dissipates, the temperature of the downdraft air differs little from the environment it merges into. Thus, for $q_m > q$, the equivalent potential

temperature of the downdraft air has to be larger than the environment. Since the minimum environmental equivalent potential temperature occurs in the middle troposphere, to be able to moisten the environment, the downdraft air has to originate from the upper troposphere. This again suggests the importance of the upper level precipitation.

Upper level clouds consist in saturated updrafts and downdrafts, therefore the moistening from upper level clouds may also be written in the above form with the replacement of q_m by q^*

$$E_c = \frac{\sigma}{\tau}(q^* - q) \tag{6.15}$$

Thus $\alpha_c = \frac{\sigma}{\tau}$.

The simple parameterization with a constant α is equivalent to assuming that the precipitation downdrafts have a constant relative humidity. A more realistic approach is to explicitly calculate the vertical distribution of q_m by coupling a model for the precipitation downdraft. Such a treatment immediately reveals the potential importance of details of the precipitation particles, such as the total water content and the size distribution of precipitation particles, in affecting the vertical distribution of water vapor in the large-scale flow.

6.5.3 The role of the size spectrum and water content of hydrometeors

The budget of the hydrometeors and water vapor within the precipitation downdraft may be represented by the following equations,

$$\frac{d((V_t + w_m)\rho)\rho_r}{dz} - \rho E_{mr} = 0, \tag{6.16}$$

$$\rho w_m \frac{dq_m}{dz} + \rho E_{mr} = 0, \tag{6.17}$$

for the free troposphere. ρ_r and q_m are the mixing ratios for hydrometeor and water vapor respectively. ρ is the density of the downdraft air and $\rho\rho_r$ is the hydrometeor water content. ρw_m is the mass flux within the precipitation downdrafts, which will be

assumed to be constant with height. V_t and E_{mr} are respectively the mass weighted mean terminal velocity and the evaporation rate of hydrometeors. The boundary conditions for ρ_r and q_m may be written as:

$$\rho_r(z_t) = h_c;\ q_m(z_t) = q^*(z_t) \tag{6.18}$$

where h_c is the mixing ratio of precipitating particles at z_t, the height of the upper cloud base where precipitation originates. At that level, the precipitation downdraft may taken as saturated. $q^*(z_t)$ is the saturation mixing ratio of water vapor.

Assuming the size spectrum of the hydrometeors is exponential $N(r) = N_0 exp(-\lambda r)$(r is the radius of a hydrometeor and $N(r)dr$ is the number of hydrometeors with radii between r and r+dr per unit volume), the evaporation rate of hydrometeors can be further written as

$$E_{mr} = -4\pi D C_v N_t \bar{r} \frac{1}{1+\epsilon}(q_m - q^*), \tag{6.19}$$

where D is the molecular diffusion coefficient, and q^* is the saturation water vapor mixing ratio. $\epsilon = \frac{D}{K}\frac{e_s(T)}{R_v T^2}(\frac{L}{R_v T} - 1)L$, R_v is the gas constant of water vapor, T is the temperature, $e_s(T)$ is the saturation pressure of water vapor, K is the coefficient of thermal conductivity of the air and L is the latent heat. $\bar{r} = B(\rho\rho_r)^{\frac{1}{4}}$ and $B = (8\pi N_0 \rho_i)^{-\frac{1}{4}}$. $\bar{r}$ is the mean radius of the hydrometeors and ρ_i is the density of the hydrometeors. $N_t = \int N(r)dr = N_0\bar{r}$. C_v is the ventilation coefficient which is related to the mean terminal velocity by $C_v = 0.78 + 0.28R_e^{\frac{1}{2}}$. $R_e = \frac{2\bar{r}\rho V_t}{\mu}$ is the Reynolds Number (Roger and Yang 1989), μ is the dynamic viscosity, and V_t is the mass weighted mean terminal velocity, $V_t = \frac{\int v_t(r)N(r)dr}{\int m(r)N(r)dr}$. $v_t(r)$ and $m(r)$ are the terminal velocity and the mass of the hydrometeors with radius r. Taking $v_t(r) = kr$, the mass weighted mean velocity can be related to the hydrometeor water content by $V_t = A(\rho\rho_r)^{\frac{1}{4}}$ where $A = \frac{4k}{(8\pi N_0 \rho_i)^{\frac{1}{4}}}$ (Mason 1971, Roger and Yau 1989).

Ground level observations show the size spectrum of continental rain can be well represented by an exponential form (Marshall and Palmer 1951). The upper level precipitation spectrum is less known. Observations of cirrus show the size spectrum

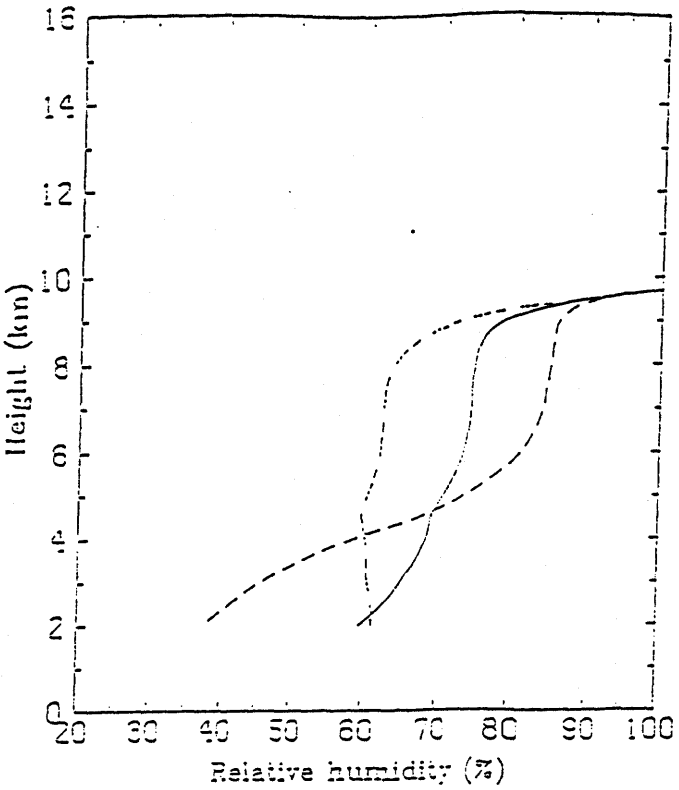

Figure 6-6: Sensitivity of the relative humidity distribution within the precipitation downdraft to the change of spectrum of hydrometeors. Relative humidity here is with respect to liquid water. Parameters are: $z_t = 9.7\,\mathrm{km}$, $\rho w_m = 0.2\ \mathrm{kg}/(m^2 s)$ and $h_c = 0.5$ g/kg. Solid line: $N_0 = 0.8 \times 10^7\ m^{-4}$. Long-dashed line: $N_0 = 0.8 \times 10^8\ m^{-4}$. Short-dashed line: $N_0 = 0.8 \times 10^6\ m^{-4}$

of ice crystals in the upper level clouds can be represented by the sum of two exponential distributions (Heymsfield 1984). For our present purpose, such a form may be sufficient.

Numerical solutions for equations 6.16,6.17 and 6.18 with different values for N_0 and h_c are presented in Figures 6-6 and 6-7 (Note that the curves are for the relative humidity instead of the mixing ratio q_m). The temperature within the downdraft cannot differ considerably from its environment when the downdraft is in its dissipating stage and therefore, it is assumed to be t he same as that of the mean environment. It is apparent from the three curves in Figures 6-6 and 6-7 that the vertical distribution of the relative humidity within the precipitation downdrafts is sensitive to the spectrum of the hydrometeors as well as their mixing ratio (Recall the mean radius $\bar{r} \sim N_0^{-1/4}$.)

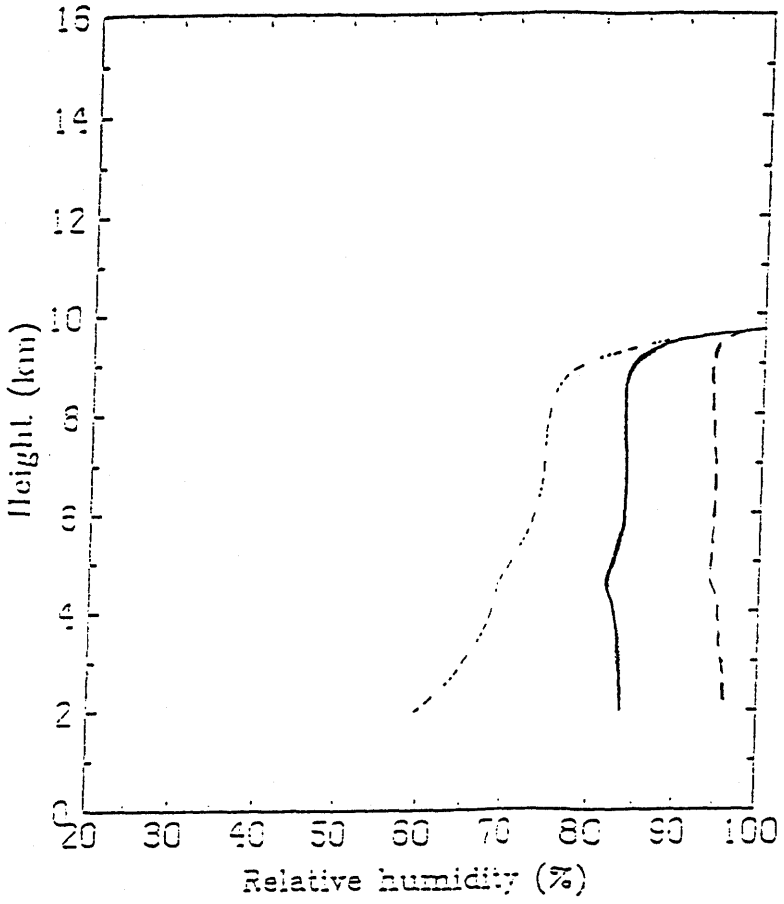

Figure 6-7: Sensitivity of the relative humidity distribution within the precipitation downdraft to the water content of hydrometeors. Relative humidity is with respect to liquid water. Parameters are: $z_t = 9.7\,\mathrm{km}$, $\rho w_m = 0.2\ \mathrm{kg}/(m^2 s)$ and $N_0 = 0.8 \times 10^7\ m^{-4}$. Solid line: $h_c = 1.0$ g/kg. Long-dashed line: $h_c = 5.0$ g/kg. Short-dashed line: $h_c = 0.5$ g/Kg

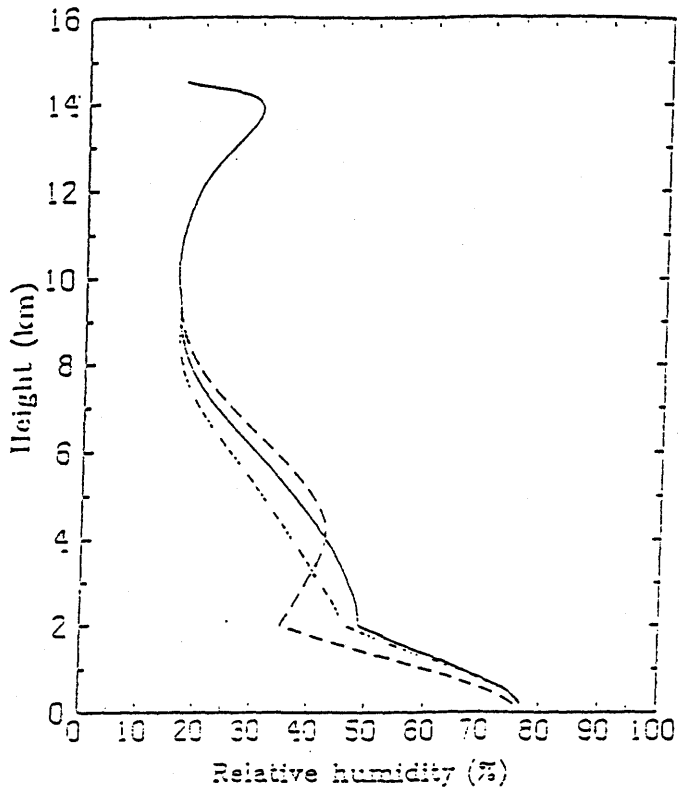

Figure 6-8: Sensitivity of the mean relative humidity distribution to the relative humidity within the precipitation downdraft. Relative humidity is with respect to liquid water. The three curves shown correspond, each with the same notation, to the three precipitation downdraft relative humidity profiles of Figure 6-6 Other parameters are: $\frac{\tau}{\sigma} = 7days$, $z_{t+} = 14.5\,\mathrm{km}$,$z_t = 9.7\,\mathrm{km}$,$z_b = 2\,\mathrm{km}$ and $K = 3.4m^2/s$.

Since the profile of q_m is sensitive to the properties of the hydrometeors, so will the vertical distribution of water vapor of the large scale flow (equation 6.12). Its dependence on the size spectrum of the hydrometeors is shown in Figure 6-8. In the calculation, equations 6.10 and 6.11 are replaced by equation 6.16 and equation 6.14 respectively and q_m is given from the simple model for precipitation downdrafts. We see that precipitation downdrafts with smaller hydrometeors tend to moisten the upper troposphere more.

6.5.4 Dissipation of deep convective towers

Deep convective towers at the dissipating stage consist in downdrafts. Conceptually, we may parameterize their contribution to ambient humidity in the same way we parameterized the moistening from precipitation. If we view the upper level clouds and

the associated hydrometeors as an extension of deep convective towers, we may have a unified description of how deep convection moistens the large scale flow in which it is embedded. Deep convection uses the moisture from the convective boundary layer to generate small scale, spatially isolated moist regions. Water vapor in these isolated regions is then transported to the surrounding flow by diffusive and convective processes. The subsiding motion in the surrounding flow, induced by deep convection itself, constantly advects the water vapor downward to where it comes from; namely, the convective boundary layer.

6.6 Simulation of the horizontal variation of relative humidity in the Hadley domain

In this section, we introduce a two-dimensional model based on the one-dimensional model presented above in order to simulate the horizontal variation of water vapor in the Hadley domain. We will show the decrease of relative humidity from the ITCZ to the subtropics throughout the free troposphere is due to the sharp decrease in the amount of hydrometeors deposited in the upper troposphere by deep convection and the relatively flat distribution of subsidence in between clouds.

The water vapor budget equation is given by equation 4.12 . In the following discussion, we omit the zonal and time mean symbols (i.e. overbar and brackets) for brevity. The horizontal transport term can be ignored compared with the term for the vertical transport. After introducing a new variable, $M_c^* = M_c - \rho w$, equation 4.12 simplifies to

$$0 = M_c^* \frac{\partial q}{\partial z} + \rho E \tag{6.20}$$

The latitudinal variation of M_c^* may be estimated from the energy equation

$$M_c^* \frac{\partial S}{\partial z} - R_c = 0. \tag{6.21}$$

where S is the dry static energy and R_c is the net radiative cooling including both the

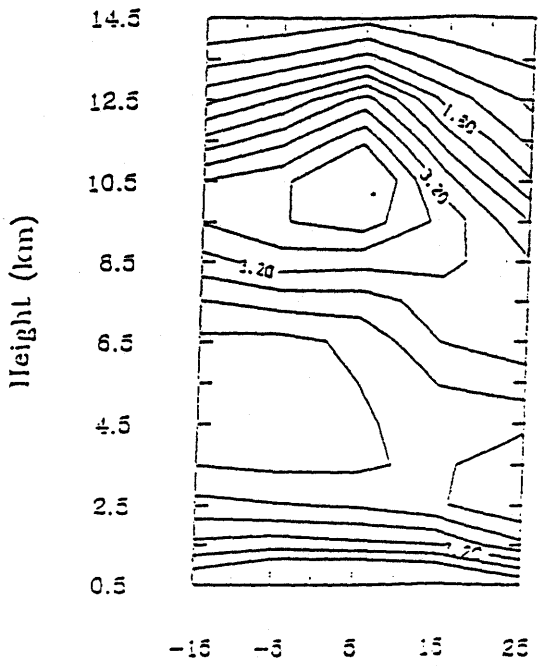

Figure 6-9: The meridional distribution of M_c^* within the domain of the Hadley circulation (see text for further detail; unit is $10^{-3}\ kg/(m^2 s)$)

solar heating and infrared cooling. The same approximations are made in deriving equation 6.21 as in deriving equation 6.21 (i.e., large-scale eddy transport and the horizontal advection by the mean circulation are ignored; refer to chapter 4 for a detailed derivation) This equation is only valid away from the boundary layer (where sensible heating by boundary layer turbulence is considerable).

The meridional structure of M_c^* in January deduced from the above equation is plotted in Figure 6-9. R_c is from Dopplick (1972) and S is from Oort (1983)(In Dopplick's calculation, clouds were also taken into account). Figure 6-9 shows that the latitude dependence of M_c^* is relatively weak. Again, we divide the atmosphere vertically into three regions: the outflow region, the free troposphere and the convective boundary layer. In the free troposphere, $E = \alpha(y)(q^* - q)$; where y represents latitude. In the outflow region, $E = \alpha_c(y)(q^* - q)$; α_c is assumed to be proportional to α. In the convective boundary layer, $E = \frac{\partial}{dz}(K\rho\frac{\partial q}{dz})$; K is the bulk diffusion coefficient for the turbulent boundary layer. Now α and α_c are functions of latitude, and their meridional variation may be assumed proportional to the upper level cloud cover (Recall equation 6.14 and 6.16). The meridional variation of upper

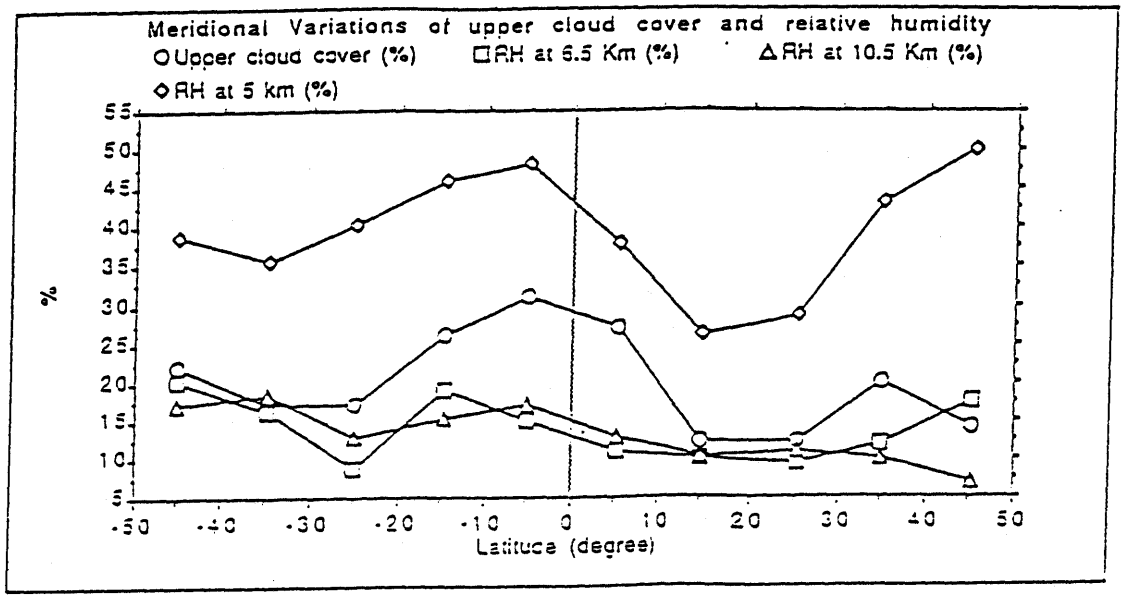

Figure 6-10: The meridional variation of upper cloud cover and the variation of the tropical tropospheric relative humidity. Upper cloud cover is from Barton, 1983. Relative humidity at 6.5 km and 10.5 km is calculated from SAGE II measurements (Rind et al 1991). Relative humidity at 5 km is from Oort (1983)

cloud amount is well correlated with the variation of the middle and upper tropospheric relative humidity (see Figure 6-9). The upper level clouds are almost always associated with the outflow of storms (Liou 1986). The decrease of the upper cloud amount is, therefore, less likely a result of a decrease of the relative humidity of the environment and is more likely a cause. Figure 6-11 shows the simulated horizontal variation of relative humidity in the Hadley domain. The similarity with the observed distribution is apparent. This shows that the difference in the water vapor content between the convergence zone and the large scale subsidence region may be just due to the distribution of hydrometeors.

The meridional distribution of hydrometeors from the ITCZ to the subtropics is largely controlled by the Hadley circulation. Deep convection tends to occur where the sea surface temperature is highest. Accompanying the deep convection are large scale circulations driven by the sea-surface temperature gradient. The subsiding motion of the large-scale circulation suppresses convective motion elsewhere, i.e. the

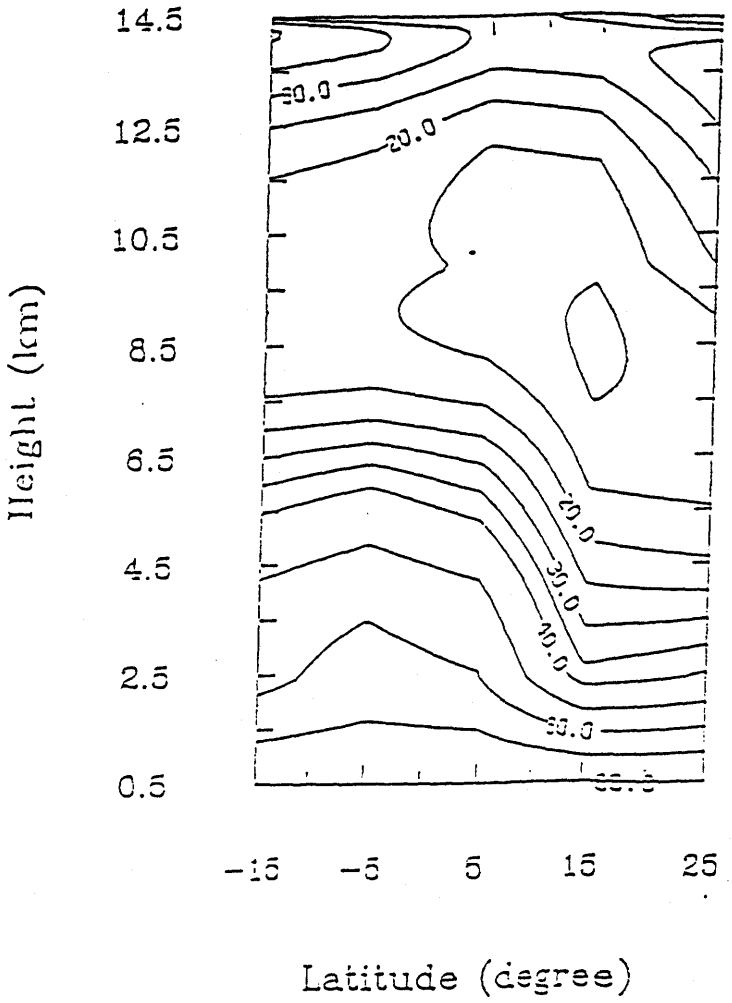

Figure 6-11: A simulation of the horizontal variation of the tropical tropospheric relative humidity ((with respect to liquid water) α and α_c are both assumed to be proportional to the upper level cloud cover with $\alpha/\alpha_c = 2$. $z_t^* = 14.5\,\mathrm{km}$, $z_t = 9.7\,\mathrm{km}$, $z_b = 2.0\,\mathrm{km}$ and $\frac{K\rho_0}{M_c} = 2.0\,\mathrm{km}$ in the convective boundary layer. The surface relative humidity is specified as 80 percent and the specific humidity at 14.5 km is fixed as 4.3×10^{-3} g/kg. Within the convective boundary layer, M_c^* is assumed to remain constant with height

subtropics. This is the reason for the decrease of the moisture source above the convective boundary layer as one moves from the ITCZ to the subtropics.

Clearly, the difference of water vapor content between the ITCZ and the subtropics is related to the existence and direction of the large-scale circulation. In a thermodynamic sense, the water vapor content of the air above the trade inversion over the subtropics is not directly related to the sea surface temperature immediately below; the air is subsiding and isolated from the boundary layer by a strong trade inversion. The inference by Rind et al (1991) ignores the interplay between the deep convection and the tropical zonal mean circulation and also ignores the vertical structure of the tropical convection.

Since places distant from each other are connected by dynamic transports, geographical variations can not be a surrogate for climate change. In studying global climate changes, the paleo-climate record bears special importance because it allow us to examine different climate regimes. In Chapter 7, we will introduce the mountain-snow line record for the last glaciation and investigate its implication about the nature of feedback of water vapor and lapse rate in global climate change.

6.7 Summary and discussion

In this chapter, by using a conceptual model for tropical convection and available data for water vapor, we investigated the maintenance of the tropical tropospheric water vapor distribution. Calculations were performed to see if the observed water vapor distribution could be explained in this simple context, and also to highlight some potentially important physical processes in determining the observed distribution and its sensitivity.

The important processes determining the humidity of the tropical troposphere, as highlighted by the present study, are the amount of hydrometeors transported to the upper troposphere by deep convective towers, the hydrometeor size spectrum, and the strength of the large scale subsidence induced by deep convection.

The amount of hydrometeors in the upper troposphere is related to the strength

of the updrafts of deep convective towers (Williams et al 1992). The strength of the updrafts is a function of the convective available energy of the environment. Thus, the water vapor content in the free troposphere is related to the entire vertical structure of the tropical tropospheric temperature. This finding challenges the traditional viewer that water vapor content is only dependent on the local temperature in the way described by the Clasius-Clapeyron equation. The stronger the updrafts in the convective tower, the larger the hydrometeor amount that will be present in the upper troposphere. The reason is that if the updraft is weak, more hydrometeors begin to fall before they are lofted to high altitude. There are no obvious reasons for deep convection to become more violent in a perturbed climate when CO_2 is increased, though that has been widely assumed (Houghton et al 1990). The deepening of the lapse rate in the last glaciation suggests that a colder tropical climate can have a much larger lapse rate and consequently more CAPE (Broecker and Denton 1989). A larger CAPE may have led the presence of more hydrometeors in the upper troposphere and consequently a moister free troposphere. As we will see in the following chapter, the maintenance of a deeper lapse rate also requires a higher relative humidity in the free troposphere. Over land, a more relevant parameter determining the updraft velocity of deep convection is the magnitude of the diurnal change of surface temperature. In a warmer climate, the surface evaporation (and also infrared radiation) is more efficient in cooling the surface, and the diurnal variation may become smaller, which will consequently reduce the build up of environmental CAPE. A detailed study of the diurnal cycle of the convective boundary layer is needed to appropriately address this issue.

The life cycle of deep convective updrafts is also expected to be an important factor in determining the amount of hydrometeors present in the upper troposphere. If the updraft can persist longer, there will be more water substance transported to the upper troposphere. It is generally observed that the onset of precipitation signals the decay of the updraft. In a warmer climate, the surface air will likely contain more water vapor and the warm rain process will be more efficient. Consequently the onset of rain may become faster (Fletcher 1962). An estimate based on the simplest

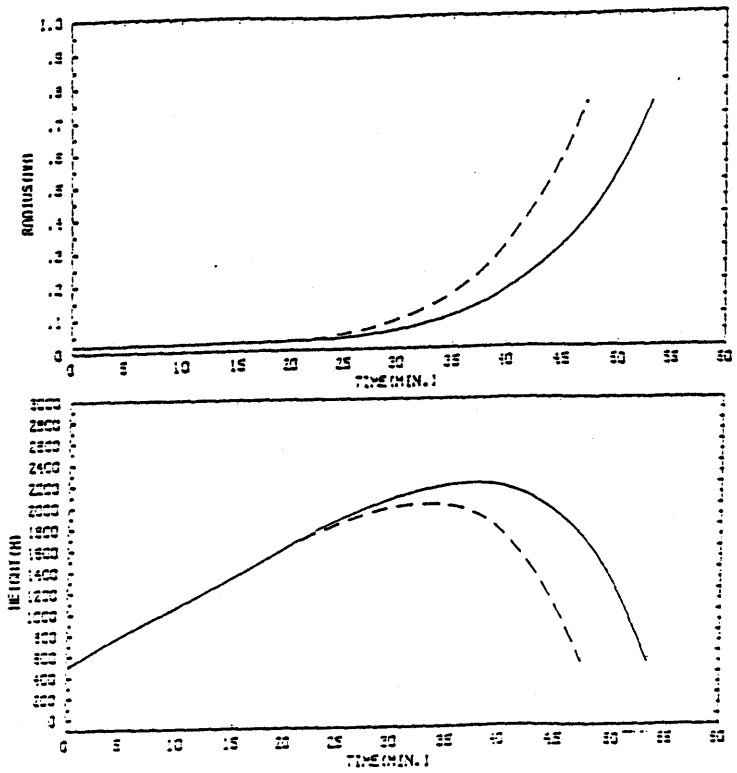

Figure 6-12: Sensitivity of the growth of a rain drop in a constant updraft to the change of surface air temperature. Upper panel: Growth of the rain drop as a function of time. Lower panel: Trajectory of the rain drop. Solid line: surface air temperature is 300 K. Dashed line: surface temperature is 302 K. Surface relative humidity is 80% and is assumed constant. Cloud water content is assumed to be constant with height. For the surface temperature of 300 K, the cloud water content is chosen as 1 g/m^3. When surface temperature changes, the relative change of cloud water content is assumed to be the same as the relative change of the surface specific humidity. The size spectrum of cloud water is assumed to be uniform and not subject to change when surface temperature changes. The radius is chosen as 0.01 mm.

continuous growth model, the Bowen model (see Bowen 1950 and Fletcher 1962) was made (Figure 6-12), which shows that the onset of rain can be 15 percent faster when surface temperature is increased by 2 K and when the relative humidity of surface air is fixed at 80%.

The size spectrum of hydrometeors is also related to the strength of the convective updrafts. Heymsfield's observational study suggests that it may also be dependent on the environmental temperature. The higher the environmental temperature, the more the shift to larger radius for the size spectrum (Heymsfield 1984). From our calculations (Figure 6-6 and 6-8), we see the possibility that the upper troposphere of a warmer climate may have a smaller relative humidity provided that the total

amount of hydrometeors does not increase proportionally.

This Chapter reveals a special role of upper level clouds and the precipitation they produce in the tropical tropospheric moisture budget. These clouds help to dry out the outflow from the deep convective towers and moisten the air below. However, we do not adequately understand how these clouds develop, grow and finally dissipate in the outflow of convective towers; nor do we completely understand the survival of upper level precipitation in a subsaturated environment (Braham and Duran 1967). The evaporative cooling and the drag of precipitation generate currents which can penetrate deep into the large-scale flow and form small-scale, isolated regions of higher moisture content. How water vapor flows from these small isolated regions to the surrounding flow and how these small regions dissipate and finally merge into the surrounding flow are issues which have not been given much attention. Proper models need to be developed for these small-scale currents to simulate their interaction with the environment during their full life cycle. Unfortunately, we still lack appropriate models for the upward jet driven by the release of the latent heat and the downward current driven by the loading of precipitation and its evaporative cooling.

Finally, we emphasize that the water vapor distribution is coupled with the distribution of clouds and the precipitation they generate. It appears that upper level precipitating clouds play an important role in determining the tropospheric relative humidity throughout the free troposphere. The precipitating clouds are optically thick and their effect on albedo may offset their greenhouse effect (Ramanathan and Collins 1991). Further climate studies will have to address water vapor and clouds in a more internally consistent way. Here, we have provided a simple approach to connecting them.

Chapter 7

Nature of water vapor and lapse rate feedback in climate change

The use of paleoclimate data offers a unique advantage in the investigation of the nature of feedback from the water vapor distribution or temperature distribution on global climate change. Paleo-climate data allow us to look at the variations of the fundamental physical quantities between different climate regimes, while instrument records only cover periods which differed little from the present. As we have seen in the previous Chapters, geographical variations are hardly useful in addressing the issue of water vapor feedback because of the inherent difficulties in isolating the role of dynamical transport from one place to another. In this chapter, we will show how we may extract information about the nature of the feedback of water vapor and lapse rate on the global climate change from the inferred changes in the mountain-snow line from the last glaciation to the present.

We begin with a discussion of the mountain-snow line record and its implications for a change in the lower tropical tropospheric lapse rate. We then show how the lapse rate change indicated by the mountain-snow line record requires a change of cooling rate and, consequently, of the relative humidity in the free troposphere.

7.1 Introduction

Notable among paleoclimate records is the CLIMAP reconstruction of the Earth's climate 18,000 years ago (ybp) (CLIMAP, 1976) during the last major glaciation. A remarkable finding of this extensive study is that the average tropical sea surface temperature was only about 1°C colder than at present. Equally remarkable is the finding that the snow line on high mountains descended about 1 km – even on equatorial peaks (Broecker and Denton, 1989, Rind and Peteet, 1985). This represents a cooling of about 5°C at about 5 km (Rind 1990, Rind and Peteet 1985), and hence a 20% increase in averaged lapse rate below this level.

The 1 km descent of the mountain snowline was found over widely dispersed geographic regions and the lowering on the wet side of the mountains was about the same as on the adjacent dry side (Broecker and Denton 1989). This suggests that the descent of the mountain snowline is unlikely to have been caused by changes in local circulations. More importantly, the temperature decrease observed on mountains is likely to be characteristic of the tropics. This is because the Rossby radius of deformation is extremely large in the equatorial tropics. The dynamics appropriate to the equatorial tropics simply does not permit large gradients to develop (especially over the large averaging periods pertinent to the paleoclimatic record), so temperatures above the trade wind boundary layer are virtually horizontally uniform.

Such a change in lapse rate is not a feature of recent instrument records, and might call into question the paleoclimatic record. All that can be said is that the CLIMAP program involved a large part of the paleoclimatic community, and the data were as carefully and critically assessed as is currently possible. Uncertainties of the order of 1°C are possible, but it is generally agreed that the quality of the data is high. Our approach in this paper is to take the data at face value, and see what they imply.

The above behavior of the lapse rate during the last glaciation is incompatible with simple notions of convective adjustments which maintain either fixed lapse rates or moist adiabats. A moist adiabatic profile permits lapse rate change, but the change is too small to account for the inferred lapse rate in the last glaciation. For a surface

relative humidity of 80 percent (a representative number for the tropics which is not sensitive to small temperature differences. We discuss possible changes later), a moist adiabatic profile gives about a 1.5 degree reduction of temperature at 5 km for a 1 K surface temperature decrease (say from 300 K to 299 K). It should be emphasized that both the notions of constant lapse rate and moist-adiabatic adjustment are empirical. Though the temperature profile within clouds is close to moist adiabatic and probably remains so when climate changes, there is no *a priori* reason to believe this is the temperature profile of the mean field in which only a small percentage area is covered by clouds. The departure of the present tropospheric temperature profile from moist-adiabatic may be regarded as small, but the departure may change considerably when the climate regime changes.

As we showed in Chapter 5, the vertical structure of the tropical atmosphere is determined primarily by a balance between subsidence heating, $M_c \frac{\partial s}{\partial z}$ (where s=dry static energy, and M_c=cumulus mass flux), and radiative cooling. Since M_c, averaged over the tropics, is determined approximately by integrated evaporation divided by surface specific humidity (Equation 5.8), a quantity not expected to change significantly in a slightly cooler tropics, changes in $\frac{\partial s}{\partial z}$ must be balanced by reduced radiative cooling. Intuitively, this would appear to call for increased infrared opacity in the middle and upper troposphere.

In order to address this possibility, we try, in Section 2, to simulate the vertical temperature structure during the last glaciation making different assumptions about the relative humidity profile in the middle and upper troposphere. It is shown that only a higher relative humidity than at present in the middle and upper troposphere gives a greater lapse rate in the lower troposphere than would a moist-adiabatic profile. The higher the relative humidity, the greater the lapse rate. Consistent with our original hypothesis, it will be shown that the change in the distribution of radiative cooling rate accompanying a higher middle and upper tropospheric relative humidity is indeed characterized by a reduction in the low troposphere. In addition, there is enhanced cooling in the upper troposphere. We show that temperature profiles with the inferred lapse rates do, in fact, have substantially greater CAPE than the present

tropical atmosphere.

In Sections 3–5, we carefully examine the assumptions involved. Section 6 discusses alternative efforts to explain the mountain snowline record. In Section 7, we examine the implications of the inferred dependence of water vapor on surface temperature for climate sensitivity to the increase of CO_2. We find that the water vapor feedback is now strongly negative, virtually eliminating the warming due to a doubling of CO_2, at least in the tropics. By comparing sensitivity studies from the present model with those from a model with a constant tropospheric lapse rate, we show the feedback from the lapse rate change is also considerable. Section 8 discusses the apparent contradiction between the present result and earlier published results which have claimed to demonstrate a positive water vapor feedback.

7.2 Numerical experiments

The model presented in Chapter 5 shows how the vertical structure of tropospheric temperature is calculably related to the distribution of radiative cooling rate. This allows us to infer, from the inferred temperature change, the tropical water vapor distribution during the last glaciation.

In many previous climate sensitivity studies, relative humidity throughout the troposphere is assumed to be independent of climate change. As pointed out by Lindzen (1991) and Betts (1991), little is concretely known about the maintenance of the moisture budget in the free troposphere (i.e., the troposphere above the boundary layer) and its sensitivity to radiative perturbation. In attempting to simulate the tropospheric temperature profile during the last glaciation, we adjust the relative humidity in the free troposphere in order to obtain a vertical temperature structure which resembles that one indicated by the mountain snowline record. Since observations show that the relative humidity within the convective boundary layer (up to about 700 mb) is relatively insensitive to surface temperature change, we fix the relative humidity below 700 mb in the following calculations. It should be emphasized that the moisture budget within the convective boundary layer is largely determined

by small scale turbulent processes driven by surface fluxes. Thus, the dependence on sea surface temperature of the relative humidity in the convective boundary layer may be inferred by comparing values observed in different places. On the other hand, the dependence of the relative humidity in the free troposphere cannot be related to the local sea surface temperature. Over much of the tropical oceans, the influence of local sea surface temperature is restricted to the region below the trade inversion; away from active cumulus towers (which occupy only about 0.1% of the tropical area), air above the trade inversion is subsiding, and the temperature and moisture fields are largely determined by the temperature and moisture fields over the regions where deep convection frequently occurs. We will return to this point later when we discuss claims of a positive feedback due to water vapor.

As already noted, we use 'solar flux' as a surrogate for the effects of cloud albedo and heat export from the tropics. We adjust this flux to produce equilibrium profiles with both the present surface temperature and a surface temperature 1 K colder than at present. Different relative humidity profiles in the middle and upper troposphere are assumed to accompany the colder climate. Figure 7-1 shows three cases of the temperature departure from the present climate as a function of height. The long-dashed line corresponds to the case in which the relative humidity is assumed to be the same as the present. The short-dashed line represents that in which the relative humidity between 300 mb and 700 mb is only 80% of the present value. The solid line is for a case in which the relative humidity between 300 mb and 700 mb is 20% larger than that of the present profile (i.e. present relative humidity plus 20%)[1].

From Figure 7-1, we see that when the relative humidity is assumed not to have changed when the surface temperature is decreased by 1 K, the temperature reduction in the middle troposphere is less than 2 K — the lapse rate behavior above the convective boundary layer is basically the same as that obtained by assuming a moist-adiabat. When a smaller relative humidity in the free troposphere is assumed to accompany the colder climate, the reduction of temperature in the middle tropo-

[1] 160 mb, the cloud detrainment level can be used instead of 300 mb. There is no substantial difference in the results. On physical grounds, we expect little change of relative humidity at the detrainment level. See Section 4 for further discussion.

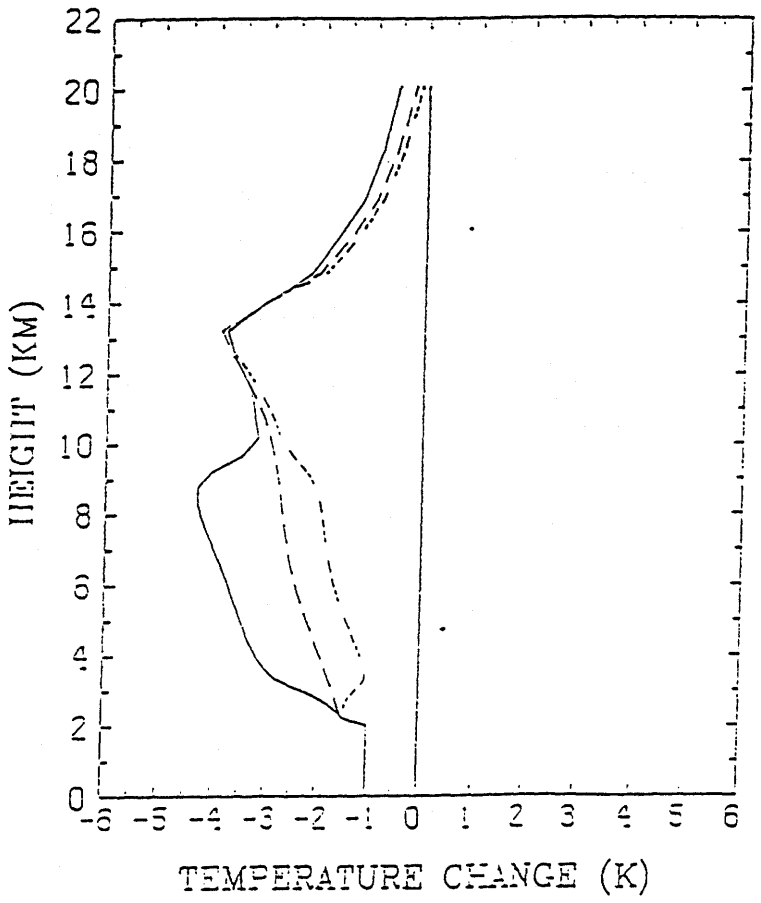

Figure 7-1: Temperature change as a function of height for a surface temperature decrease of 1 K. Different assumptions about the change of the relative humidity (RH) between 700 mb and 300 mb are made. Solid line: RH is increased by 0.2. Long dashed line: RH is the same as the present. Short dashed line: RH is 80% of the present value.

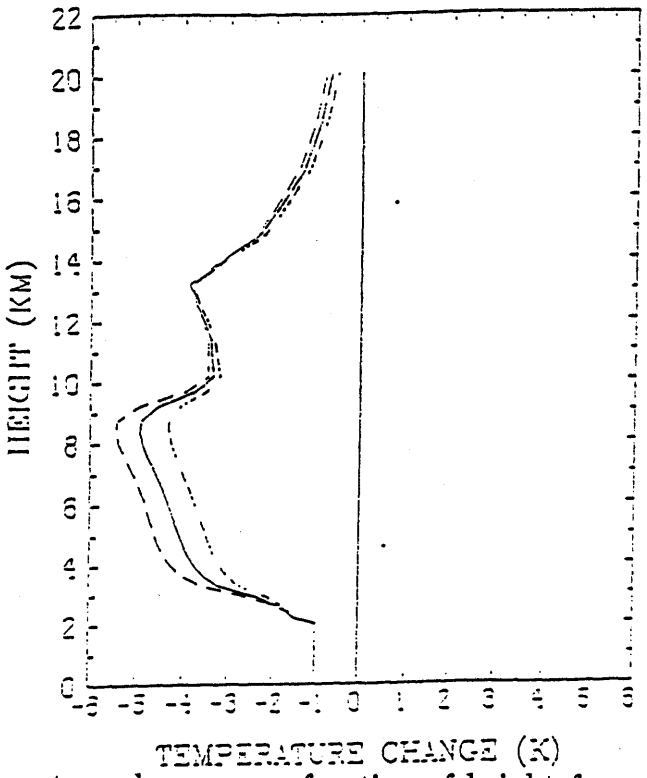

Figure 7-2: Temperature change as a function of height for a surface temperature decrease of 1 K. Relative humidity between 300 mb and 700 mb is assumed to increase by a specified value when the surface temperature is decreased. Relative humidity increases are: 0.2 (short-dashed line), 0.3 (solid-dashed line), 0.4 (long-dashed line)

sphere is also no larger than the surface temperature decrease. When the relative humidity in the free troposphere is assumed to be 20% higher than at present, the reduction in the middle troposphere is about 3.5 K, which is about the 70% of the reduction indicated by the mountain snowline record.

From the three cases, it is apparent that only an increase of relative humidity in the free troposphere can lead to a greater reduction of temperature in the middle troposphere than that which a moist-adiabatic profile produces. It is further found that the steepening of the lapse rate in the free troposphere is proportional to the increase of relative humidity in the free troposphere, though not linearly so. Figure 7-2 shows the departure of temperature from that of the present as a function of height when still higher relative humidity is assumed to accompany the colder climate. A 5 K temperature reduction at the mid-troposphere requires an increase of relative humidity of about 40%. What a physically plausible increase should be, will be discussed shortly.

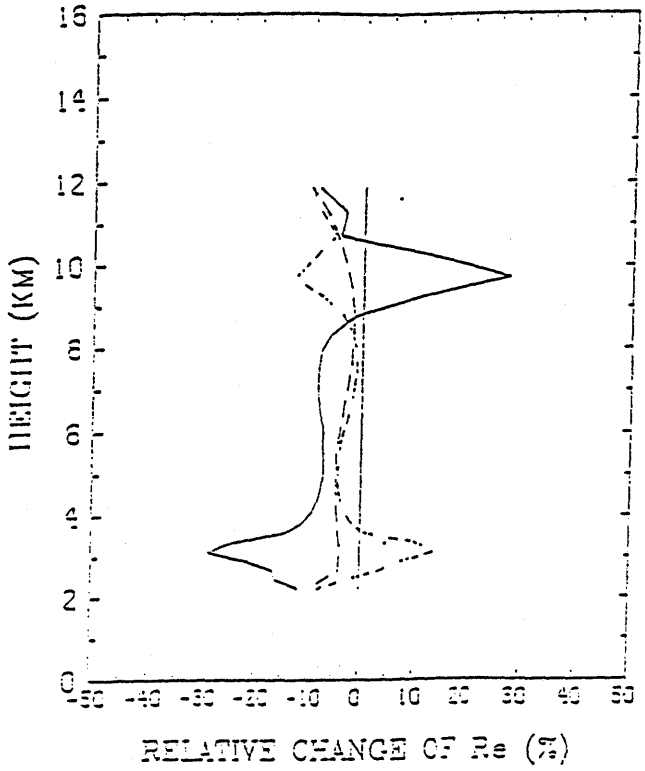

Figure 7-3: Relative change of tropospheric radiative cooling as a function of height for a surface temperature decrease of 1 K. Different assumptions about the change of the relative humidity (RH) between 700 mb and 300 mb are made. Solid line: RH is increased by 0.2. Long dashed line: RH is the same as the present. Short dashed line: RH is 80% of the present value.

Physically, the changing lapse rates are associated with changes in radiative cooling below about 6 km (viz Equation 1). Increasing humidity decreases local cooling rates by increasing the infrared opacity above, and decreased cooling rates are associated with decreasing ds/dz or, equivalently, increasing lapse rate. Figures 7-3 and Figure 7-4 show the change in the distribution of radiative cooling rate for various choices of humidity distribution. M_c and the tropopause height, determined by the neutral buoyancy level, are both found for all cases to be almost the same in both the present climate and the colder climate (assumptions involved in the calculations will be considered in greater detail later). When there is more water vapor in the middle and upper troposphere, the radiative cooling rate change is characterized by an increase in the upper troposphere (due to enhanced emissivity) and a reduction in the lower troposphere (due to increased opacity above). The temperature reduction maximizes in the middle troposphere.

Increased upper level cloud coverage can also contribute to the change in the dis-

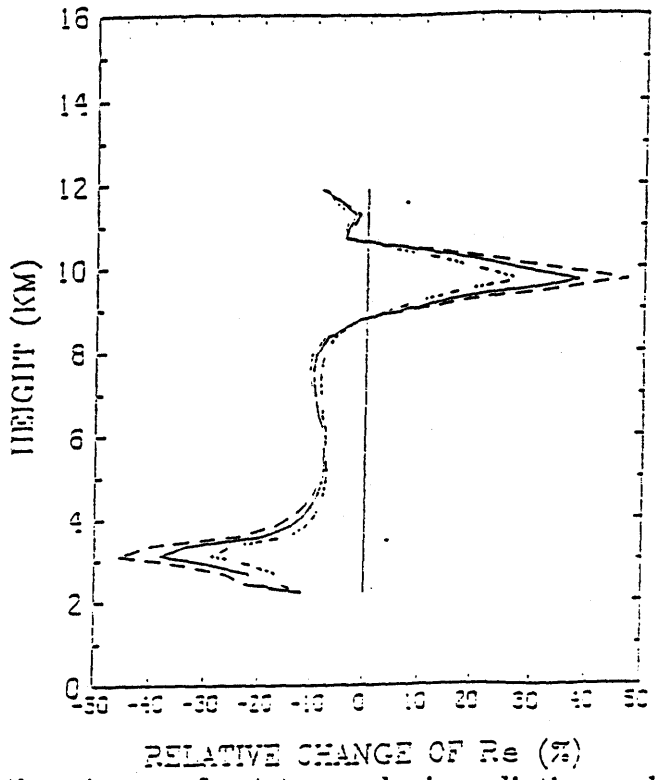

Figure 7-4: Relative change of net tropospheric radiative cooling as a function of height for a surface temperature decrease of 1 K. Relative humidity (RH) between 300 mb and 700 mb is assumed to increase by a specified value. The increases for RH are: 0.2 (short-dashed line), 0.3 (solid line) and 0.4 (long-dashed line)

tribution of radiative cooling rate. Indeed, considerable increase in the high cloud amount, either in the form of increased thickness or wider horizontal coverage, is expected to accompany an increase of relative humidity in the free troposphere. We will show later that the free troposphere is largely moistened by evaporation of hydrometeors falling from upper level clouds. In this sense, the increase of relative humidity may be somewhat smaller than 40%. However, due to the uncertainties in the radiative properties of clouds, it is premature to quantify the effects with confidence. All that can be said at this point is that upper level cloud amount is not expected to increase without an increase of relative humidity in the free troposphere.

Another reason that the actual increase of relative humidity may be less than 0.4 is that a more moist atmosphere would facilitate the descent of the snowline (Rind, 1989). Though the controlling factor for its position is the temperature, relative humidity may also matter. Thus, should the relative humidity in the middle and upper troposphere be considerably higher than at present, the temperature reduction

Table 7.1: Conditional available potential energy (CAPE) associated with various assumed distribution of relative humidity

T_s(K)	$\triangle R$	CAPE(joules) $rh_s = 0.8$	CAPE(joules) $rh_s = 1.0$
300	0	670.5	2200.3
299	+0.2	1047.2	2610.9
299	+0.3	1156.8	2749.7
299	+0.4	1255.9	2841.0

corresponding to a 1 km descent may be less than 5 K.

The lapse rate change leads to an interesting feature of the colder states: namely, the air participating in deep convection will experience enhanced buoyancy. In other words, the environmental profile has more convective available potential energy (CAPE). CAPE is essentially the work done by buoyancy on a parcel of surface air rising in a cloud. This is proportional to the integral over the cloud of the difference between the equivalent potential temperature of cloud and ambient air. Our calculations of equivalent potential temperature follow Bolton (1980). Table 7.1 summarizes the CAPE of the different profiles discussed above. The steeper the lapse rate, the larger the CAPE. The increase of CAPE during the last glaciation is 40% to 100%, and suggests why the relative humidity in a colder climate might have been higher than at present.

Deep convection, associated with larger CAPE, is observed to generate a larger number of hydrometeors in the middle troposphere and upper troposphere (Williams, et al, 1992). Sage II measurements also show that cirrus occurs much more frequently over the tropical land than over the tropical ocean (Chiou, et al, 1990). It is known that deep convection over the land is associated with more CAPE than over the ocean. That the number of hydrometeors present in the middle and upper troposphere increases with increasing CAPE is also expected on the basis of results from comprehensive numerical cloud models (M.K. Yau, personal communication). While the quantitative relationship between the number of the hydrometeors and the en-

vironmental CAPE has not yet been firmly established, the sign is not in serious doubt.

Besides the change in the amount of hydrometeors, the spectrum of hydrometeors is also expected to change. When the environment has more CAPE, convective updrafts will be stronger. The hydrometeors carried into the middle and upper troposphere will have smaller sizes because they will have less time to grow before they reach the middle and upper troposphere. From the calculations shown in Chapter 6, this will also lead to a moister upper troposphere.

This finding about the water vapor behavior is different from the popular view (Houghton et al 1991). As we will show later, this finding implies a strong negative feedback of water vapor on climate change. Considering the importance of the topic, we now more carefully examine the assumptions involved

7.3 Dependence of the averaged convective mass flux on the low level relative humidity

Based on the assumption that the low level relative humidity is mostly controlled by boundary layer small-scale processes, we fixed the surface and low level relative humidity in the above experiments. The relative humidity below the trade inversion is determined by a balance between the subsidence drying and surface evaporation. The subsidence drying is related to the magnitude of the large-scale subsidence and the mixing ratio of water vapor in the free troposphere, both of which are related to the properties of deep convection. Thus the low level relative humidity is also dependent on deep convection and the associated large-scale circulation. However, this dependence appears to be weak. Figure 7-5 and Figure 7-6 show the sensitivities of the surface relative humidity to the water vapor mixing ratio and to the magnitude of the subsidence above the inversion. The relative humidity is insensitive to the change of these two parameters. This is because of the dependence of the surface evaporation rate on the surface level relative humidity. An enhanced subsidence drying will lead to more evaporation, and a decreased subsidence drying will lead

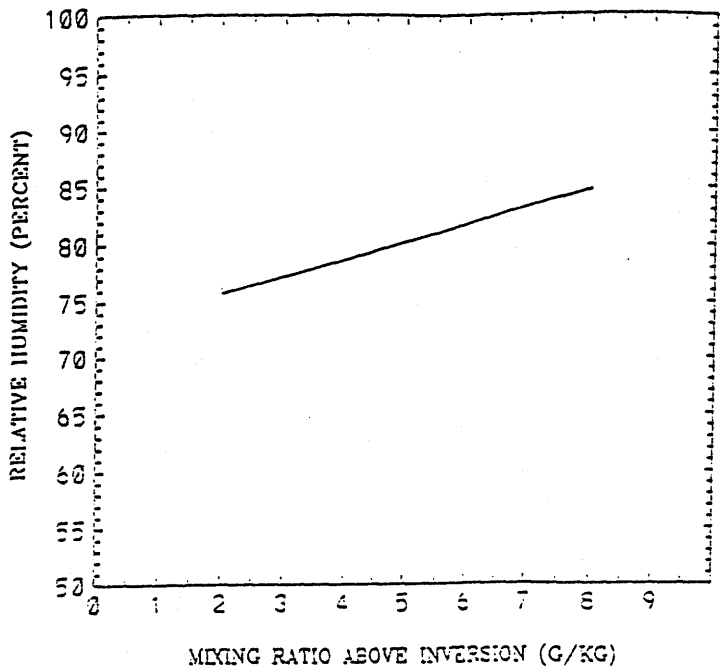

Figure 7-5: Dependence of the surface relative humidity on the water vapor mixing ratio above the inversion. The water vapor budget for the region below the inversion is given by $C_d V_s(q_s - q_0) = w_0(q_0 - q_t)$. C_d is the aerodynamic coefficient, V_s is the surface level wind, q_s is the saturation mixing ratio of water vapor at the sea surface temperature, q_0 is the surface level water vapor mixing ratio, q_t is the water vapor mixing ratio above the inversion, and w_0 is the subsidence. In the calculation, sea surface temperature is 300 K, air's temperature at the surface level is 299 K, $C_d = 0.0013$, $V_s = 6.7$ m/s and ρw_0=40 mb/day (Betts and Ridgeway, 1989)

to less evaporation. More sophisticated modelings in which radiative and convective flux are coupled with each other have shown that the relative humidity in the tropical convective boundary layer remains approximately the same when the sea surface temperature is changed by several degrees (Betts and Ridgeway 1989).

Nevertheless, we investigated the matter of whether or not a decreased surface and low level relative humidity during the last glaciation will affect our conclusion derived from the above numerical experiments. As discussed above, the physical reason for the requirement of a moister middle and upper troposphere to maintain the decreased vertical stability in the low troposphere is that a decreased vertical stability requires a decreased radiative cooling rate if the magnitude of the subsidence M_c remains unchanged. In the above numerical experiments in which the relative humidity below 700 mb is assumed invariant, M_c is insensitive to the surface temperature decrease. However, in light of equation 5.8, M_c may increase if the surface relative humidity

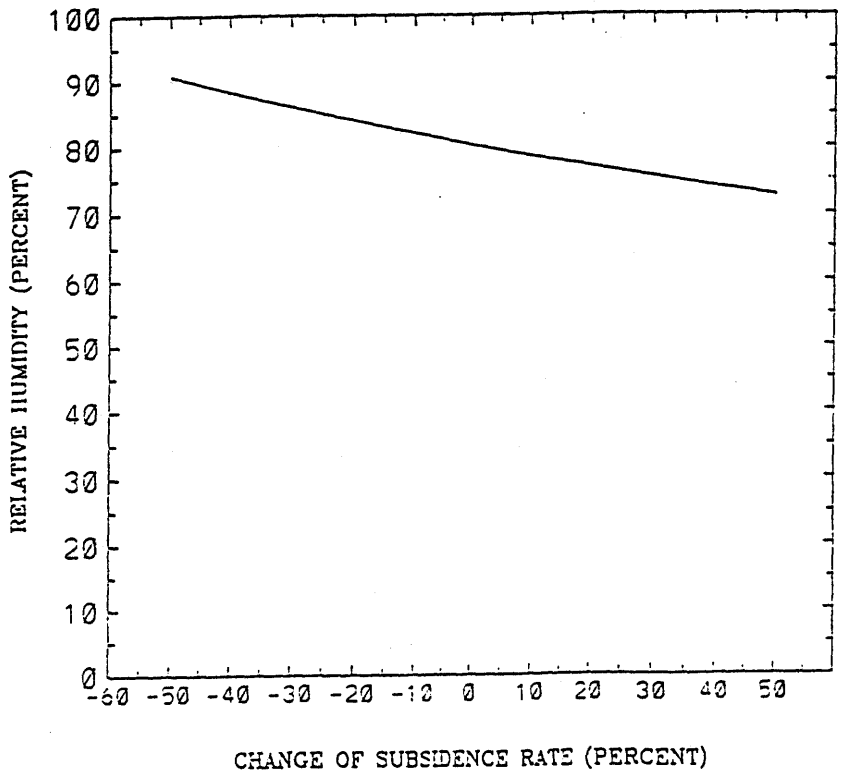

Figure 7-6: Dependence of the surface relative humidity on the the magnitude of the subsidence. The water vapor budget for the region below the trade inversion is given by $C_d V_s(q_s - q_0) = w_0(q_0 - q_t)$. C_d is the aerodynamic coefficient, V_s is the surface level wind, q_s is the saturation mixing ratio at the sea surface temperature, q_0 is water vapor mixing ratio at the surface level, q_t is the mixing ratio of water vapor above the inversion. w_0 is the subsidence. In the calculation, sea surface temperature is 300 K, surface air's temperature is 299 K, $C_d = 0.0013$, $V_s = 6.7$ m/s, $q_t = 5.0 g/Kg$ and the reference value for the subsidence is 40 mb/day (Betts and Ridgeway, 1989)

Table 7.2: Change of M_c in response to 10% decrease in the surface and low level relative humidity. The surface level relative humidity in determining the tropopause height is the same as the mean surface relative humidity. When sea surface temperature is decreased by 1 K, the relative humidity below 700 mb (RH_L) is assumed to decrease by 10% and various assumptions about the change of relative humidity between 300 mb and 700 mb (RH_{mu}) are made. $\triangle T_s$ is the decrease of sea surface temperature, $\triangle M_c$ is the relative change of M_c, and $\triangle T_{600mb}$ is the temperature change at the level of 600 mb

$\triangle T_s$(K)	RH_L(%)	RH_{mu}	$\triangle M_c$(%)	$\triangle T_{600mb}(K)$
-1	-10	same as present day	5.0	-3.4
-1	-10	present day value +20%	0.3	- 4.3
-1	-10	80%× present day	7.0	-2.9

decreases. A larger M_c will lead to an increase of the lapse rate even if the radiative cooling rate is not subject to change. Consequently, our conclusion derived from the numerical experiments presented in the above section may not hold. However, it turns out that the qualitative aspects of our conclusion about the water vapor behavior during the last glaciation remain unchanged even when a substantial decrease of surface and low level relative humidity is assumed to accompany the surface cooling.

Table 7.2 shows the results of the numerical experiments in which the surface and low level relative humidity during the last glaciation is assumed to be 10% lower than the present value (i.e., the present value –10%). Various assumptions about the relative humidity in the middle and upper troposphere are assumed to accompany the surface cooling. The results show that M_c indeed increases. The magnitude of the increase is dependent on the change of relative humidity in the middle and upper troposphere. This is because the surface moisture budget is coupled with the surface heat budget. Again, we see that only an increase of relative humidity in the middle and upper troposphere can lead to a cooling in the middle troposphere consistent with the mountain-snow line record.

Table 7.3: Change of M_c in response to 1 K surface temperature decrease and 0.5 K increase in the sea-air temperature difference. Various assumptions about the change of relative humidity are made. $\triangle T_s$ is the sea surface temperature, RH_{mu} is the relative humidity between 300 mb and 700 mb. Relative humidity below 700 mb is fixed. $\triangle M_c$ is the relative change of M_c

$\triangle T_s$(K)	RH_{mu}	$\triangle M_c$(%)
-1	same as the present day	0.7
-1	presen day value +20 %	-0.8
-1	80% × present day value	3.6

7.4 Dependence of the averaged convective mass flux on the sea-air temperature difference

The dependence of M_c on the sea-air temperature difference is summarized in Table 7.3. When the surface temperature is decreased by 1 K, we assume that the sea-air temperature difference increase from 1 K to 1.5 K. M_c is quite insensitive to the change in sea-air temperature difference. This is probably related to the large opacity in the low atmosphere (Manabe and Strickler 1964). Thus our inference about the water vapor behavior is not strongly dependent on the assumption made about the sea-air temperature difference.

7.5 Final caveats

In all numerical experiments presented above, the vertical structure of M_c is assumed not to subject to change, though its magnitude is determined through the surface moisture and heat budget. In the present climate, the lapse rate appears always to adjust itself to a value which is quite close to moist-adiabatic. M_c is largely determined by the large-scale radiative forcing (Emanuel 1991). Considerable changes in the vertical structure of M_c again suggest considerable changes in the radiative forcing field in which water vapor is a dominant contributor.

Perhaps the more severe caveat in our analyses is the fact that the present tro-

pospheric lapse rate is very close to moist-adiabatic, which indicates a very tight control of moist convection on the lapse rate (Betts 1982, Xu and Emanuel 1988). There is insufficient reason to believe that this tight control will change considerably in a different climate. This notion is also supported by the work of Renno (1992), who throughly and carefully analyzed the nature of radiative convective equilibrium of a moist atmosphere. Various parameterization schemes for moist convection were examined including the most promising scheme of Emanuel (1991). Though Renno did not use his sophisticated models to examine the mountain snow line record, his sensitivity studies of the response of the atmosphere to the increases of CO_2 do not support the idea that the equilibrium profile of a moist atmosphere can significantly deviate from a moist diabatic profile.

Next, we discuss Betts (1991) and Emanuel's (1990) alternative efforts to explain the mountain-snow line record, which are based on the safer assumption that the tropical tropospheric lase rate during the last glaciation was moist adiabatic.

7.6 Alternative efforts by Betts and Emanuel

Betts (1991) assumed that the tropospheric temperature profile can be represented by a moist-adiabatic profile. The freezing level is thus related to the low level equivalent potential temperature θ_e. He found that a snowline decrease of 950 m requires 14 K drop in θ_e. For a fixed relative humidity, this requires a 3.3 K decrease in SST, which is far beyond that which the uncertainties of paleoclimate data allow. Taking into account the mean sea level pressure change during the last glaciation and assuming 2 K decrease in SST, he was still unable to achieve the required drop of θ_e unless he assumed that there was also a considerable decrease in the surface relative humidity. The best scenario according to his estimate is that SST decreased by 1.4 K, surface pressure increased about 10 mb and surface relative humidity decreased by about 8%. However, he also pointed out that 8% decrease in the surface relative humidity requires a 30% drop in the surface wind, which is a " rather large fall of surface wind ". He concluded that it remains difficult to reconcile the observations that the snowline

on the tropical mountains fell 950 m, while the tropical sea surface temperature fell only 1-2 K.

Emanuel (1990) offered a more promising explanation for the mountain snowline record . By assuming that the virtual temperature lapse rate in the equatorial atmosphere is always nearly moist adiabatic, and that the sum of the latent and sensible heat flux from the tropical ocean was no greater during the last glacial period than it is today, he found

$$\delta T \approx 2.09\delta T_s - 0.73\delta p_s \tag{7.1}$$

where δT is the change of temperature at 5 Km, δT_s is the change in SST, and δp_s is the change in the sea level pressure. For $\delta T_s = -2$ K, $\delta p_s = 12$ mb, the formula gives $\delta T \approx 5$ K. Describing this analysis in a letter to Dr. Wally S. Broecker, Emanuel concluded that ' a 5 K drop in temperature near the freezing level in the equatorial zone is consistent with a $2°C$ drop in SST, but not a $1°C$ drop in SST '.

It appears that if one takes into account the maximum error in the data, one indeed can explain the snowline record based on the apparent safer assumption that the tropical tropospheric lapse rate remained close to the moist-adiabatic value during the last glaciation. However, it should be emphasized that the best estimate of SST change is 1 K. According to Fairbridge (1991), the tropical SST is not likely to have changed more than 1 K or so over a billion years, based on the premise that temperatures can be inferred from the distributions of forams in the sediment. The tropics are the region of maximum temperature, and changes of more than a degree or so in the maximum temperature would lead to extinctions of foram species. No such extinctions have been observed.

In the next section, we estimate the implications for the nature of water vapor feedback in tropical climate change of our inferences from the mountain snowline record.

7.7 Estimating the feedback factor of water vapor and lapse rate in doubling CO_2

We have, thus far, estimated the change in humidity in the tropical free troposphere accompanying a 1 K decrease in tropical sea surface temperature. Since our calculations are specific to the tropics, we cannot readily use these results to infer the sensitivity of global climate to a doubling of CO_2. However, our results do enable us to estimate the sensitivity of tropical surface temperature to a doubling of CO_2.

Noting that a 1 K cooling of the tropical sea surface lead to an increase in relative humidity of as much as 0.4, we will assume that tropically averaged surface temperature changes result in proportional changes in relative humidity. For reasons we have already discussed, a 40% change in tropical relative humidity for a 1 K change in average tropical surface temperature is probably an upper limit. Thus, in calculating the response of tropical surface temperature to a doubling of CO_2, we consider a range of values for the expected increase of relative humidity per 1 K decrease of surface temperature (ΔR_{-1}). The formula used is simply

$$\Delta R(300\,\mathrm{mb} - 700\,\mathrm{mb}) = -\Delta R_{-1} \times (T_s - 300\,\mathrm{K}). \tag{7.2}$$

Of course, a more appropriate approach would involve using something like Equation 4.6 to explicitly calculate relative humidity. This would, however, require fairly sophisticated cloud modeling. Although we are engaged in such efforts, they go beyond the scope of the present work. For the moment, Equation 7.2 can be viewed as a linearization. To be sure, if $(T_s - 300\,\mathrm{K})$ proves large, this linearization would break down. However, as we see in the results summarized in Table 7.4, $(T_s - 300\,\mathrm{K})$ remains small for a doubling of CO_2. We see that for fixed specific humidity, we would expect an increase in tropical surface temperature of 0.66 K. However, for a 40% increase in R per 1 K decrease of average surface temperature the response decreases to 0.09 K, and even for a 10% increase of R per 1 K decrease of surface temperature, the response is still only 0.23 K. These values may be contrasted with results from models

Table 7.4: Tropical surface temperature change ΔT, for a doubling of CO_2 and associated feedback factor, f, for different assumed changes in relative humidity (between 300 mb and 700 mb) for a 1 k decrease in sea-surface temperature (ΔR_1). Lapse rate permitted to vary.

ΔR_{-1} (%)	$\Delta T(K)$	f
Fixed q	0.66	0
10	0.23	-1.9
20	+0.15	-3.5
30	+0.12	-4.6
40	+0.09	-6.4

wherein a doubling of CO_2 produces a 4 K increase in global mean temperature. In these models, tropical temperatures increase by 2 K or more.

In Table 7.4 we also show feedback factors, f, defined by the relation

$$\text{response} = \frac{\text{response for fixed specific humidity}}{1 - f}. \tag{7.3}$$

These feedback factors, while germane to the tropical half of the earth, may not be applicable to the whole globe. For example, during the last glaciation, global mean temperatures were several degrees lower than at present even though tropical temperatures were only 1 K lower. On the other hand, glacial climate changes were almost certainly not associated with changes in the global radiative forcing, but rather with changes in the meridional heat flux and regional inhomogeneities in radiative forcing. In such a case, the change in global mean temperature is likely to be a peripheral consequence of the increase in equator–to–pole temperature gradient, and the relevance of simple feedback factors is dubious. However, for sensitivity to a globally homogeneous forcing such as a doubling of CO_2, these factors could very well have a more general relevance, and the numbers in Table 7.4 may be indicative of global as well as tropical feedbacks.

It should be further noted that associated with a change in the relative humidity profile, there is a change in the lapse rate. As emphasized by Cess (1991, 1990), the

Table 7.5: Tropical surface temperature change $\triangle T$, for a doubling of CO_2 and associated feedback factor, f, for different assumed changes in relative humidity (between 300 mb and 700 mb) for a 1 k decrease in sea-surface temperature ($\triangle R_1$). Lapse rate permitted to vary.

$\triangle R_{-1}$ (%)	$\triangle T(K)$	f
Fixed q	1.11	0
10	0.74	-0.5
20	+0.44	-1.4
30	+0.32	-2.4
40	+0.24	-3.6

feedback from the lapse rate is potentially as important as the water vapor feedback, though the two always go together. To isolate the role of lapse rate change from the change of relative humidity in the free troposphere, we employ a radiative-convective model with constant lapse rate adjustment to investigate the role of water vapor feedback in double CO_2 experiments. The results are summarized in Table 7.5.

By comparing Tables 7.4 and Table 7.5 , we see that the feedback factor from the lapse rate change is as large as that from the change of water vapor, and that both have the same sign. However, it should be emphasized that the two are dynamically coupled, though their roles in affecting radiative transfer in the atmosphere are physically different. Indeed, Lindzen, et al (1982) found a similar effect, noting that it was related to the fact that the physical parameterization of cumulus heating lead to a higher deposition of heat than is implicit in simple convective adjustment.

Give that current observations and modeling studies suggest that a moist atmosphere is unlikely to have an equilibrium profile which is considerably different from a moist adiabatic profile, (Betts 1982, Xu and Emanuel 1988, Renno 1992)), the above results regarding the lapse rate should be taken cautiously. They probably correspond to the upper limit.

7.8 Summary and discussion

We have used a radiative convective model to investigate what changes of water vapor above the convective boundary layer can lead to a picture consistent with the vertical structure of the tropical tropospheric temperature indicated by the mountain snowline record; i.e., a steeper lapse rate in the low troposphere (or equivalently a reduction in static stability) requiring a concomitant reduction in radiative cooling rate. Under the assumption that the vertical structure of the averaged M_c and the low level relative humidity are not subject to change, we have found that only an increase of relative humidity in the middle and upper-troposphere during the last glacial period can explain this change in cooling rate. This conclusion remains unchanged when the low level relative humidity is assumed to decrease substantially when the surface temperature is decreased. We have also noted that the vertical temperature profile during the last glaciation had more CAPE, which would have led to the production of more and smaller hydrometeors in the middle and upper troposphere — both of which factors would lead to enhanced moisturization of the free troposphere, consistent with the humidity changes required to produce a steeper lapse rate in the low troposphere which, in turn, produced the enhanced CAPE.

We have also investigated the implication for the atmospheric response to a doubling of CO_2 of the increase of relative humidity in the free troposphere or a decrease in surface temperature . We found that for plausible values of relative humidity change inferred from the snowline record, the feedback of water vapor severely reduces the warming induced by the increase of CO_2. We have further noted that the large negative feedback factor is partially due to the lapse rate change associated with the change of water vapor distribution, and stressed that the lapse rate change is not consistent with the current observation and more sophisticated modeling, so the results should be taken cautiously.

The nature of water vapor feedback suggested by this study is contrary to that which GCMs have predicted. The major problems of GCMs in dealing with water vapor feedback lie in the parameterization schemes employed for calculating convective

transports. As we have discussed in Chapter 1, the schemes employed by GCM models were not originally designed to address the issue of water vapor and have not been significantly improved in this regard. In particular, they lack adequate treatments of microphysical processes in precipitation formation and dissipation, which we have shown in Chapter 6 are important elements in the tropical tropospheric water vapor budget (relevant discussions can also be found in Emanuel, 1991). In addition, there are numerical problems (Rasch and Williamson, 1990).

There are earlier observational studies which have claimed a positive dependence between sea surface temperature and relative humidity in the free troposphere (Rind et al, 1991, Raval and Ramanathan, 1990). These results were obtained by comparing observed values of relative humidity or other related physical quantities over different places in the present tropics. However, above the convective boundary layer, air is subsiding and the physical properties of air, including water vapor and temperature, are strongly correlated over large distances through dynamic transport. Thus location (or season) cannot be used as surrogates for global climate change.

Alternative efforts to explain the mountain snow line record were discussed. When SST is assumed to have decreased by 2 K instead of the best estimate 1 K, it is also possible to explain the mountain snowline record under the moist adiabatic assumption.

Chapter 8

On the extratropical zonal mean tropospheric temperature and wind

8.1 Introduction.

In this Chapter, we report on an attempt to explain the maintenance of the zonal mean temperature and wind structure, primarily from the point of view of the transport of potential vorticity (PV) and marginal instability.

The maintenance of the observed zonal mean temperature and wind distributions in the extratropics is a classical problem in the context of the general circulation. There have been many attempts to solve it. However, past literature has largely looked at the problem in isolation from the tropics. The focus has been on the mean tropospheric temperature gradient and the heat flux rather than the global structure of temperature and wind. The conceptual models involved were those originally designed for the description of synoptic-scale disturbances. They cannot appropriately take into account the meridional variations of many important quantities, such as wind, lapse rate and planetary vorticity gradient. The tropospheric lapse rate, tropopause height and potential vorticity gradient along isentropes were treated as given parameters, rather than quantities to be explained. As a result, many outstand-

ing questions concerning the mean temperature and wind structure remain either unanswered or inadequately explained. Below are a few examples:

Observations show that the extratropical tropospheric lapse rate is close to the mean tropical tropospheric lapse rate and does not show much seasonal change. Is this an accident or does it have something to do with the transport properties of baroclinic eddies and the way they interact with the tropical circulation? For the maintenance of the lapse rate, what's the relative importance of the large-scale advection by adiabatic eddies and the local diabatic processes associated with precipitation processes? To what degree are the temperature and wind distributions dependent on the surface conditions?

The mass and momentum (or temperature and wind) of the zonal mean state are closely coupled with each other by the balance equations. The meridional distribution of zonal wind, particularly the meridional distribution of the surface wind, is clearly constrained by the requirement for the global angular momentum balance (Lorenz 1967). Is the temperature distribution also greatly affected by this requirement?

Another seemingly trivial, but equally puzzling question concerns the sharp rather than smooth transition of the lapse rate from the tropospheric value to the stratospheric value. Do the stratospheric PV and PV gradient have any role in affecting the zonal mean tropospheric temperature and wind?

The mean state of the extratropical troposphere is dependent on the transfer properties of baroclinic eddies which result from instability of the extratropical tropospheric flow. A fundamental property of the unstable baroclinic eddies is that they mix potential vorticity along isentropic surfaces. The most fundamental quantity that determines whether a large-scale flow can generate and sustain baroclinic eddies is the potential vorticity distribution of the large-scale flow, particularly the gradient of potential vorticity along isentropic surfaces (Charney and Stern 1962). In this chapter, we use PV and balanced dynamics to study the zonal mean temperature and wind of the extratropical troposphere as a function of the gradient of PV along isentropic surfaces. We are particularly interested in an extratropical troposphere with constant PV along isentropic surfaces. It has been noted that such a

troposphere with a proper elevation of the tropopause is neutral for baroclinic disturbances (Lindzen 1992). Thus it represents a limiting state which the baroclinic eddies and the mean flow can equilibrate to. The major goal of this chapter is to obtain the temperature and wind distribution of a such troposphere. By comparing it with the real atmosphere and investigating its maintenance, we wish to identify and highlight the important physical processes which have not drawn much attention and to shed some light on the three questions listed above.

This Chapter is organized as follows. Section 2 briefly reviews the past efforts in this area. The review is not intended to be exhaustive, but rather to provide the necessary background for what we address here. In Section 3, we present the distribution of Ertel potential vorticity (EPV) of the observed zonally averaged time mean flow for each of the four seasons. The overall structure suggests the neutral state noted recently by Lindzen (1992) is likely to be relevant to the real atmosphere. In Section 4, we calculate the temperature and wind distribution which corresponds to a well mixed PV along isentropes, and investigate the implication of this efficient mixing of PV for the connection between the extra-tropical tropospheric lapse rate and the tropical lapse rate. In Section 5, we investigate the sensitivity of the temperature and wind distribution in the extratropical troposphere to the tropical lapse rate and position of the edge of the Hadley circulation. The major purpose is to further assess the importance of the tropical impact on the extratropical temperature and wind. In Section 6, we study the sensitivity of the temperature and wind in the extratropical troposphere to changes in the gradient of PV along isentropes. Section 7 provides our summary.

8.2 Background

The zonal mean distribution of temperature and wind in the troposphere is dependent on how heat is transported from the equator to the pole and how heat is transported vertically from the ground to the tropopause. In the extratropics, the chief agent in fulfilling this heat transfer is baroclinic eddies, with sizes ranging from synoptic scale

to the planetary scale.

Obviously, the physical processes involved are many and interactions between them have appeared very complex. Past efforts have been largely foucused on searching for a simple relationship between the observed state with the marginal instability criterion obtained from idealized models which have been demonstrated to be relevant to the real atmosphere in certain aspects.

8.2.1 Ideas based on neutrality

The models which have been developed to investigate the instability of the extratropical flow are Charney's model, Eady's model and Phillips' two layer model (Charney 1947, Eady 1949, Phillips 1962). Each of the models grasps some features of the extratropical troposphere while each of them has obvious over-simplifications. For example, Eady's model has a constant planetary vorticity and a rigid lid with a fixed height, and Phillips' model only has two layers. Charney's model is more general than Eady and Phillips's models, but none of the three models allows meridional variations of wind and lapse rate, and none has realistic lateral boundaries. These limitations exclude their ability to address the maintenance of the extratropical zonal mean temperature and wind in a global context.

The marginal stability of the three models is defined by their potential vorticity distribution (Charney and Stern 1962; Pedlosky 1979 and Hoskins et al 1985). Vertical wind shear or the meridional temperature gradient (or the available potential energy) alone does not tell whether the flow is stable or not (Lindzen and Farrell 1980, Gill 1982). However, the meridional temperature gradient in the interior of the extratropical troposphere shows little seasonal change. In Phillips' two layer model, because of the fixed vertical stability, the marginal stability is also related to a critical shear (or meridional temperature gradient below which instability is impossible). This motivated attempts to relate the the observed meridional temperature gradient to this critical shear (Pocinki 1955, Thompson 1961, Stone 1978). The hypothesis that the extratropical troposphere tends to equilibrate itself to this critical state has been termed ' baroclinic adjustment '.

Phillips' model is a two layer model whereas the atmosphere is continuous. Whether the marginal instability criterion obtained from the Phillips' model can be directly applied to the atmosphere is in question. Observations have further shown that the major contributor to the meridional heat transport are waves which have a smaller zonal wave number than the most unstable wave in the linear models. More importantly, the model cannot predict the meridional distribution of temperature unless the vertical stability is given. To require a fixed vertical stability and a reference value of the planetary vorticity is a limitation for all models based on quasi-geostrophic (QG) theory in the investigation of the mass and momentum distribution on a global scale. And finally, the two layer model has fixed vertical scale and therefore cannot address where the troposphere ends.

To examine the baroclinic adjustment hypothesis in the non-linear regime, there have been many studies done in the context of Phillips' two layer model despite its obvious problems when applied to the real atmosphere (Cehelsky and Tung 1991, Ceheslsky 1987, Vallis 1988, Vallis and Roads 1984, Salmon 1980, 1978). These non-linear studies have shown that the meridional temperature gradient of the mean state is significantly super-critical. A large number of concepts have been introduced to describe the model results, such as wave-mean flow equilibration, wave wave equilibration and stochastic equilibration. The picture of the maintenance of the extratropical mass and momentum distribution tends to assume substantial complexity.

Closely accompanying these non-linear studies is the concept of geostrophic turbulence. To describe the non-linear interaction between eddies (or waves) with different scales, the concept of two-dimensional homogeneous turbulence has been introduced and modified in some fashion to describe the quasi-geostrophic systems (Charney 1971; Salmon 1978, 1980). The knowledge of two-dimensional homogeneous turbulence and its application to the large-scale atmospheric flow has proven helpful in understanding the energetics of the atmospheric flow, but has not contribute much to the understanding of the maintenance of the time and zonal mean structure of the extratropical troposphere. The theory for homogeneous turbulence is only appropriate for small-scale eddies in a region far from the boundary. Its application to the

description of the planetary scale eddies and the maintenance of the zonal mean flow is obviously limited.

Realizing the limitation of the two layer model and the fundamental importance of the PV distribution, Lindzen and Farrel (1980) proposed a stimulating scheme for parameterizing the heat transport of eddies . In the paper, they assumed that the atmosphere in the extratropics could be represented by the Charney model and addressed the question what modification to the vertical wind profile is needed to make the atmosphere stable. This scheme predicts the meridional distribution of the vertically averaged troposphere well, though the approach has its tentative nature (Hoskins 1983). Perhaps more importantly, it draws the researcher's attention to the distribution of PV–the fundamental quantity which determines the stability of the flow. Again, the approach of this paper is based on an assumption that the time mean flow in the extratropical troposphere should be close to marginally unstable.

The studies discussed above were based on (QG) theory. As is well known, QG theory is limited in its ability to describe the mean state of temperature and wind on a global scale.

8.2.2 Vertical scale of eddies and the radiative constraint

A different approach to understanding the mean state of the extratropical troposphere originates from radiative-convective equilibrium calculations. This approach is based on one-dimensional averaged models with empirical assumptions about the mean lapse rate, and therefore its merit is obviously limited. A useful finding in the context of the radiative-convective equilibrium calculations is that the tropopause height can be determined through the radiative-constraint if the lapse rate is given and vice versa. This finding appears to have motivated Held's speculative arguments (Held 1982) about the tropopause height and the tropical tropospheric lapse rate in both the tropics and the extratropics. Basically, Held suggested that in the extratropics the dynamics of baroclinic eddies largely defines the vertical extent of the heat flux, presumably the tropopause height, and that the overall lapse rate is determined by the radiative constraint. The problem with this argument is that it is not very clear

that the tropics and the extratropics can be considered separately when the radiative constraint is applied.

8.2.3 Eady Type of Instability and the neutrality of the troposphere

Synoptic analysts have long noticed the role of the upper level PV anomaly and its interaction with the surface in the development of the extratropical cyclone (Pettersson and Smebye 1971; Sanders 1986, 1988). Numerical simulations of the life cycles of non-linear waves have further shown that averaged over a life cycle, the waves behave more like what is predicted by the Eady model (Simmons and Hoskins 1978, 1980). Some theorists have thus realized that the Eady type instability may be more germane to real atmospheric extratropical cyclone development (Hoskins 1985, 1990). However, to look at the maintenance of the extratropical large-scale flow from the perspective of the Eady type instability is a very recent idea (Lindzen 1992). In this pioneer paper, Lindzen noted that the extratropical tropopause may be just at the height at which waves with the scale of the physical geometry cannot see each other if they travel along the the tropopause and the surface. In Eady's model, there is no internal gradient of pseudo potential vorticity (QGPV) along isobaric surfaces (equivalently, no gradient of the EPV along the isentropic surfaces).

This hypothesis has offered an entirely new perspective to look at the instability and maintenance of the large-scale extratropical flow including the time and zonally averaged flow. First, it emphasizes that both the tropopause height and the gradient of PV along isentropic surfaces are not only the parameters which define the properties of unstable eddies in interacting with their background flow, but also they are a consequence of this interaction. Secondly, it points out that the extratropical temperature and wind distribution is connected to how PV is transported and distributed along isentropic surfaces. Also inherent in this hypothesis is the inviscid and adiabatic assumptions, which force us to divide the flow into different regions: boundary layer and the interior flow. Thus it creates a new setting in which the potential role

of the tropics, the stratosphere and the surface layer are highlighted.

Another feature of this hypothesis is the emphasis on the role of eddies with the largest scale in maintaining the time-mean state. These eddies play an important role in any turbulent flow and determine the overall structure of the turbulent flow (Landau and Lifshitz 1981). Though in the atmosphere, the synoptic-scale eddies are very energetic, their horizontal scale limits their importance in transporting both potential vorticity and heat. More importantly, they live and die in the setting created by the eddies with the planetary scale.

The eddies with a larger horizontal scale also have a larger vertical scale, so the presence of the stratosphere is obviously more important in affecting planetary scale eddies. Given the much larger value of the EPV in the stratosphere, what affects most the planetary scale eddy may be the tropopause height (ie. where the reservoir of the EPV is positioned), not the small gradient along isentropic surfaces in the interior of the troposphere. In this sense, Lindzen's hypothesis about the tropopause height may not be really dependent on whether the gradient of PV along isentropic surfaces is identically zero. Yet a small gradient of PV along isentropic surfaces can render waves with smaller scale unstable, which in turn will try to diminish the gradient of PV along isentropes. Note that the raising or lowering of the mean tropopause necessarily involves the exchange of air between the stratosphere and the troposphere. We thus may expect that the generation of PV gradient along tropospheric isentropes has something to do with the very large value of PV in the stratosphere and the intrusion of the stratospheric air into the troposphere. Thus Lindzen's hypothesis about the tropopause height raises a possible cooperation between eddies with different scales in mixing PV downgradient.

In the following section, we will show the distribution of the EPV of the time and zonal mean flow at four seasons, whose overall structure indeed suggests the relevance to the real atmosphere of the neutral state noticed by Lindzen

8.3 Distributions of the Ertel potential vorticity

Ertel potential vorticity bears very special importance among the quantities which describe a large-scale baroclinic flow. First, it is a conserved quantity when the diabatic and frictional effects are negligible. In the interior of the atmospheric large-scale flow the adiabatic effects and friction can indeed generally be ignored. Second, its spatial distribution defines the stability of the flow (Charney 1947; Eady 1949; Charney and Stern 1962; Hoskins 1974; and Hoskins et al 1985). Third, with suitable boundary conditions and the balance requirement, it contains all the information which describes the large-scale flow (Hoskins et al 1985).

The isentropic approximation of EPV for the zonal mean flow is simply $-g(f + \zeta_\theta)\frac{\partial\theta}{\partial p}$. g is the gravity constant, f is the planetary vorticity, θ represents the zonal mean potential temperature, ζ_θ is the relative vorticity of the zonal mean flow evaluated along isentropes and p is the pressure. The distributions of the EPV for the time and zonal mean flow over the four seasons in the extratropics are plotted in Figure 8-1 to 8-4, together with the corresponding potential temperature distributions. In terms of the value of EPV and its gradient along isentropic surfaces, the distribution of potential vorticity over all seasons is characterized by three regions: the surface layer with small values of EPV but large gradients along isentropic surfaces, the interior troposphere which extends to the immediate region of the tropopause which is characterized by vanishing EPV gradients along isentropic surfaces, and the region immediately below the tropopause (usually defined by the 1.5 PV unit contour) with high values of EPV and strong EPV gradients along isentropic surfaces.

The simple structure of the EPV distribution is analogous to the mass or momentum distribution of a turbulent flow in which there is no reference rotation. This again demonstrates that the most fundamental quantity the baroclinic eddies transport is PV, rather than heat.

In all seasons, ζ_θ is an order of magnitude or more smaller than f. The chief contributor to the EPV distribution is $-gf\frac{\partial\theta}{\partial p}$. Thus the EPV distribution offers a straightforward tool with which to look at the lapse rate distribution. The former is

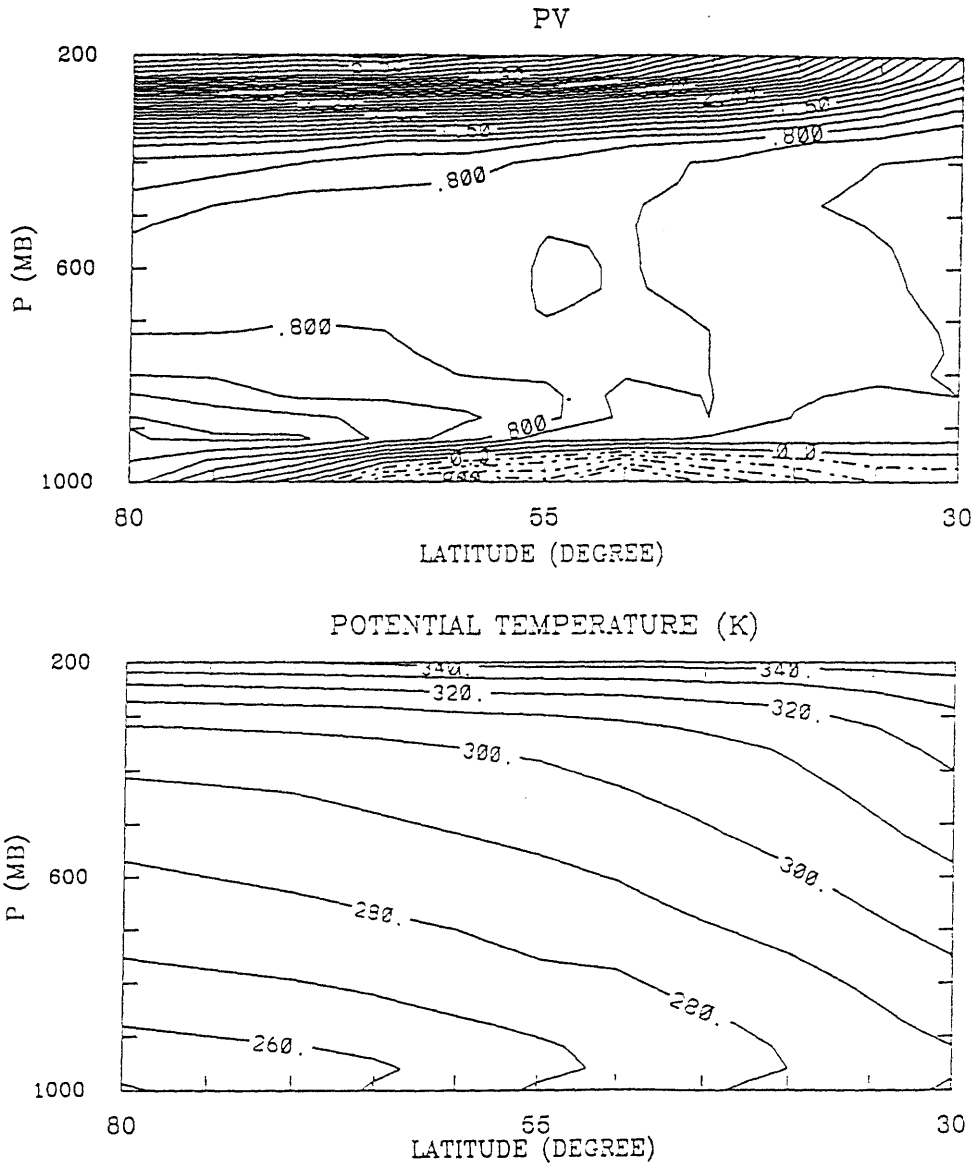

Figure 8-1: Potential vorticity (in standard PV unit ($10^{-6}m^2s^{-1}KKg^{-1}$)) and potential temperature distribution for the seasonally averaged zonal mean flow (Winter)

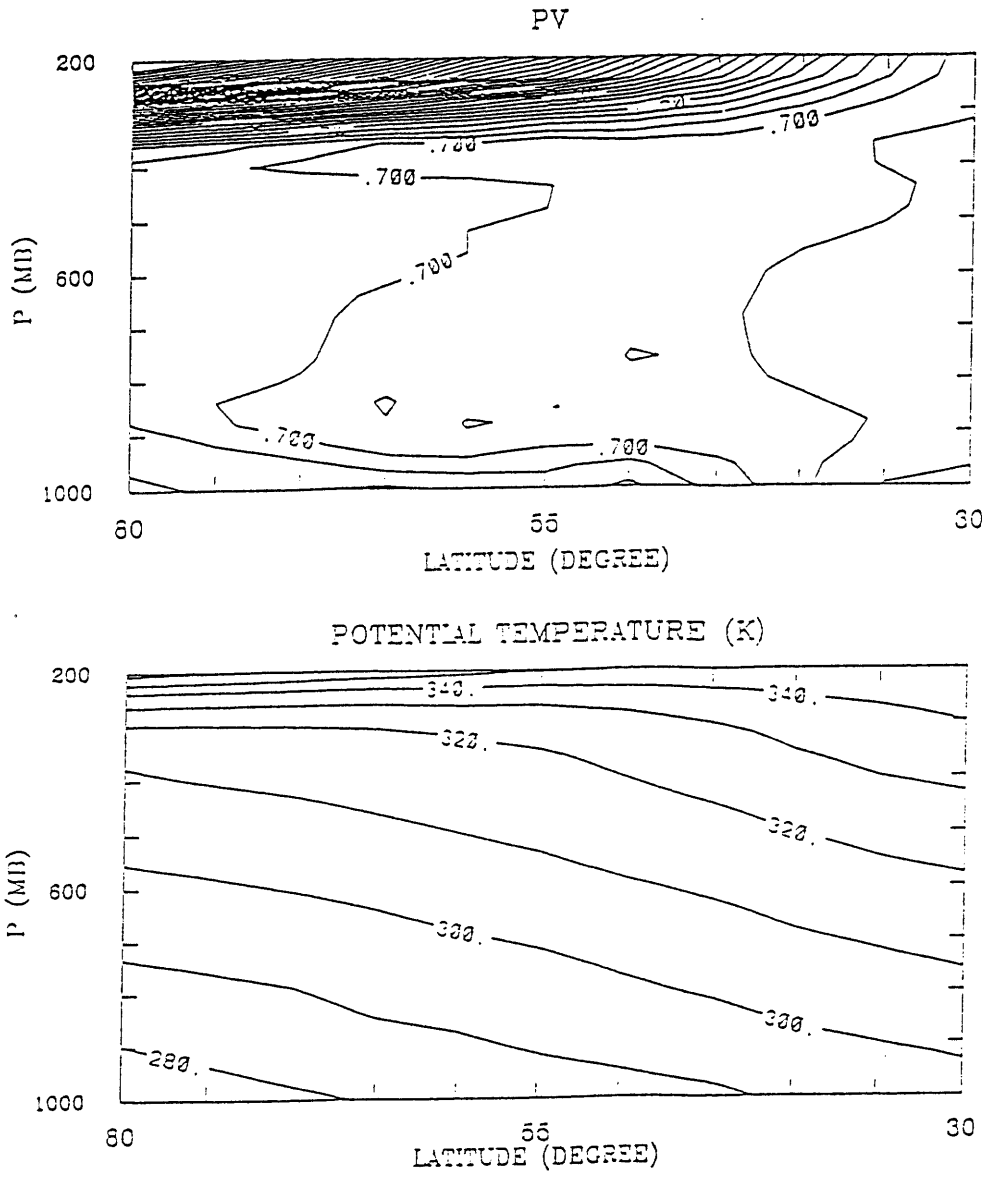

Figure 8-2: Potential vorticity (in standard PV unit) and potential temperature distribution for the seasonally averaged zonal mean flow (Summer)

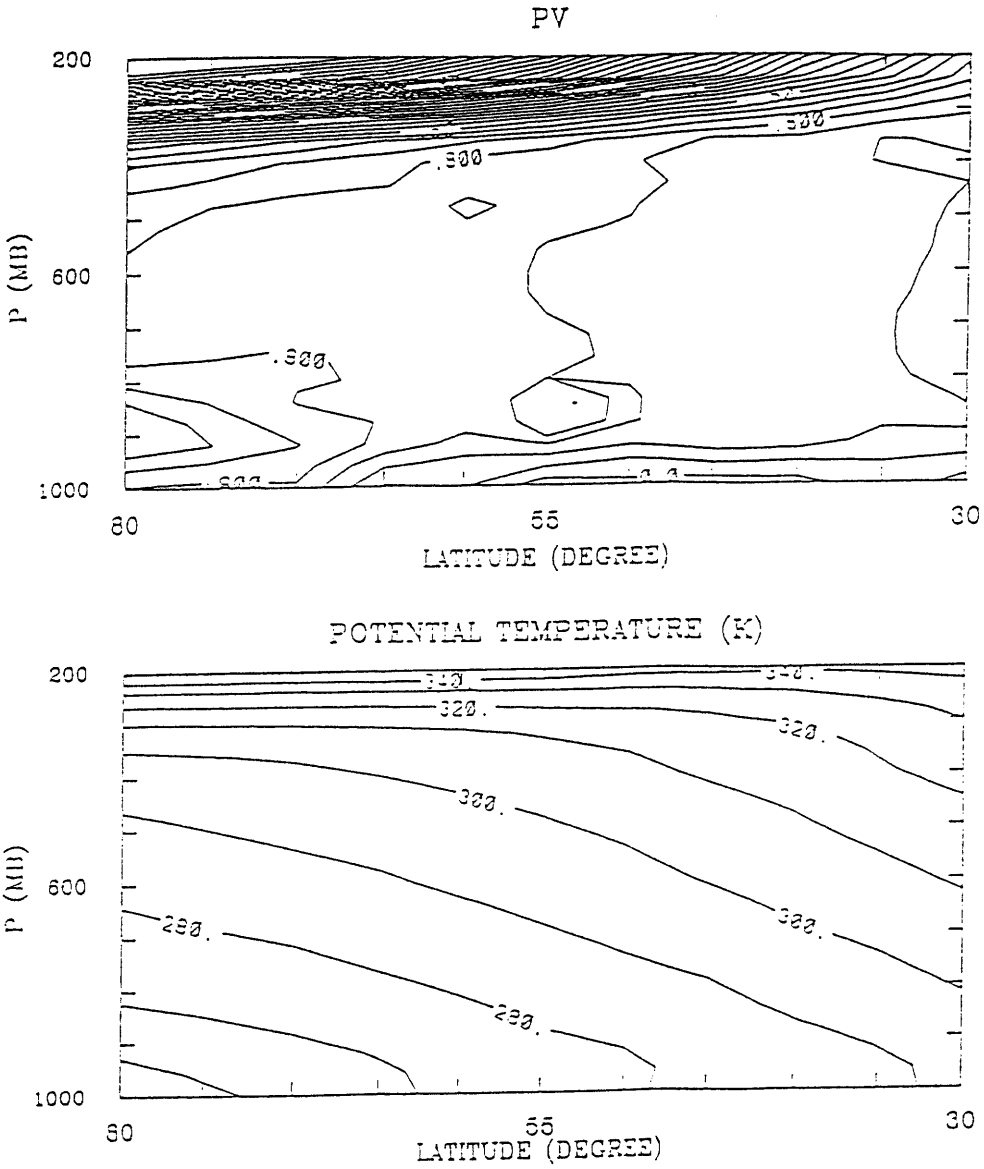

Figure 8-3: Potential vorticity (in standard PV unit) and potential temperature distribution for the seasonally averaged zonal mean flow (Spring)

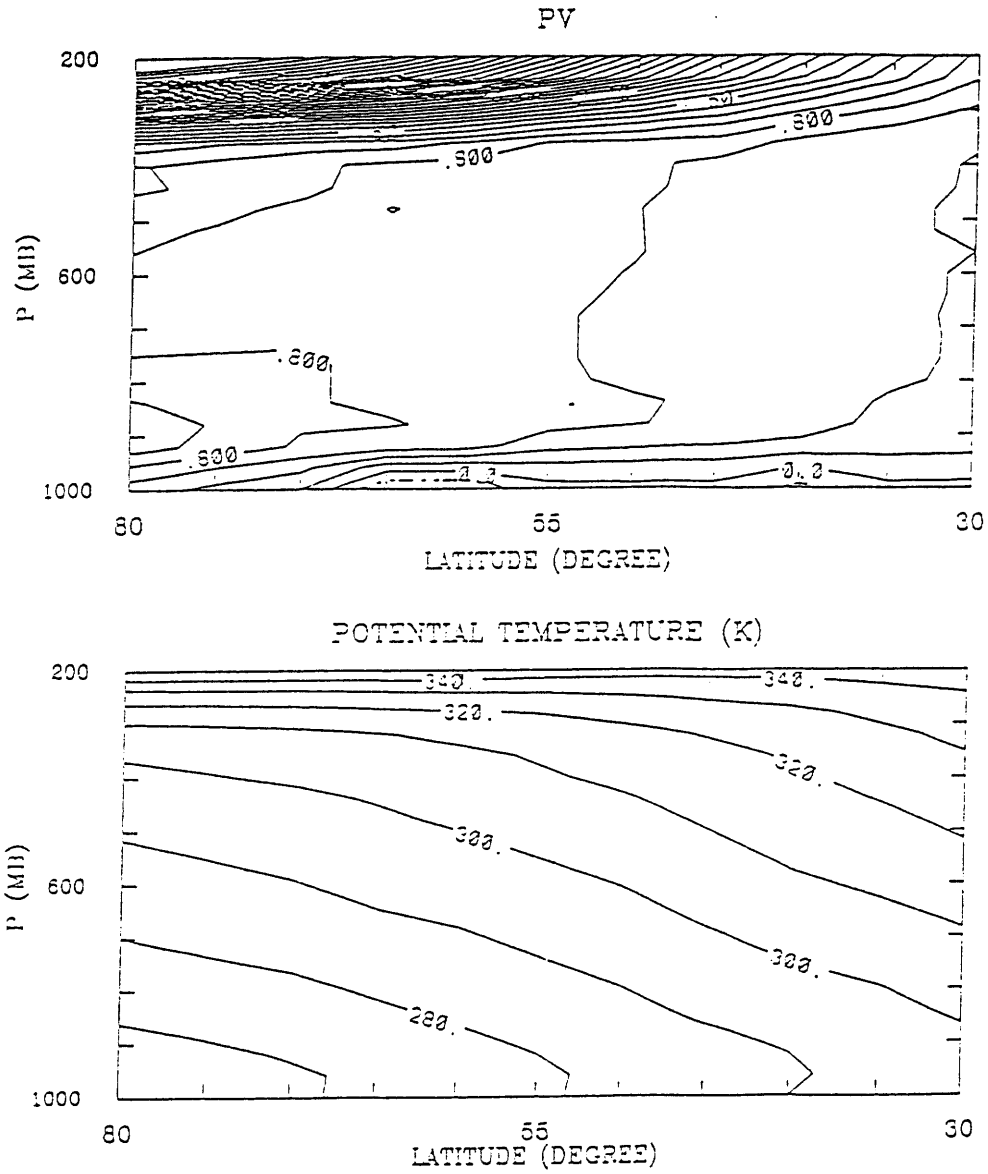

Figure 8-4: Potential vorticity (in standard PV unit) and potential temperature distribution for the seasonally averaged zonal mean flow (Autumn)

a conserved quantity for an inviscid and adiabatic flow, while the latter has a much less direct dynamic meaning.

An important feature evident in these maps is that the EPV distribution in the bulk of the interior region away from the polar region shows no considerable seasonal change. It would appear that the lack of seasonal change of the lapse rate is associated with the lack of seasonal change of PV.

In contrast, the surface boundary layer is characterized by profound seasonal change, particularly the meridional distribution of potential vorticity. In the winter, the surface boundary layer is most distinguishable. There are also considerable seasonal change in the EPV of the low stratosphere (more clearly seen from data than the contour maps presented here) and distinguishable seasonal change in the transitional region from the interior troposphere to the stratosphere, particularly in the polar region.

In winter, radiative forcing is strongest and so is eddy activity, we therefore focus on the winter case in the following analyses.

To examine the EPV distributions along the isentropic surfaces more closely, we plotted the EPV distribution in winter along three representative isentropic surfaces (Figure 8-5, 8-6 and 8-7)

The first originates in the tropics and intersects the tropopause. The second one originates from the extratropical surface and also intersects the tropopause before reaching the pole. The third originates from the surface and passes over the pole without intersecting the tropopause. The EPV distribution on each surface reenforces our impression that it is indeed characterized by the boundary layer and interior flow structure. Note that on the first surface, the gradient of EPV between 15 and 25 N is clearly much larger than that in between 25N and 45 N, the section which lies in the interior of the extratropical troposphere. The third surface only has a surface boundary layer.

In general, the EPV gradient along the isentropes is positive. Though much smaller, the PV gradient away from the boundary layer section appears distinguishable from zero. However, it should be noted that the data points are too sparse to

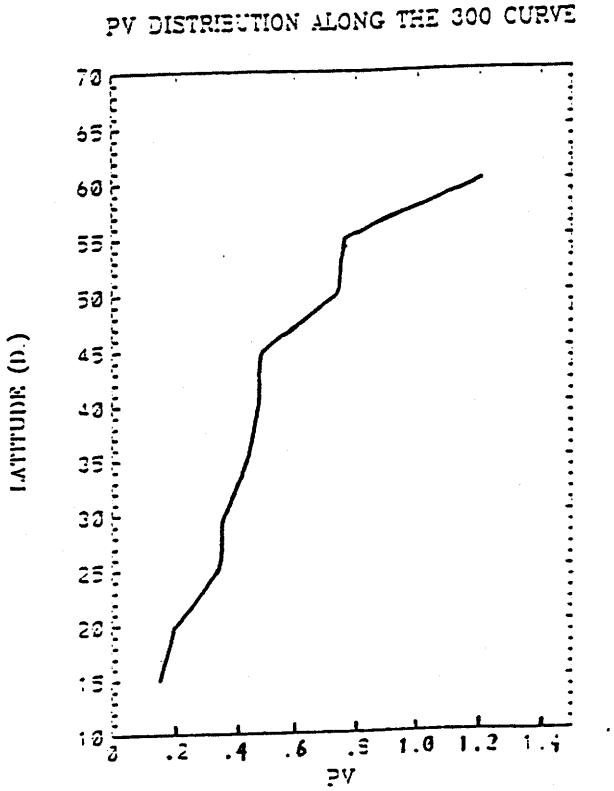

Figure 8-5: EPV distribution along the 300 K curve (in standard PV unit)

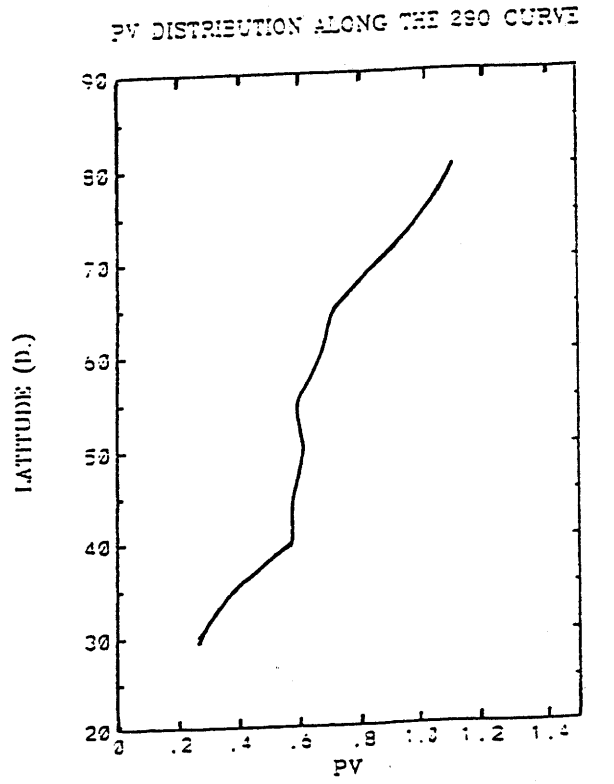

Figure 8-6: EPV distribution along the 290 K curve (in standard PV unit)

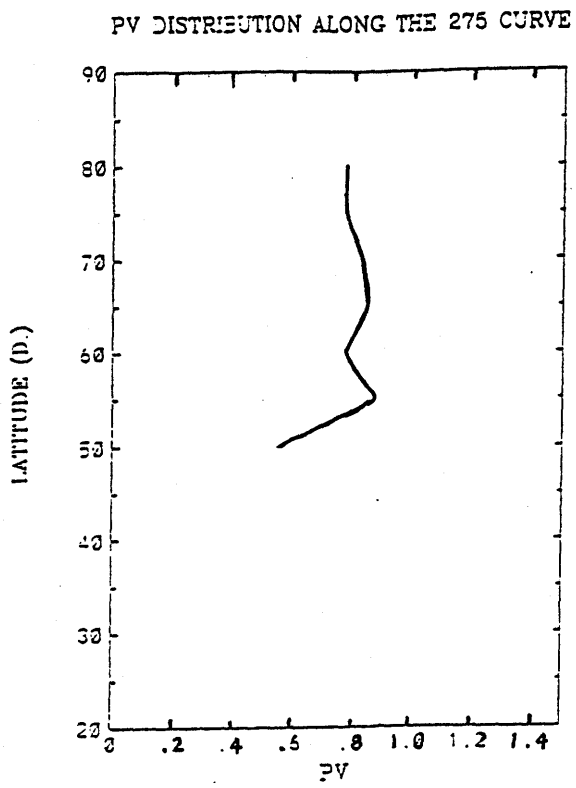

Figure 8-7: EPV distribution along the 275 K curve (in standard PV unit)

say for certain. The horizontal resolution of the data compiled by Oort is 5 degree latitude and they are available only on the standard pressure levels (ie, in between 300 mb and 800mb, there are only 3 data points). Given the large change from surface values or tropical values to stratospheric values, low resolution of the data will tend to exaggerate the gradient. An alternative way to check how significant the EPV gradient is, is to obtain the temperature and wind distribution which corresponds to a zero gradient of EPV, and then compare this temperature and wind distribution with the observed temperature and wind. This is the subject of the following section.

It is emphasized that the EPV distribution presented here is for the monthly mean and zonally averaged flow. The stability of the time mean flow is defined by the PV of the time mean flow. The stability is not defined by the time mean PV. In this regard, it may be worth noting the difference between the analysis here and that of Hoskins (1991). In his paper, the global distribution of PV is the zonally and time-averaged potential vorticity. Different from a passive chemical tracer, the distribution of potential vorticity also controls the motion which transports it. The eddy activity is intermittent and varies with longitude. The degree of PV homogenization by eddies

is expected to vary with time and longitude. Systematic analyses of the geographic variations of the degree of PV homogenization have not been performed. Morgan calculated the EPV distribution along isentropes which cross the jet maximum. He also found an almost homogeneous distribution of EPV alone these isentropes (Morgan 1992, personal communication)

The gradient of QGPV for the zonally and time-averaged flow in the extratropical troposphere has been calculated before by Pfeffer (1981) and Fullmer (1982). Since the gradient of QGPV involves the second derivative of the zonal wind, it is uncertain how large a numerical error was introduced in the calculations. This is reflected by the disagreement in many details in the results of the two calculations. Nevertheless, their results also show minimum QGPV gradients in the middle troposphere.

It should be further noted that QG theory is not expected to apply to a global scale and highly non-linear case. It requires a reference value for both the planetary vorticity and the vertical stability and therefore is inadequate in addressing the maintenance of the mean state, particularly the exchange of potential vorticity between the tropics and the middle latitudes and between the troposphere and the stratosphere. The more fundamental quantity than QGPV is the EPV (Hoskins et al 1985), in which the vertical stability is coupled with the vorticity field. In the remainder of this Chapter, by PV, we refer to EPV only.

The distribution of PV of the seasonally averaged zonal mean flow shows that the PV gradient tends to be vanishing along isentropic surfaces in the interior of the troposphere. Though not conclusive, it is worth investigating what an efficient mixing of PV by baroclinic eddies implies for the connection between the lapse rate in the extratropical troposphere and the tropical troposphere and the efficiency of the heat transport from the pole to the equator. A troposphere with constant PV along isentropic surfaces and a tropopause height determined by Lindzen's hypothesis is the limit which the mean flow and eddies can tend to. When the ratio between the time scale of advection of PV by baroclinic eddies and the time scale of dissipation approaches zero, the extratropical troposphere is expected to approach this state. Thus a clear picture of the difference between the temperature and wind distribu-

tions of the neutral state and the real atmosphere is helpful in evaluating the role of dissipative processes in the real atmosphere (Schoeberl and Lindzen 1984).

8.4 A troposphere with zero PV gradient along isentropic surfaces

8.4.1 An approximate calculation

As shown by observations, for the time and zonal mean flow of the extratropical troposphere, the relative vorticity ζ_θ is one order of magnitude or more smaller than the planetary vorticity. Therefore, to first order approximation, the PV is simply $-gf\frac{\partial\theta}{\partial p}$. This greatly simplifies the calculation as we will see later. However, whether $\zeta_\theta << f$ is obviously dependent on the how PV is distributed and what the boundary conditions for the temperature and wind are. When we take an idealized PV distribution which differs from that observed, this assumption may not be good. But this can be easily checked once the temperature and wind distributions are obtained under this assumption.

To illustrate the role of the tropics and the role of the planetary vorticity gradient in a most elementary setting, we first consider an extratropical troposphere with a uniform PV, ie. PV is well mixed horizontally as well as vertically.

A troposphere with a uniform PV

If the PV is uniform across the entire extratropical troposphere, then the vertical lapse rate in the extratropical troposphere is related to the tropical lapse rate simply by

$$f\frac{\partial\theta}{\partial p} = f_0(\frac{\partial\theta}{\partial p})_0 \tag{8.1}$$

The subscript 0 denotes the position of the edge of the domain of the Hadley circulation. We define the tropics here as the domain of the Hadley circulation.

Equation 8.1 is a first order partial differential equation. Given the surface distribution of potential temperature, the tropical lapse rate and the width of the Hadley circulation, equation 8.1 determines the distribution of potential temperature in the entire extratropical troposphere. Note that the tropopause height can be determined independently in the manner noted by Lindzen (1992). Solving equation 8.1 does not require knowledge of the position of the tropopause, though the tropopause height is a function of the solution of equation 8.1.

By equation 8.1, we see that because of the variation of the planetary vorticity f with latitude, the extratropical troposphere will not have the same lapse rate as the tropics even in this extreme case for PV mixing.

Once the temperature distribution is determined, the wind may be obtained by the thermal wind relationship with the assumption that the surface level wind is negligible

$$f\frac{\partial U}{\partial p} = \hat{R}\frac{\partial \theta}{\partial y} \tag{8.2}$$

Solutions to 8.1 and 8.2 with boundary conditions $\theta\ |_{p=p_s} = \theta_s(y)$ and $U\ |_{p=p_s} = 0$ are presented in Figure 8-8. In the calculation, we take $p_s = 900mb$. The temperature distribution at p_s is chosen as the observed distribution for winter. Consistent with the assumption of a vertically well mixed PV, we assumed that the potential temperature distribution at the edge of the Hadley circulation is linear with pressure. We further take $\frac{\partial \theta}{\partial p}$ as the mean value of that observed between 900 mb and 300 mb at 30 N, the extent of the observed Hadley circulation in winter. The observed vertical distribution of potential temperature over the tropics is indeed very close to linear with pressure. The model troposphere is assumed to end at a specified tropopause height. The tropopause level is assumed to be 200 mb at 30 N and decreases linearly with increasing of latitude to 450 mb at 80 N. For the present purpose, this may be regarded as an adequate approximation. (The same tropopause height will be used in all other calculations)

Compared with the observed temperature distribution, discrepancies are obvious.

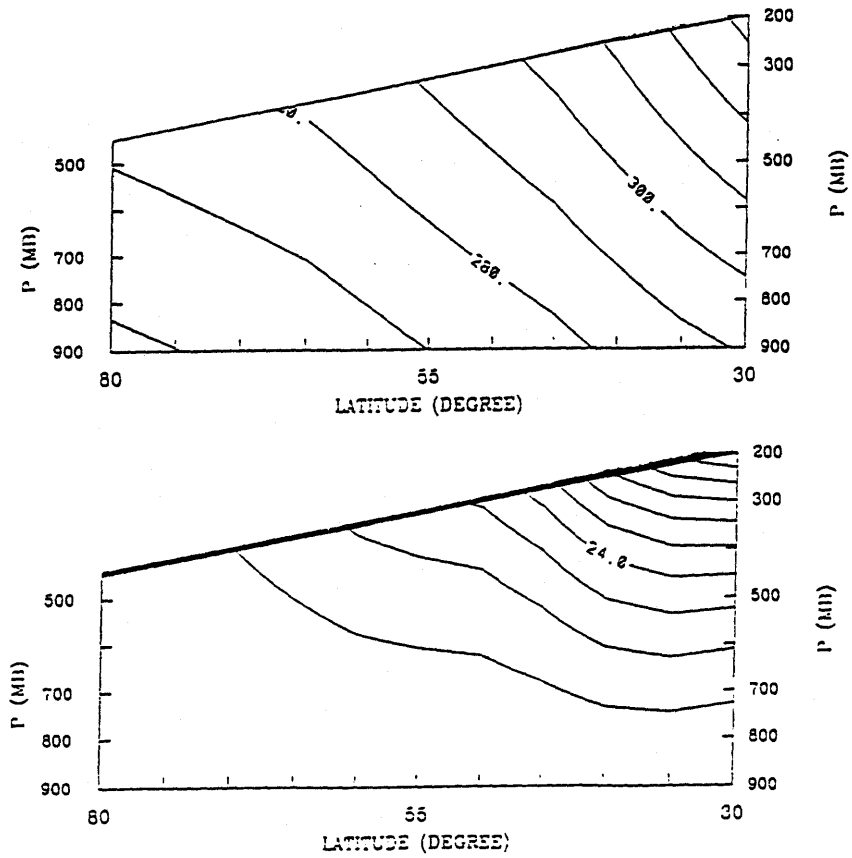

Figure 8-8: Solutions to equation 8.1 and equation 8.2. Upper: potential temperature. Lower: zonal wind. (Contour interval: 10 K for the potential temperature and 6 m/s for the wind).

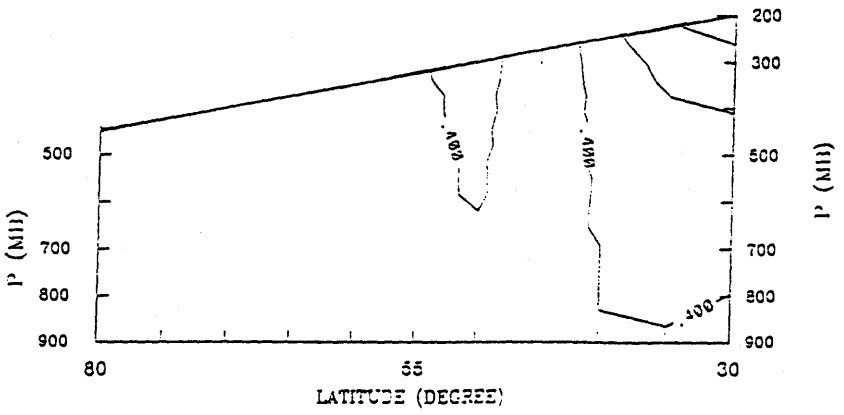

Figure 8-9: The exact PV distribution corresponding to the wind and temperature distribution in Figure 8-8 (in standard PV unit). Contour interval: 0.1 PV unit.

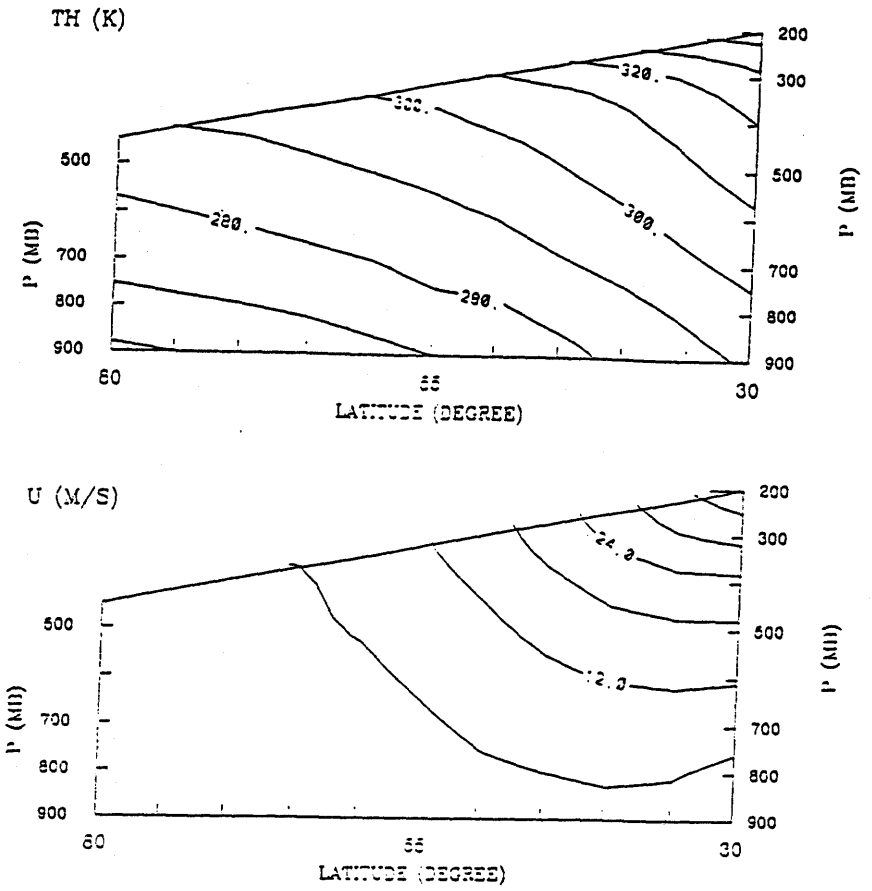

Figure 8-10: Observed zonal mean temperature and wind for the winter season (Contour interval: 10 K for the potential temperature, 6 m/s for the wind)

The slope of the isentropes in the middle and upper troposphere is much steeper than the observed value (Figure 8-10 presents the observed distribution of zonal mean temperature and wind for a quick reference). This is due to the increase of f with latitude (equation 8.1). The figure reminds us again that an efficient transport of PV is not the same thing as an efficient transport of heat as measured by the meridional temperature gradient when the planetary vorticity gradient is presented. Note that the presence of the planetary vorticity gradient limits the impact of the tropics even in the extreme case for PV mixing, though the 300 K isentrope still extends to 50°.

Figure 8-9 presents the PV distribution corresponding to the temperature and wind distributions in Figure 8-8, which demonstrates that the wind contribution to the PV distribution is indeed small.

Nevertheless, unlike circulations in the tropics where rigorous vertical mixing oc-

curs due to moist convection, extratropical circulations are quasi-horizontal and transport PV primarily along isentropic surfaces. We next consider a troposphere, in which PV is constant only along isentropic surfaces. The cross isentrope PV distribution can be non-uniform. By comparing the distribution of temperature and wind of such a case with the uniform PV case we just presented, we will also have an opportunity to isolate the role of the effective cross isentropic mixing due to the local diabatic processes.

A troposphere with constant PV along isentropes

Note that for any quantity F, we have

$$(\frac{\partial F}{\partial y})_\theta = (\frac{\partial F}{\partial y})_p - \frac{\partial \theta}{\partial y}(\frac{\partial \theta}{\partial p})^{-1}\frac{\partial F}{\partial p} \tag{8.3}$$

$y = a\phi$, a is the radius of the Earth, ϕ represents the latitude, and θ and p represent the potential temperature and pressure respectively. The subscripts represent the surface along which the derivative of F is evaluated.

Thus the gradient of $P_a = -gf\frac{\partial \theta}{\partial p}$ along isentropic surfaces can be written

$$-g^{-1}(\frac{\partial P_a}{\partial y})_\theta = \frac{df}{dy}\frac{\partial \theta}{\partial p} + f\frac{\partial^2 \theta}{\partial y \partial p} - \frac{\partial \theta}{\partial y}(\frac{\partial \theta}{\partial p})^{-1}\frac{\partial}{\partial p}\frac{\partial \theta}{\partial p} \tag{8.4}$$

If P_a is constant along isentropic surfaces, we may re-arrange 8.4

$$\frac{\partial}{\partial p}(\frac{\frac{\partial \theta}{\partial y}}{\frac{\partial \theta}{\partial p}}) = -\frac{1}{f}\frac{df}{dy} \tag{8.5}$$

Integrating from the surface level p_s to the level p, we have a first order partial differential equation which determines θ

$$f\frac{\partial \theta}{\partial y} - (\frac{-gf^2}{P_{as}}\frac{\partial \theta_s}{\partial y} - \frac{df}{dy}(p - p_s))\frac{\partial \theta}{\partial p} = 0 \tag{8.6}$$

$P_{as} = -gf(\frac{\partial \theta}{\partial p})_s$, which is the potential vorticity distribution at the surface level. Note that relative vorticity is ignored. Since the PV is constant along isentropic surfaces,

P_{as} is the distribution of PV across the isentropes originating from the surface level. θ_s is the potential temperature distribution at the pressure level p_s.

Compared with equation 8.1, equation 8.6 has one more parameter P_{as}. It is also a first order partial differential equation. Thus for a given θ_s, P_{as} and a potential temperature distribution at the edge of the Hadley cell, Equation 8.6 gives the temperature distribution in the entire extratropical troposphere. The zonal mean wind may then be estimated by the thermal wind relationship

$$f\frac{\partial U}{\partial p} = \hat{R}\frac{\partial \theta}{\partial y} \tag{8.7}$$

with the assumption that $U|_{p=p_s} = 0$.

A numerical solution to equation 8.6 and 8.7 is presented in Figure 8-11. In solving equation 8.6, we treated equation 8.6 as a typical transport equation with a varying coefficient (or velocity). Therefore the isentropic curves are just the characteristic lines of equation 8.6. The details of the numerical procedure are presented in Appendix I. In the calculation, we take $p_s = 900mb$. θ_s and P_{as} are taken from the observed values for the winter. The temperature distribution at the tropical side is assumed to be linear with pressure. The value for $\frac{\partial \theta}{\partial p}$ is taken as the mean observed value between 900mb and 300 mb at 30N. This gives a vertically well mixed PV when wind shear can be ignored. The solution is assumed to extend to a specified height which represents the tropopause level.

The exact PV distribution corresponding to the temperature and wind distributions in Figure 8-11 is presented in Figure 8-12. Presented also in Figure 8-12 is the PV distribution when the contribution from the relative vorticity is ignored. The difference between the two is indeed small. The temperature and wind presented in Figure 8-11 is the exact solution we get if we invert the PV distribution given in the lower portion of Figure 8-12 with the requirement of thermal wind balance. One may still wonder if the small difference can lead to a considerable difference to the balanced mass and momentum distribution. When the mass and momentum are balanced and PV is positive, both the wind and the temperature are related to the PV through an

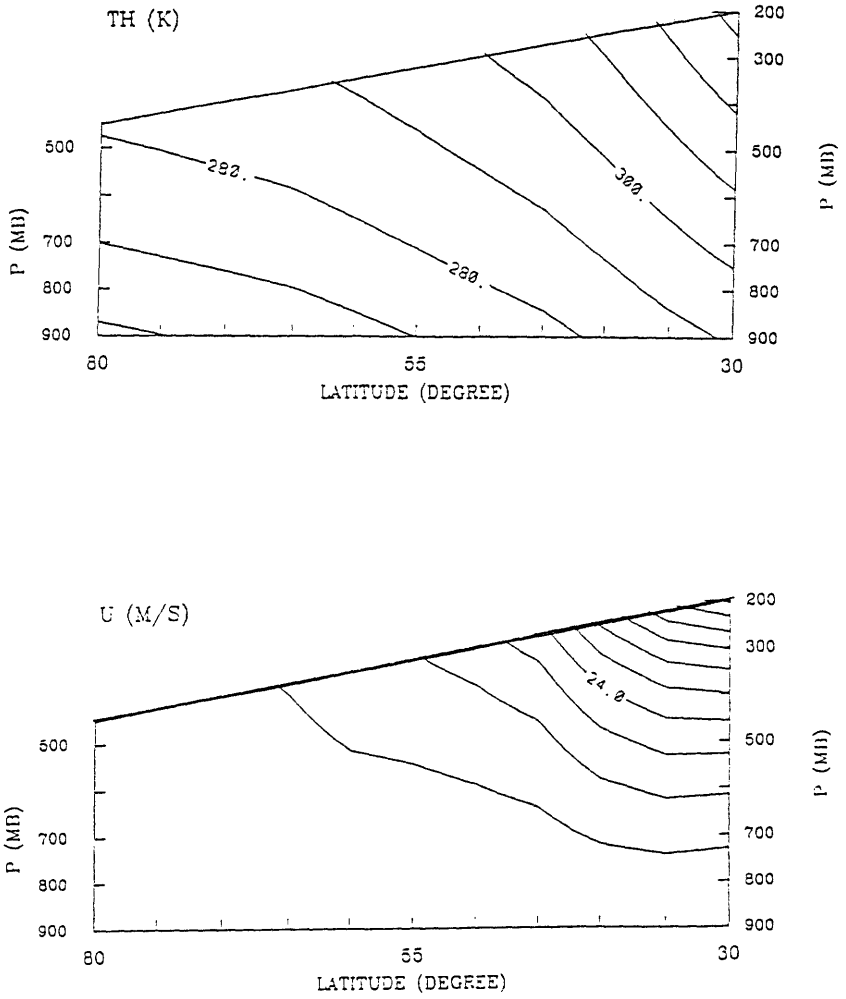

Figure 8-11: Temperature and wind distribution obtained through equation 8.6 and 8.7. Upper: potential temperature. Lower: zonal wind. Contour interval: 10 K for the potential temperature and 6 m/s for the wind. Temperature at 900 mb is chosen as the observed value. P_{as} is taken from the observed value at 800 mb.

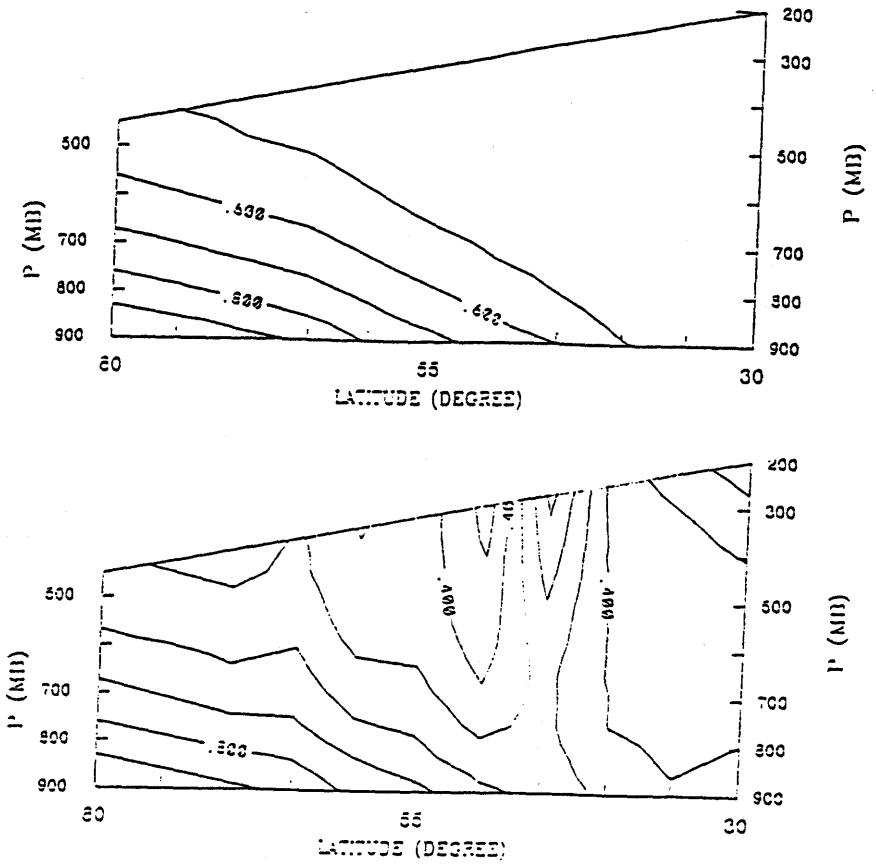

Figure 8-12: PV distributions Upper: PV distribution when ζ_θ is ignored. Lower: the exact PV distribution corresponding to the temperature and wind in 8-11 (in standard PV unit).

elliptic operator. Based on the smoothing property of the elliptic operator, we do not expect the small-scale structure appearing in Figure 8-12 will lead to any considerable difference in temperature and wind distribution. We will address this issue in a more rigorous manner in the following section. The major goal of this section is to gain a picture of the temperature and wind distributions when PV is approximately well mixed along isentropic surfaces and in this sense this section is self contained.

By comparing the solution with observations, one can say that this idealized solution indeed defines much of the observed distribution, though some discrepancy exists near the tropopause level, particularly at the jet region where there usually exists a break of the tropopause. The model atmosphere is colder near the jet region. This feature is reminiscent of the feature observed in connection with penetrative convection. When a layer of fluid with a stable stratification is heated from below, penetrative convection develops and the density (or potential temperature if the fluid

is air) tends to be well mixed within the convective region. However, the convective region is usually capped by an inversion. The fluid in the convective region is colder than the fluid immediately above. In the atmosphere, such an inversion cannot be expected to be observed, not only because of the presence of small scale mixing, but also because of the presence of radiation. As is well known, the time scale of radiative heating or cooling is dependent on the spatial scale of the temperature distribution (Goody and Yung 1989). A sharp jump in temperature renders the radiative cooling as effective as the dynamic transport. Thus the potential vorticity is not expected to be well mixed in the immediate region near the tropopause and a transition region is expected there.

Accompanying a colder upper troposphere near the jet region, the jet is also much stronger than that observed. The isentropes originating from the tropics have a slightly larger slope than observed. The tropical impact is still limited by the increase of f with latitude. The meridional extent of the isentropes originating from the tropics is slightly larger than the uniform PV case.

The good agreement with observations in the overall structure suggests that advection by quasi-adiabatic eddies is the dominant process in transporting PV and determining the temperature distribution in the extratropical troposphere. The much better agreement with observations compared with the uniform PV case shows the importance of the meridional variation of the surface conditions in creating the nonuniformity in the cross isentrope PV distribution. This non-uniformity also provides the means for diabatic processes such as latent heat release to generate gradients of PV along isentropic surfaces. Note that small scale moist processes tend to homogenize PV vertically.

The implicit role of the stratosphere

So far as the wind contribution to the PV expression can be ignored, it seems that the temperature distribution can be determined without the need to know where the troposphere ends and the thermal and wind conditions in the stratosphere. In the two cases investigated above, ignoring the relative vorticity in the PV expression

appears to be a good approximation. However, it is emphasized that this does not necessarily mean that there is no role for stratospheric PV in affecting the tropospheric temperature. Intrusion of stratospheric air will affect the mean PV budget of the troposphere and generate gradients along isentropes against the mixing affects of eddies. We will explore these issues later. Next we quantify the seemingly small effect of wind in affecting the PV distribution. A more subtle role of the stratosphere in affecting tropospheric wind comes to light.

8.4.2 A more accurate calculation

So far we have ignored the contribution to the PV distribution from the relative vorticity of the zonal wind in calculating the temperature distribution. In the following, we obtain the distributions of temperature and wind simultaneously by inverting a given PV distribution under the requirement that mass and momentum are balanced.

PV expression and balance equations

In the potential temperature– latitude coordinate $(\theta - \phi)$, the PV and the balance equations may be written

$$P_v = -g(f + \zeta_\theta)\frac{\partial \theta}{\partial p} \tag{8.8}$$

$$fU = -\frac{\partial M}{a\partial \phi} \tag{8.9}$$

$$\prod(p) = \frac{\partial M}{\partial \theta} \tag{8.10}$$

in which $f = 2\Omega sin\phi$, $\prod(p) = c_p(p/p_0)^{\frac{R_d}{c_p}}$, $M = c_pT + \Phi$. p is the pressure, $p_0 = 1000$ mb, f is the planetary vorticity, T is the temperature, $\prod(p)$ is the Exner function, Φ is the geopotential and M is the Montgomery potential. c_p and R_d are the specific heat and specific gas constants for dry air respectively. U denotes the zonal wind and $\zeta_\theta = -\frac{\partial}{acos\phi}Ucos\phi$, which is the relative vorticity of the zonal mean flow. Using

equation 8.9 and 8.10, equation 8.8 can be re-written as

$$\frac{\partial^2 M}{\partial \phi^2} - \frac{2}{sin2\phi}\frac{\partial M}{\partial \phi} + 2\Omega a^2 sin\phi \frac{P_v}{g\hat{R}}\frac{\partial^2 M}{\partial \theta^2} + (2\Omega a sin\phi)^2 = 0 \qquad (8.11)$$

in which $\hat{R} = \frac{d\prod}{dp} = \frac{R_d}{p_0} c_p^{\frac{c_v}{R_d}} (\frac{\partial M}{\partial \theta})^{-\frac{c_v}{R_d}}$. Thus equation 8.11 is non-linear. To emphasize this, we re-write the equation in the following form:

$$\frac{\partial^2 M}{\partial \phi^2} - \frac{2}{sin2\phi}\frac{\partial M}{\partial \phi} + 2\Omega a^2 sin\phi \frac{P_v}{g}\frac{p_0}{R_d} c_p^{-\frac{c_v}{R_d}} (\frac{\partial M}{\partial \theta})^{\frac{c_v}{R_d}} \frac{\partial^2 M}{\partial \theta^2} + (2\Omega a sin\phi)^2 = 0 \qquad (8.12)$$

Equation 8.12 is a second order elliptic equation for a positive PV distribution.

An ill-posed problem

To follow closely calculations presented above, we may wish to choose the surface boundary conditions as a fixed potential temperature distribution and zero wind, and to leave the upper boundary open. In terms of M, the boundary conditions are

$$\begin{aligned} M &= 0 \quad at \quad \theta = \theta_s(p_s, \phi) \\ \frac{\partial M}{\partial \theta} &= \prod(p_s) \quad at \quad \theta = \theta_s(p_s, \phi) \end{aligned} \qquad (8.13)$$

in which p_s is the surface level pressure. Notice that with a non-zero gradient of potential temperature, the lower surface defined by a constant pressure appears in the (θ -ϕ) plane as a curve whose shape is related to the exact distribution of surface temperature. Equation 8.12 with boundary condition 8.13 constitutes an ill-posed problem in the following sense. The solution exists, and is unique, but is not continuously dependent on the surface temperature distribution (Garabedian 1964). Physically, this is related to the fact that adjustment between the mass and momentum distribution is mutual. Suppose a perturbation is introduced into the potential temperature distribution at the surface level after a state which satisfies equation 8.12 is established, the subsequent adjustment to a new balanced state will involve changes of both temperature and wind. Fixing both of them at a line is physically impossible. As is

well known for elliptic type equations, the boundary in general needs to be closed. Therefore, we must supply an upper boundary condition and lateral boundary conditions at the polar and the tropical extremities. This also suggests that the role of the stratosphere will have to be taken into account when the wind is also a variable to be solved for.

The effect of the zonal wind

To estimate the error introduced by ignoring the relative vorticity of the zonal wind, we need to quantify the differences between the balanced mass and momentum (temperature and wind) distributions corresponding to the two PV distributions presented in Figure 8-12. The balanced temperature and wind distribution corresponding to the PV distribution in the low portion of Figure 8-12 is just the one in Figure 8-11. What we need is to obtain the balanced temperature and wind distribution corresponding to the PV distribution presented in the upper portion of Figure 8-12.

To invert the PV distribution presented in the upper portion of Figure 8-12, we need four boundary conditions. To compare with the approximate calculation presented above, we demand that the vertical distribution of wind at 80 N, the vertical distribution of potential temperature at the tropical boundary, and the meridional distributions of potential temperature at the lower and at the upper boundary are the same as those in the approximate calculation.

In mathematical terms, these boundary conditions are:
Lower and upper boundary conditions

$$\frac{\partial M}{\partial \theta} \mid_{\theta=\theta_s(p_s,\phi)} = \prod(p_s). \tag{8.14}$$

$$\frac{\partial M}{\partial \theta} \mid_{\theta=\theta_t(p_t,\phi)} = \prod(p_t) \tag{8.15}$$

p_s and p_t are the pressures which define the vertical domain. p_s and p_t represent the lower boundary pressure and the upper boundary pressure respectively. They can vary with latitude. θ_s and θ_t are the potential temperature distributions at the lower

and upper boundary respectively. They are in general functions of latitude.
Right and left lateral boundary conditions

$$M\mid_{\phi=\phi_r} = M_r(\theta) \tag{8.16}$$

$$M\mid_{\phi=\phi_l} = U_l(\theta) \tag{8.17}$$

M_r is the Montgomery potential at the tropical boundary. For a given vertical distribution of temperature and a reference value, it is uniquely determined. U_l is the wind at the polar boundary.

Equation 8.12 with the boundary conditions 8.14 , 8.15, 8.16 and 8.17 can be solved based on the traditional non-linear overrelaxation methods (Ames, 1969). Numerical techniques to force the solution to satisfy the lower and the upper boundary conditions are given in detail in Appendix II. The numerical method can be directly applied to study the structure of an axially symmetric baroclinic vortex. To expand to three dimensional flow is also straightforward. The advantage of this inversion for a given PV distribution in potential temperature coordinates is threefold: first , it does not require the coordinate transformation such as is needed in semi-geostrophic theory; secondly, it does not involve any approximation in the expression of PV; finally, it can be used to study the momentum and mass distributions as a function of PV gradient along isentropic surfaces, which directly connects the instability of the balanced flow (either the balanced flow is zonal mean flow or a synoptic-scale vortex). Its application to the diagnostics of storm structure requires a separate study.

When the upper boundary is not a surface of constant pressure, the numerical difficulty is greater. For our present purpose, which is to check whether the small differences in the two PV distributions in Figure 8-12 will lead to considerable differences in the corresponding balanced temperature and wind distributions, it is not necessary to choose a sloping upper boundary. Note that the approximate calculation does not require knowledge of the position of the tropopause. Instead assuming that the solution to equations 8.6 and 8.7 extends to a region such as shown in Figure

8-12, we can assume that the solution extends to the 200 mb level at all latitudes. We then solve equation 8.12 over a region which is slightly higher than the region of interest. For any given potential temperature distribution at the 200 mb level, there will be a corresponding temperature distribution at the sloping tropopause.

By solving equation 8.12 with the boundary conditions, we obtain the distribution of M as a function of latitude and pressure. We then use the balance equations 8.9 and 8.10 to obtain the pressure and wind distributions as functions of latitude and potential temperature. Finally, we obtain potential temperature and wind distributions in the pressure and latitude coordinates. The balanced temperature and wind distributions corresponding to the PV distribution in the upper potion of Figure 8-12 are presented in Figure 8-13. The tropopause pressure is again specified as a linear function of latitude. In the calculation, we chose a higher vertical domain, which is bounded by a constant pressure surface (200 mb). Figure 8-13 only shows the section below the sloping tropopause, which is what we are interested in. Recall that the present purpose is to estimate the error introduced in obtaining the tropospheric temperature and wind by ignoring the relative vorticity in the PV expression.

We see that both the temperature and wind are quite similar to the approximate solution obtained assuming contribution to the potential vorticity distribution by the zonal wind is ignored. In fact there is no distinguishable difference between the temperatures. Weak (no larger than 2 m/s) eastlies occur at surface level at high latitudes. The surface wind turns out to be very sensitive to the temperature distribution at the tropopause, as we will show shortly.

For a solution with u_l set to zero, no significant change occurs (Figure 8-14).

Tropopause temperature and surface level wind

Figure 8-15 and 8-16 show how the wind distribution is sensitive to the temperature distribution at the tropopause . The cross isentrope PV distributions for Figures 8-15 and 8-16 are the same. The boundary conditions to obtain Figure 8-15 are also the same as in obtaining Figure 8-14 except a slightly different temperature distribution at the upper boundary is used, which leads to a slightly different distribution at the

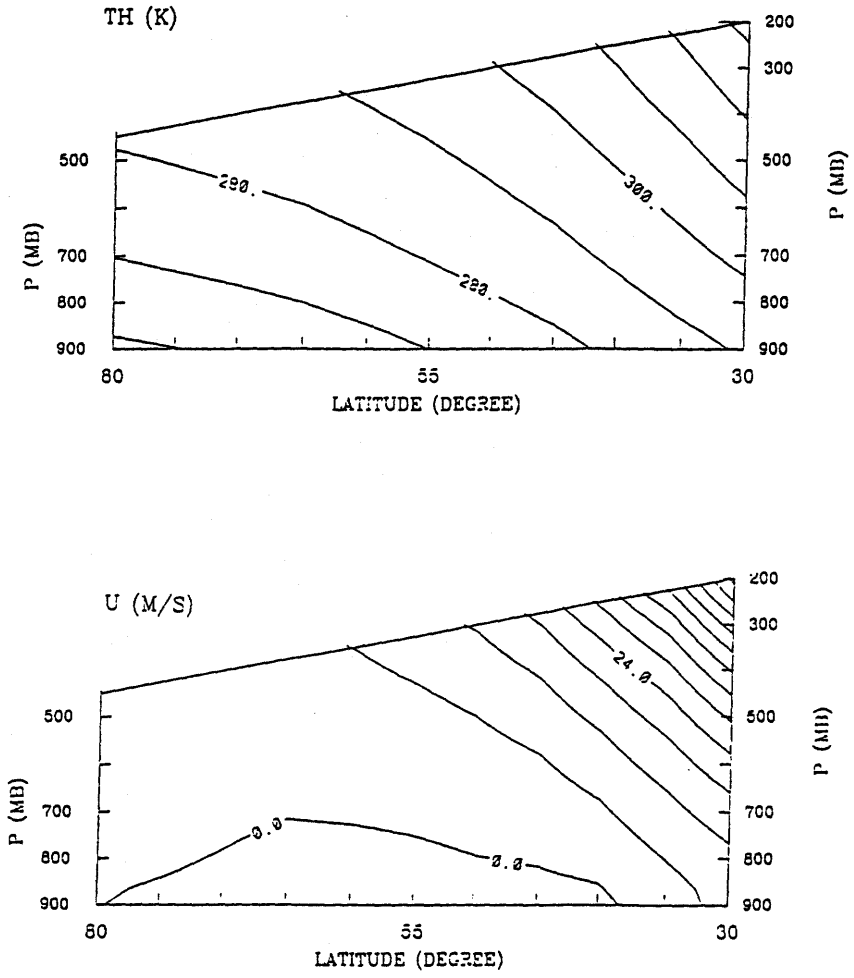

Figure 8-13: Balanced potential temperature and wind. Upper: potential temperature: lower: wind. Contour interval: 10 K for the potential temperature and 6 m/s for the wind. See text for more details

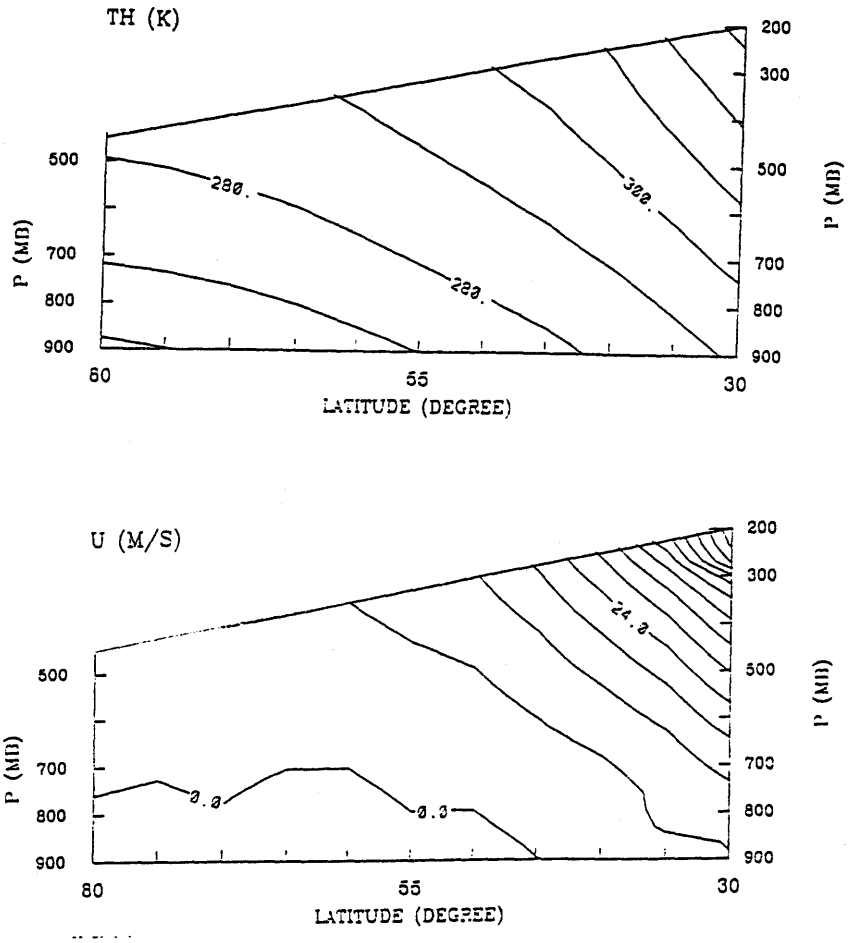

Figure 8-14: Balanced potential temperature and wind. Upper: potential temperature: lower: wind. Contour interval: 10 K for the potential temperature and 6 m/s for the wind. See text for more details.

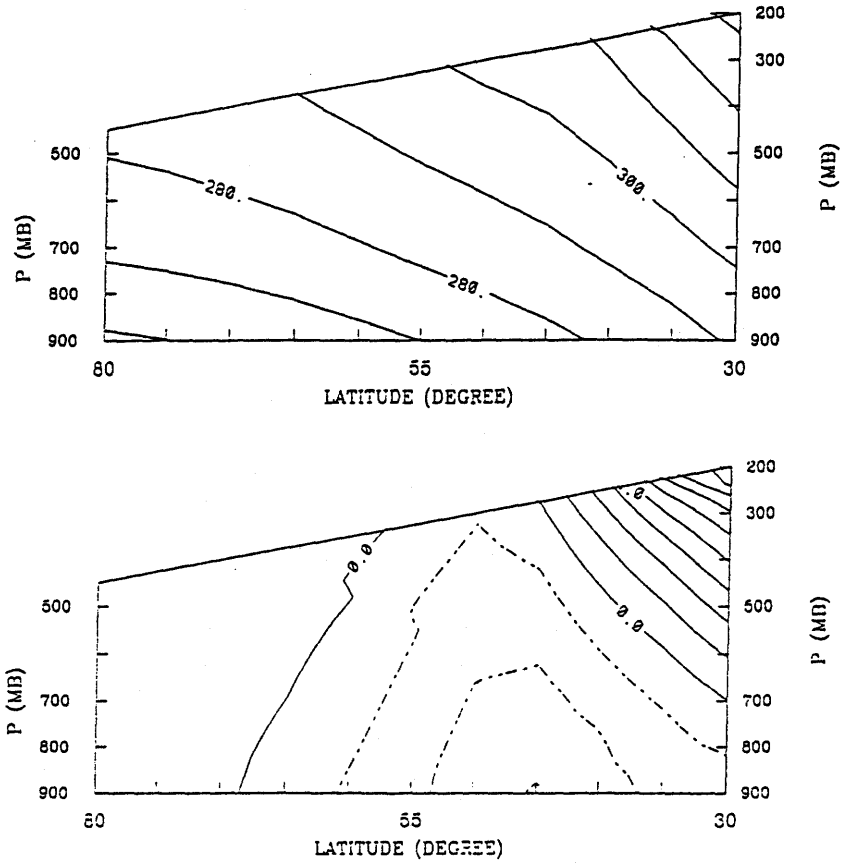

Figure 8-15: Balanced potential temperature and wind. Upper: potential temperature: lower: wind. Contour interval: 10 K for the potential temperature and 6 m/s for the wind. See text for more details.

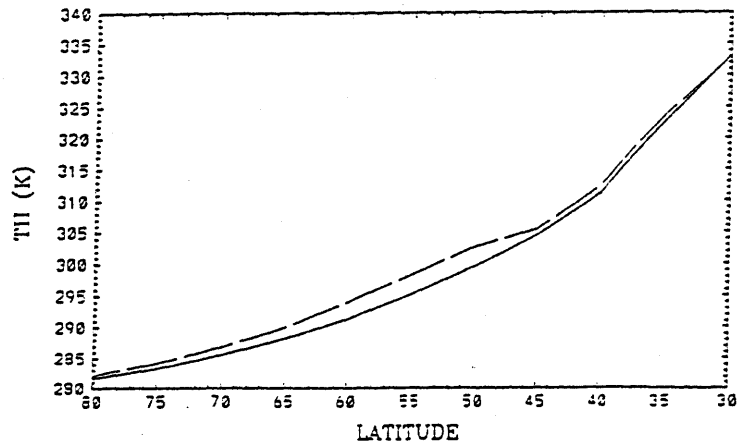

Figure 8-16: Meridional potential temperature distribution at the tropopause in Figure 8-14 and Figure 8-15.

the specified tropopause level. Figure 8-16 shows the temperature distributions at the specified tropopause level which correspond to those obtained in 8-14 (solid line) and 8-15 (Dashedline).

Note how a slight difference in the temperature structure can greatly affect the wind distribution. Clearly, the solution presented in Figure 8-16 is unlikely realizable in nature, at least not as a steady state. Note that surface wind over the bulk of the extratropics is strong easterly, and there is no way to satisfy the global momentum budget when surface friction is considered. On the one hand, this example demonstrates how the extratropical climate cannot be accurately determined unless it is put into a global context and how inappropriate an inviscid model such as Charney' model, Eady's model or Phillips' two layer model is. On the other hand, since wind distribution is so sensitive to a small change in the temperature structure, the requirement for the global momentum balance has no practical impact in determining the temperature structure. This offers some justification for using the energy balance models so far as the temperature is concerned. The physical reason for the negligible effect of wind distribution on the temperature distribution is that over planetary scales, the relative vorticity is more than one order smaller than the planetary vorticity. This is obviously dependent on the magnitude of the wind, and more fundamentally on the meridional temperature gradient. For a much larger pole to equator temperature difference, the wind effect may not be negligible. That the relative vorticity is much smaller than the planetary vorticity is equivalent to $\frac{\Delta\theta}{\theta_0} << (\frac{\Omega a}{C_0})^2$. $\Delta\theta$ is the pole to equator temperature difference, θ_0 is the mean tropospheric potential temperature, Ω is the angular velocity of the earth and a is the earth's radius. $C_0 = (gH_0)^{\frac{1}{2}}$, g is the gravity constant and H_0 is the tropopause height.

Note that once the temperature distribution at the tropopause level is fixed, the role of the stratospheric PV and its gradient in affecting the tropospheric temperature and wind is implicitly taken into account. A fixed tropopause temperature gradient in the meridional direction is equivalent to an infinite gradient of PV (Bretherton, 1966). In addition, with the temperature distribution at the tropopause fixed, the perturbation of temperature induced by a PV anomaly in the stratosphere must

be zero at the tropopause. Mathematically, the situation can be accounted for by introducing a PV anomaly with the opposite sign in the troposphere. Thus with the tropopause temperature distribution fixed, any change in stratospheric conditions will be instantaneously reflected in the troposphere.

8.4.3 Important factors in determining the extratropical climate

In the above section, we have shown what a neutral extratropical troposphere may look like. Note that the tropopause height can be determined in the manner of Lindzen (1992). This state is the limit that the baroclinic eddies and their background flow can equilibrate to. We have shown that even in this limit, the temperature and wind are dependent on a number of parameters, among which are the position of the edge of the Hadley circulation, the tropical lapse rate, surface level temperature distribution and the PV distribution across the isentropes originating from the extratropical surface (we use P_{vas} to represent it). Details in surface temperature distribution will not be properly addressed without considering the ocean. Maintenance of the tropical lapse rate has been discussed in Chapter 5. Here we briefly discuss the width of the Hadley circulation and the PV distribution across the isentropes originating from the extratropical surface (P_{vas}).

The width of the Hadley circulation

The global circulation has been traditionally divided into two regions: the Hadley circulation and the baroclinic eddy regime. This division is supported by observation as well as theory. Schneider(1977), and Held and Hou (1980) demonstrated that a zonally symmetric, eddy-free circulation driven by differential heating on a sphere is indeed confined to the equatorial region. Held and Hou (1980) were also able to calculate precisely the width by observing the heat conservation within the symmetrical circulation, which was termed by ' equal area argument '. However, with the presence of eddies, the ' equal area argument ' cannot apply to determine the width of the

Hadley circulation any more because there is heat flux carried poleward by eddies.

However, an important property of the Hadley circulation is the creation of a potential vorticity gradient. In the inviscid limit, it generates an infinite gradient at its edge (Held and Hou 1980, Hou and Lindzen 1991). With the presence of the vertical mixing by cumulus convection, the wind is much weaker and the ability of the Hadley circulation to generate potential vorticity gradient is much weaker. Nevertheless, this property is opposite to what baroclinic eddies do. In principle, the separation line between the Hadley circulation regime and baroclinic eddy regime can be determined if we can parameterize the creation and destruction of the PV gradient along isentropic surfaces by the two different processes. This of course requires a separate study.

PV distribution across the isentropic surfaces originating from the extratropical ground

Clearly, P_{vas} is related to the dynamics of the surface boundary layer where diabatic processes and viscosity cannot be assumed negligible in the generation and destruction of PV compared with the advective effect of PV by the large-scale eddies. Note that the thermal boundary layer and the viscous boundary layer may not have the same height, particularly when the low atmosphere is convectively unstable and surface heat flux is associated with convection.

Perhaps to say P_{vas} is completely determined by the surface boundary layer dynamics is unfair to the stratosphere. The potential vorticity there may affect the value of PV in the interior. There are some observations which have suggested some specific ways by which the stratospheric potential vorticity can be mixed into the troposphere (Hoskins 1991; Shapiro 1980). So far as we have understood it, the essence of baroclinic instability is the interaction between anomalies of PV aloft with perturbations at surface level. The unstable baroclinic waves necessarily advect PV down-gradient.

To study the matter of the exact distribution of P_{vas} is also beyond our present purpose. This issue is related to the global balance of potential vorticity, whose

understanding is far behind the understanding of the global energy balance and the global momentum balance, at least conceptually (Hoskins 1991). In the following section, we investigate the sensitivity of the extratropical zonal mean temperature and wind distribution to changes in these seemingly important factors which have been highlighted in the above section.

8.5 Sensitivity to changes in the tropics and in the cross isentrope PV distribution

The sensitivity studies in this section are again restricted to the extreme case of PV mixing: PV is constant along isentropic surfaces. We use the same procedures as presented in Section 8.4.2 to obtain the temperature and balanced wind distributions. We first solve 8.6 and 8.7 to obtain the temperature distribution at the upper boundary (200 mb) and the vertical distribution of wind at 80 N, which will be used as two of the four boundary conditions (equation 8.14, 8.15, 8.16 and 8.17) to invert the PV (equation 8.12) to obtain the balanced temperature and wind distribution.

Sensitivity to the vertical distribution of PV/lapse rate in the tropics

We first examine the sensitivity of the temperature and wind to the vertical distribution of PV at the tropical boundary. When wind shear is small, PV is mainly determined by the lapse rate. Figure 8-17 and 8-18 show the potential temperature and the balanced wind distributions for two cases corresponding to different vertical distributions of PV at the tropical boundary. Figure 8-19 shows the distribution of PV. In one case, the PV at the tropical side boundary is assumed to be well mixed with height, and in the other case it is assumed to increase slightly with height. In both cases, the surface temperature distribution is the same. The PV distribution across the isentropic surfaces originating at the extratropical ground are assumed to increase linearly with latitude to the value of 1 PV unit at 80 N. We see that a slight change affects both the temperature and wind significantly. The slope of those isen-

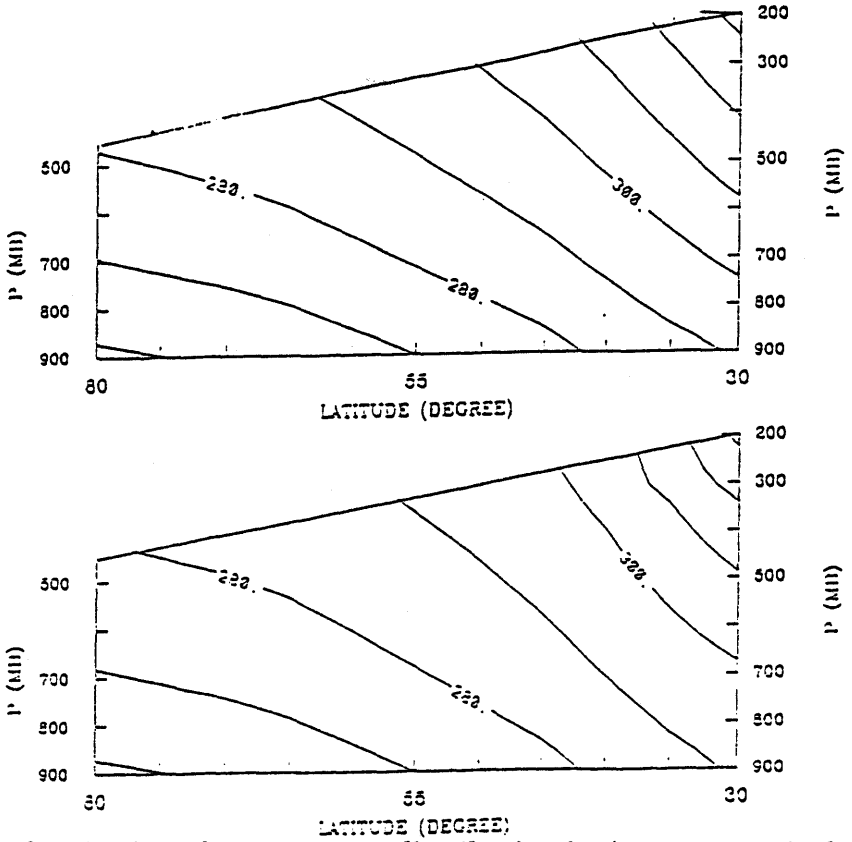

Figure 8-17: Sensitivity of temperature distribution in the extratropical troposphere to the vertical distribution of PV at the tropical boundary (Contour interval: 10 K)

tropes which originate from the tropics has a smaller value in the case of constant PV at the tropical boundary. This suggests that the more vigorous the tropical convection in mixing the potential vorticity vertically, the more impact the tropical region has on the extratropics. The magnitude and the width of the jet are approximately the same, but there are considerable differences in the detailed spatial distribution of the wind.

Sensitivity to the position of the tropical boundary

By position of the tropical boundary, we mean the division line between the eddy regime and the regime of the Hadley circulation. For simplicity, we assumed that the thermal structure within the domain of the Hadley circulation can be characterized by a fixed surface temperature and a constant $\frac{\partial \theta}{\partial p}$ (the moist adiabatic assumption may be more appropriate, but the difference between them is small). The pole to equator temperature difference is assumed to be fixed and the surface temperature distribution outside of the tropics is assumed to be linear with latitude. We also assume that the tropopause height is a linear function of latitude. Furthermore,

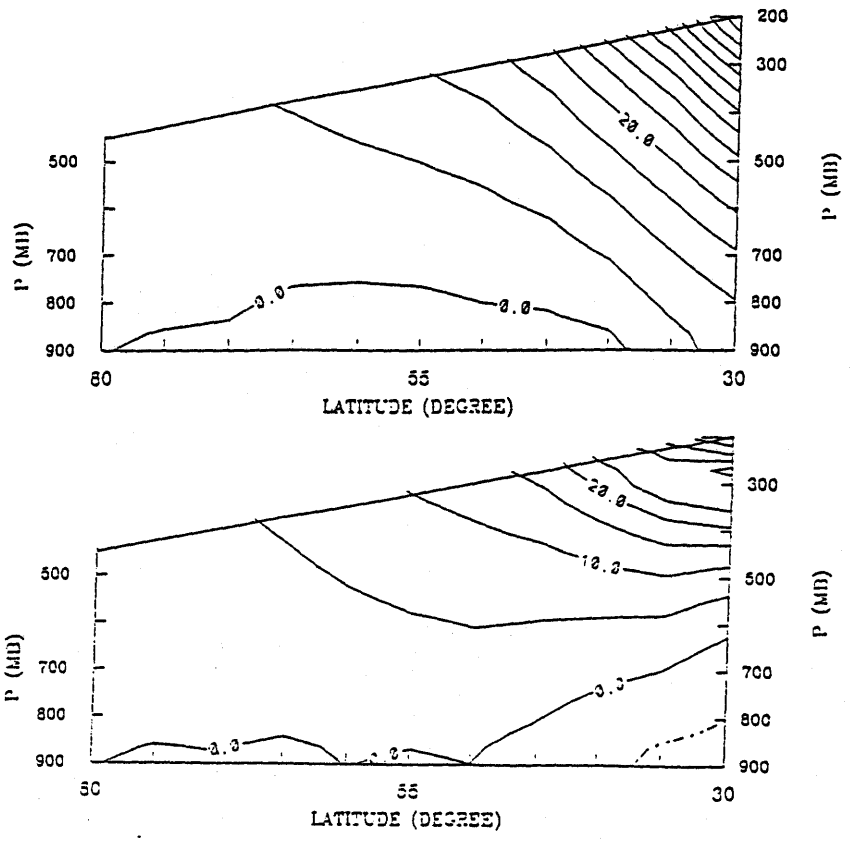

Figure 8-18: Sensitivity of wind distribution in the extratropical troposphere to the vertical distribution of PV at the tropical boundary (Contour interval: 5 m/s)

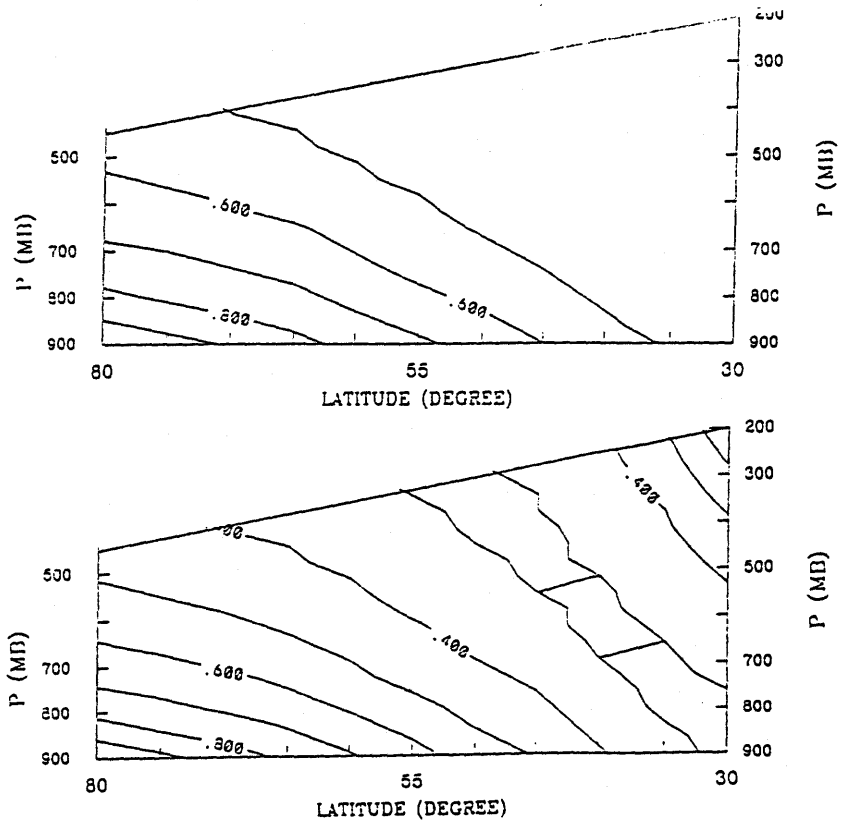

Figure 8-19: PV distributions corresponding to the temperature and wind distributions in Figure 8-17 and Figure 8-18 (in standard PV unit)

we assume that P_{vas} increases linearly from the value at the poleward edge of the Hadley circulation to 1.0 PV units at 80 N. These assumption may restrict artificially the freedom of the extratropical climate to respond to changes in the width of the tropical boundary. These issues cannot be addressed adequately without considering the ocean and the dynamics of the surface boundary layer. Under these assumptions, the change of the position of the poleward edge of the Hadley circulation affects extratropical temperature and wind by changing the PV value along the isentropic surfaces originating from the tropics, and by changing the meridional distribution of surface temperature and P_{vas}. The sensitivity of the extratropical temperature and wind to the position of the tropical side boundary is shown by Figure 8-20 and Figure 8-21. From Figure 8-20, we see that the difference again is limited to the troposphere of the lower middle latitudes and the upper troposphere of the middle latitudes. For a smaller width of the domain of the Hadley circulation, the PV to be mixed into the middle latitudes along the isentropes originating from the domain of the Hadley circulation is smaller. Consequently, the vertical stability becomes smaller in the the region where the isentropes originating from the tropics pass through. In addition, there are also noticeable differences in the balanced wind distribution.

It should be noted that in the above calculations, we emphasize the transport of PV by adiabatic processes (transport along isentropic surfaces) and assumed no cross isentrope transport. In the real world, radiative transfer and the latent heat release associated with the precipitation processes are not negligible in the thermal energy budget of the zonal mean flow (Liou, 1979), and therefore they may also be considerable in the PV budget. As we have already mentioned, the cross isentrope transport of PV will extend the influence of the tropics throughout the troposphere in the middle latitudes. Thus, we may expect that with the diabatic processes included, the extratropical tropospheric temperature and wind may exhibit a greater degree of sensitivity to changes in the tropical circulations.

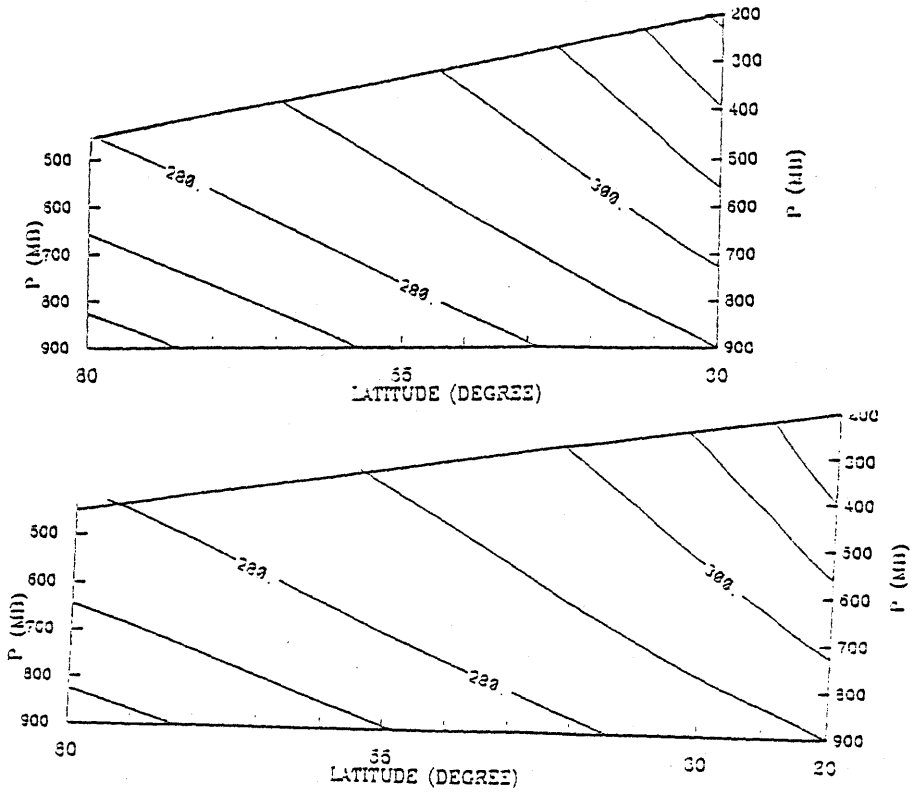

Figure 8-20: Sensitivity of temperature distribution in the extratropical troposphere to the position of the tropical boundary. Contour interval: 5 K. See text for details.

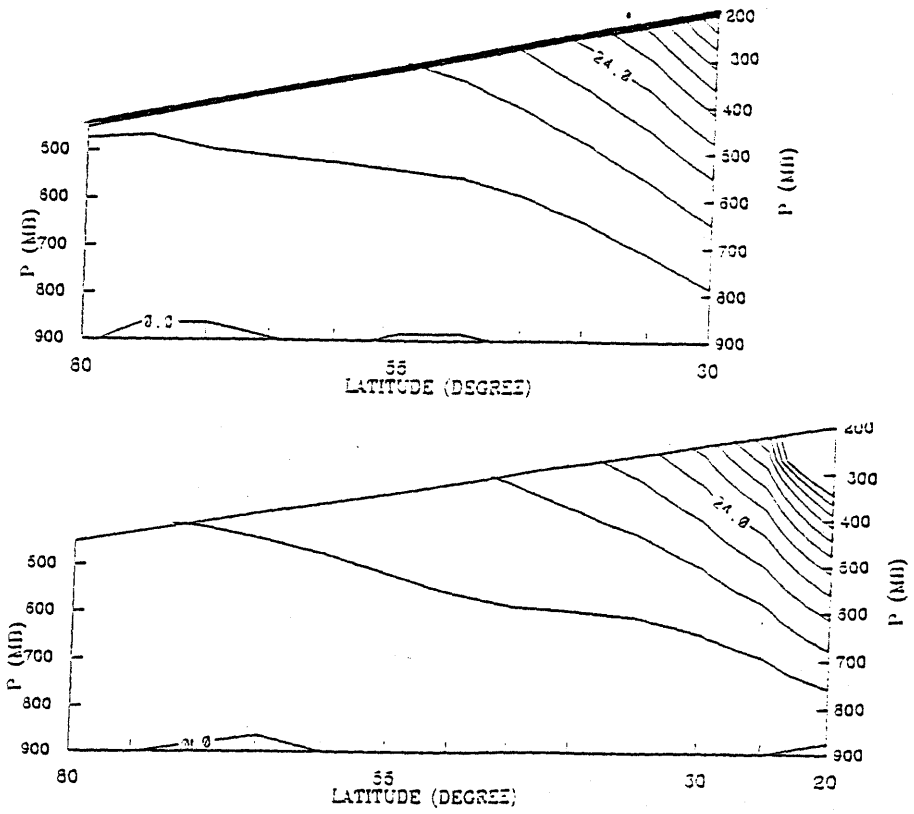

Figure 8-21: Sensitivity of wind distribution in the extratropical troposphere to the position of the tropical boundary. Contour interval: 6 m/s. See text for details

Sensitivity to the meridional distribution of P_{vas}

Figure 8-22 and 8-23 show the dependence of temperature and wind on P_{vas}. Figure 8-24 shows the two meridional distributions of P_{vas} which correspond to the temperature and wind distributions presented in Figures 8-22 and 8-23 (The solid line is for the temperature and wind distribution presented in the upper portion of Figures 8-22 and 8-23, and the dashed-line is for the lower portion). The PV value on each isentropic surface originating from the tropics is assumed to be uniform and the same in the two cases. Though the larger the PV, the larger the vertical stability, it is interesting to note that the affect on the vertical stability is not local because of the efficient transport of PV along isentropic surfaces. The jet structures in the two figures are almost the same, which shows that the jet is mainly determined by the PV distribution on the isentropes originating from the tropics. Figures 8-22 and 8-23 also show that the meridional distribution of P_{vas} also affects the slopes of those isentropes originating from the tropics. It appears that the larger the meridional gradient of P_{vas}, the higher the latitude to which an isentrope originating from the tropics can penetrate before it reaches the tropopause, though the dependence of the slope of the isentropes originating from the tropics on the meridional distribution of P_{vas} is not strong.

8.6 Sensitivity to PV gradients along isentropic surfaces

The gradient of PV along isentropic surfaces is an effective measure of how efficient the baroclinic eddies are in mixing PV. In this section, we quantify the dependence of temperature and wind in the extratropics on the gradient of PV along isentropic surfaces. The diabatic effects associated with latent heat release, radiation, and the intrusion of stratospheric air will tend to generate PV gradients along isentropic surfaces. Strong meridional variations of PV are present in the surface level as well as in the stratosphere. Diabatic processes tend to diffuse the gradient into the interior of

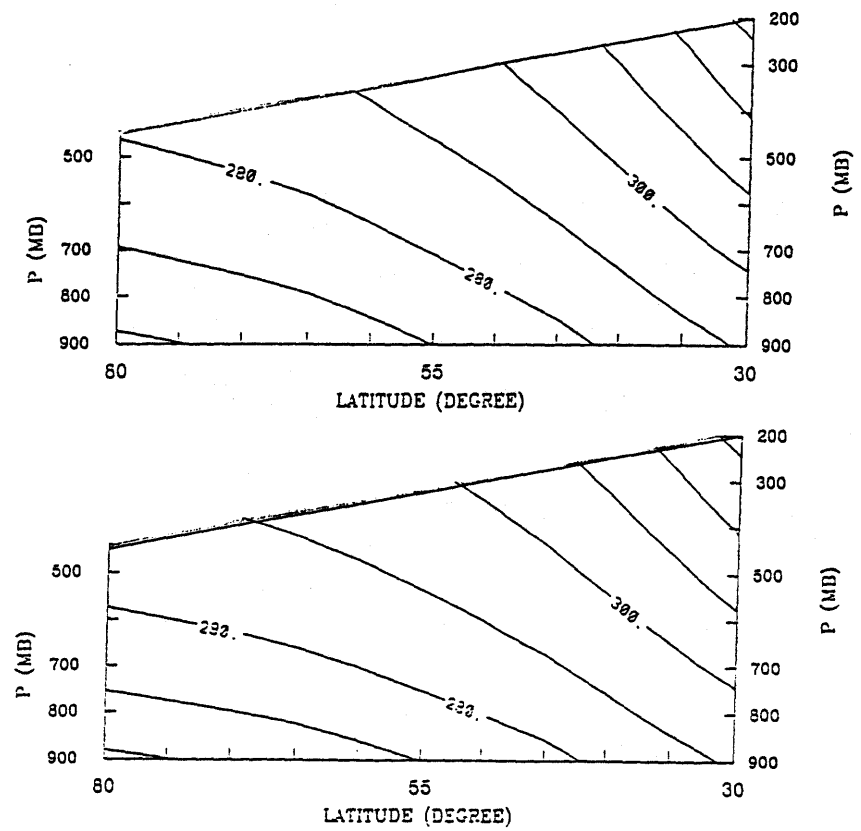

Figure 8-22: Sensitivity of temperature distribution in the extratropical troposphere to the meridional distribution of P_{vas}. See text for more details

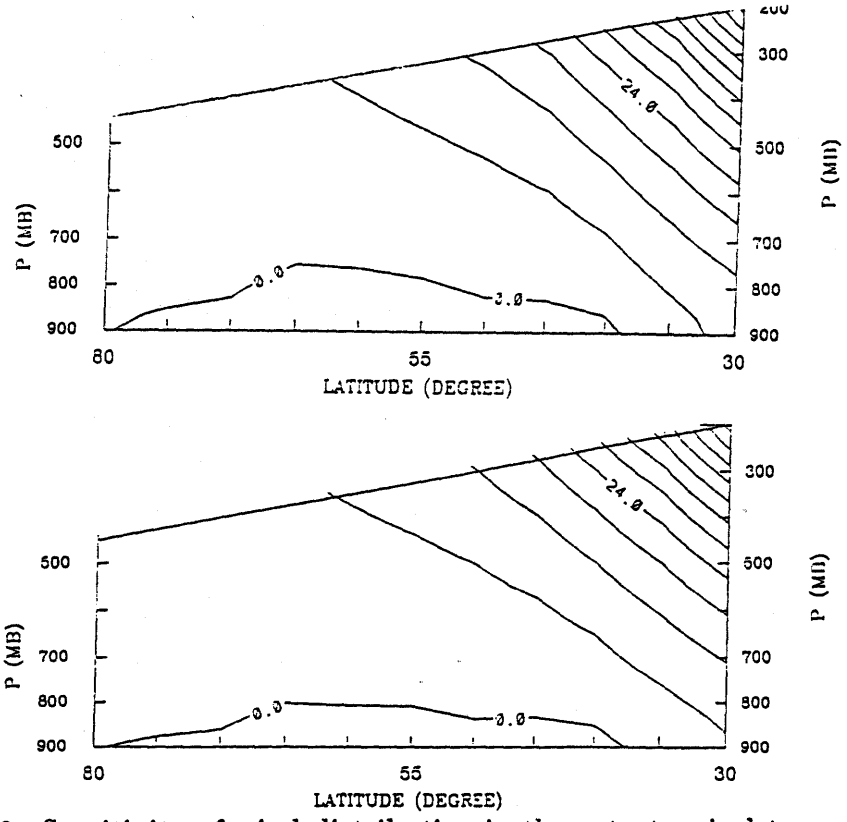

Figure 8-23: Sensitivity of wind distribution in the extratropical troposphere to the meridional distribution of P_{vas}. See text for more details

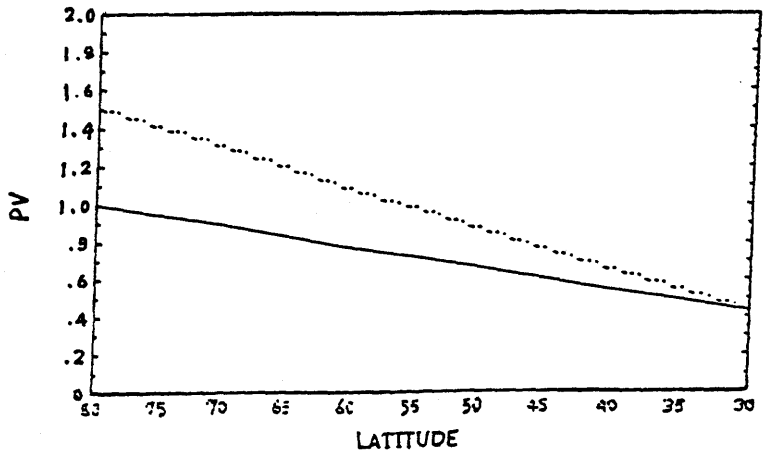

Figure 8-24: Meridional distributions of P_{vas} for the temperature and wind distribution in Figure 8-22 and in Figure 8-23 (in standard PV unit). See text for more details.

the troposphere through effective vertical mixing. Thus to quantify the dependence of the tropospheric temperature and wind distributions on the PV gradient along isentropic surfaces is an effective way to estimate the stratospheric influence and the diabatic effect associated with latent heat release.

We employ the same procedure as in Section 4. First, we solve equation 8.4 and equation 8.7 to obtain the temperature at the upper boundary and the wind at 80 N. Using this temperature and wind as the upper boundary condition and the polar boundary condition respectively for solving equation 8.12, we obtain the balanced mass and momentum distributions. To simplify equation 8.4 with a non-zero gradient of PV, we shall assume the gradient of PV can be written in the following form

$$(\frac{\partial P}{\partial y})_\theta = -g\alpha(y)\frac{\partial \theta}{\partial p} \tag{8.18}$$

$\alpha(y)$ corresponds to the QGPV gradient. When $\frac{\partial \theta}{\partial p}$ can be replaced by a reference value, α is exactly the gradient of QGPV (Charney and Stern 1962).

With this constraint, equation 8.4 can be simplified to

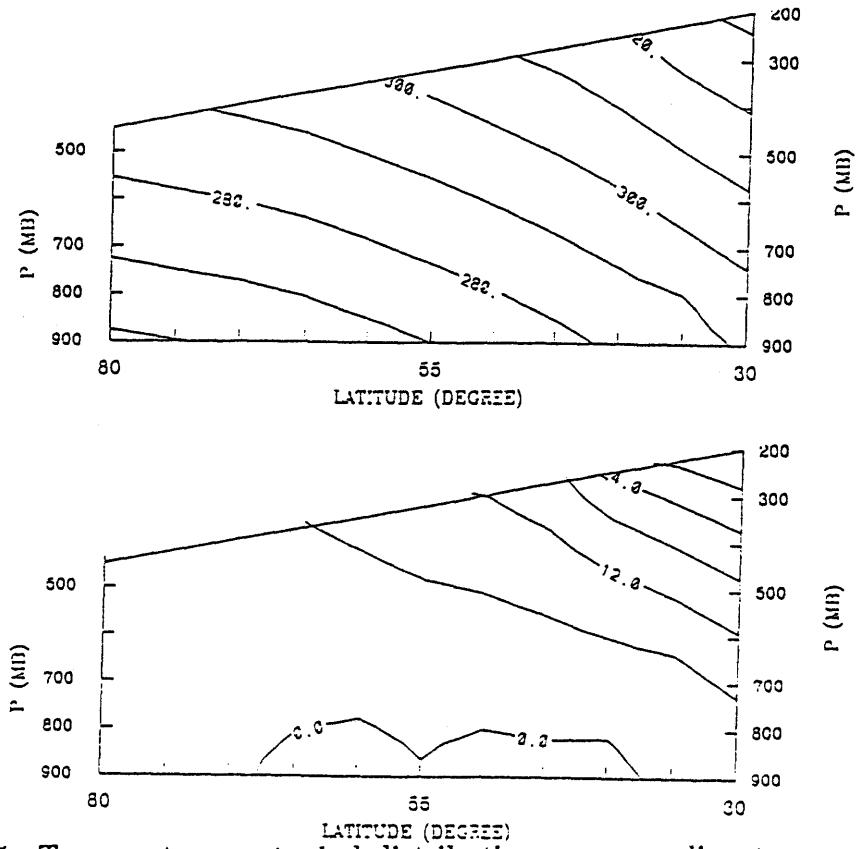

Figure 8-25: Temperature and wind distribution corresponding to $\alpha = \beta$ (Contour interval: 10 K for the potential temperature; 6 m/s for the wind).

$$f\frac{\partial\theta}{\partial y} - (\frac{-gf^2}{P_{as}}\frac{\partial\theta_s}{\partial y} + (\alpha-\beta)(p-p_s))\frac{\partial\theta}{\partial p} = 0 \tag{8.19}$$

in which $\beta(y) = \frac{df}{dy}$, the planetary vorticity gradient.

Potential temperature and the balanced wind distributions corresponding to $\alpha(y) = \beta(y)$ are presented in Figure 8-25. The PV distribution is shown in Figure 8-26. Compared with the case with zero gradient, the isentropic slope is smaller and the tropopause temperature is warmer. The maximum wind is also smaller. So far as the slope of those isentropic surfaces originating from the tropics is concerned, the presence of the PV gradient actually helps more heat to be transported to high latitudes. Note that this is not to say the presence of the planetary vorticity gradient makes the equator to the pole heat transport more efficient. As we have already seen in section 3, it is precisely the increase of planetary vorticity that causes the slope of the isentropic surfaces to increase with latitude when there is no PV gradient along isentropic surfaces.

The major difference from the case with zero gradient occurs at the jet region,

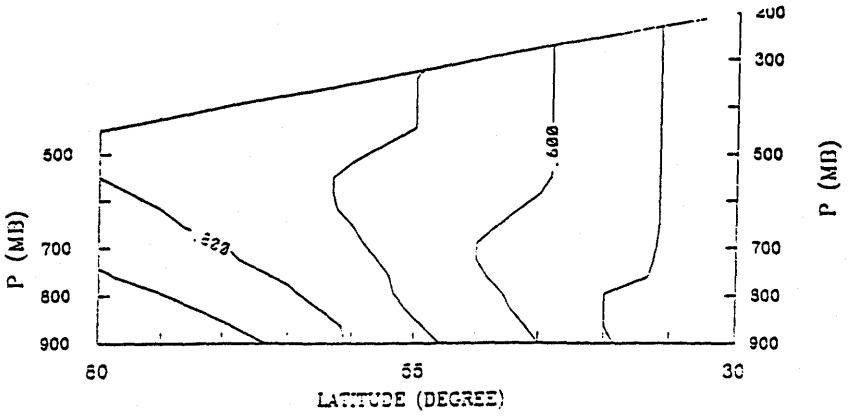

Figure 8-26: PV distribution corresponding to $\alpha = \beta$ (in standard PV unit)

which suggests the importance of the presence of a positive gradient of PV there for a warmer upper troposphere.

Potential temperature and the balanced wind distributions corresponding to $\alpha(y) = 2\beta(y)$ are presented in Figure 8-27. The PV distribution is shown in Figure 8-28. The slopes of the isentropic surfaces are still smaller as is the strength of the jet.

8.7 Discussion and summary

In this chapter, we have studied the zonal mean temperature and wind distributions in the extratropical troposphere as functions of the PV distribution, particularly the PV gradient along isentropes. We have paid particular attention to the case with zero-gradient of PV along isentropic surfaces. We have highlighted the impact of the tropics, the presence of the planetary vorticity gradient, the relative importance of large-scale advection and local diabatic processes, the importance of the surface boundary layer, the role of stratospheric PV and its gradient, and the requirement for global momentum balance.

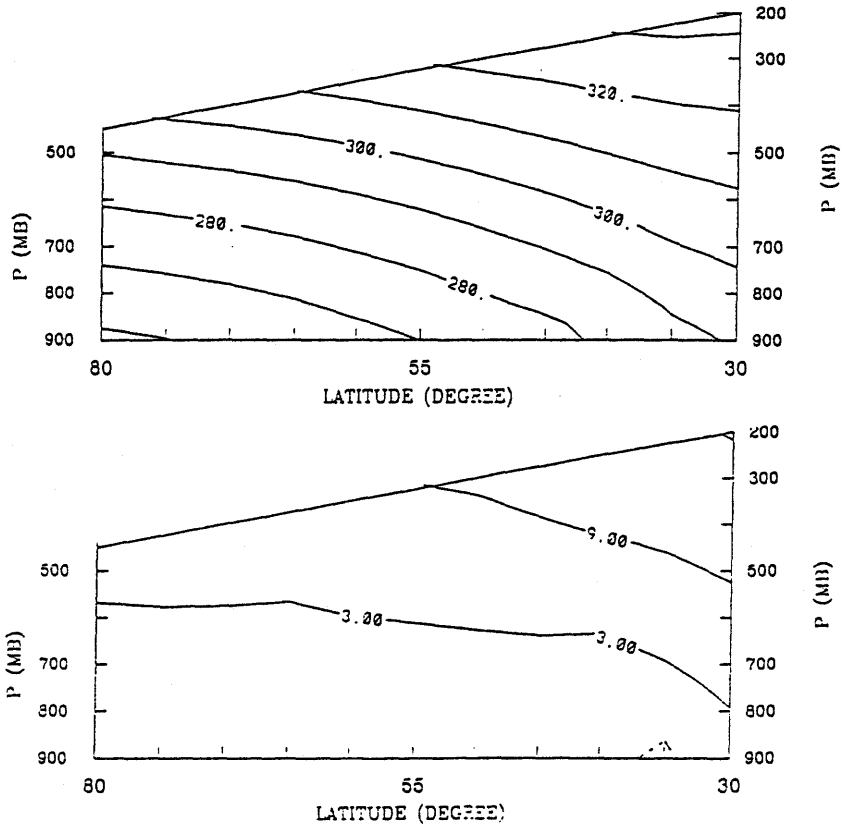

Figure 8-27: Temperature and wind distribution corresponding to $\alpha = 2\beta$ (Contour interval: 10 K for potential the temperature; 6 m/s for the wind).

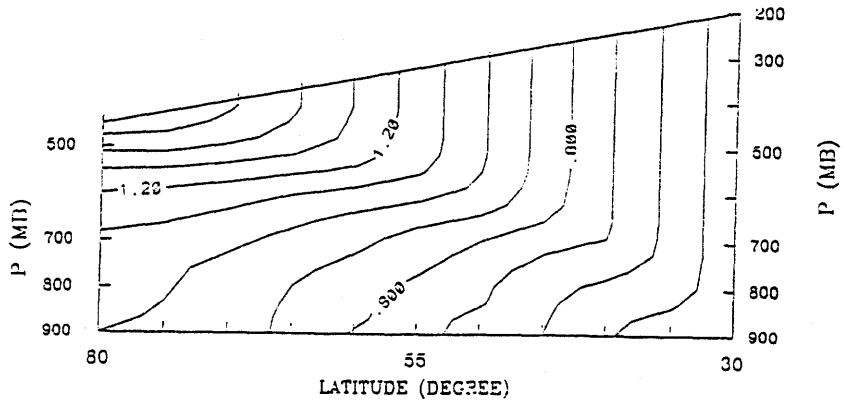

Figure 8-28: PV distribution corresponding to $\alpha = 2\beta$ (in standard PV unit)

We first calculated the PV distribution of the seasonally averaged zonal mean flow in the extratropical troposphere. We noticed that the distribution of PV over the four seasons is characterized by the " interior flow and boundary layer " structure. In the interior of the troposphere, the gradient of PV along isentropes tends to vanish. We also noticed that relative vorticity of the zonal mean flow is an order of magnitude or more smaller than the planetary vorticity. To a very good approximation, $PV \approx -gf\frac{\partial\theta}{\partial p}$. The distribution of the lapse rate in the extratropical troposphere is straightforwardly related to the distribution of PV. The key step in understanding the maintenance of the lapse rate is likely to be the investigation of the PV budget in the extratropical troposphere.

We have further obtained the temperature and wind distribution for a troposphere with well mixed PV along isentropic surfaces. For a surface temperature distribution and a tropical lapse rate as observed, the troposphere corresponding to well mixed PV along isentropic surfaces is considerably colder near the jet region than that observed. The jet is also stronger. However, the general features are very similar to those observed, including the width of the jet.

We have also shown how the presence of the planetary vorticity gradient limits the penetration of the tropical impact to the extra-tropical troposphere. In Section 8.4.1, we have shown that the extratropical tropospheric lapse rate will not be exactly the same as the tropical tropospheric lapse rate even when the PV in the extratropical troposphere is well mixed both vertically and horizontally. When the PV is only well mixed along isentropic surfaces, the slope of isentropes increases with height due to the increase of the planetary vorticity with latitude (equation 8.6 and Figure 8-11), and the penetration of the tropical impact is also found to be dependent on the PV distribution across isentropes originating from the extratropical surface. A larger meridional gradient in the cross isentrope PV distribution helps the penetration of the isentropes originating from the tropics to higher latitudes before they reach the tropopause. By comparing the temperature and wind distribution corresponding to a uniform PV with the case in which PV is only constant along isentropes, we highlighted the relative importance of the local diabatic processes versus the adiabatic

advection along isentropic surfaces.

Though the presence of a planetary vorticity gradient limits the tropical impact on the extratropical temperature and wind distribution, the isentropes originating from the tropics still reach the upper troposphere of the middle latitudes due to the relatively slow variation of the planetary vorticity. In the limit of efficient PV mixing along isentropic surfaces, both the temperature and wind distributions are sensitive to the vertical distribution of PV (or lapse rate) at the edge of the Hadley circulation. Vertically well mixed PV within the domain of the Hadley circulation helps the penetration of tropical impact to the extratropics. The temperature and wind in the extratropical troposphere are also dependent on the position of the Hadley cell. We have also noted that the effective cross isentrope transport of PV due to diabatic effects will further expand the tropical influence.

In the context of balanced dynamics, we have examined the mutual dependence between temperature, wind and PV, and have highlighted the role of stratospheric PV and its gradient. We have found that the tropospheric wind distribution is very sensitive to changes in the tropopause temperature distribution. Though the temperature and wind distributions are mutually dependent on each other and they cannot be accurately determined without reference to the global momentum balance, the meridional wind distribution has negligible effects on the temperature structure except it may play a vital role in determining the tropopause height in the manner noted by Lindzen (1992), namely, the width of the jet limits the horizontal scale of the unstable baroclinic eddies.

Finally, we have quantified the dependence of temperature and wind distributions on the gradient of PV along isentropic surfaces. The purpose was to estimate the role of the intrusion of stratospheric air into the troposphere and the effects of the diabatic processes associated with latent heat release in maintaining the tropospheric temperature and wind distributions. We have found that the larger the PV gradient along isentropic surfaces, the smaller the slope of the isentropic surfaces and the smaller the pole-to-equator temperature difference as measured in the middle troposphere, and by the strength of the jet.

It should be noted that the lapse rate in the extratropical troposphere is a function of both the surface temperature distribution and the temperature of the tropics. This dependence can be determined by applying the radiative constraint (ie. the requirement for the global energy balance). Therefore, results from the present sensitivity studies with a fixed surface temperature distribution have their obvious limitations. Nevertheless, this study sheds light on the relationship between the temperature and wind distributions and the distribution of potential vorticity, and on the roles of some important processes in the maintenance of extratropical climate, namely the impact of the tropics, the transport of PV along and across isentropes, the surface boundary layer, the potential role of stratospheric PV and its gradient ,and the requirement for the global momentum balance.

Chapter 9

Conclusions

9.1 Summary of important findings

We set out to investigate the nature of water vapor feedback in the CO_2 induced warming, particularly the dependence of water vapor on the temperature. We realized that the thermo-dynamic processes described by the Clausius-Clapeyron equation could not be the only processes which determine the tropospheric water vapor content. We conjectured that the thermal structure and moisture structure may be mutually dependent on each other in a more subtle way. The results of our investigation indeed suggest that the free tropospheric water vapor may be more related to CAPE which is a function of the entire vertical structure of temperature than to the local value of temperature.

In the radiative-convective equilibrium, we first provided an interactive picture for the maintenance of the vertical thermal structure of the tropical troposphere. We demonstrated the importance of the radiation fields and the boundary layer in maintaining the overall thermal structure of the tropical troposphere. We then provided a simple framework to explain the mean vertical structure of water vapor as well as its meridional variations. We showed the dominant role of the evaporation of hydrometeors transported to the upper troposphere in moistening the large-scale subsiding flow. Based on observations and theoretical reasoning, a leading parameter which determines the number of hydrometeors transported through deep convective updrafts

appears to be the CAPE of the large-scale environment (Williams et al 1992). This suggests that the water vapor content of the tropical tropospheric air is crucially dependent on the entire vertical structure of the tropical tropospheric temperature, not just the local temperature alone.

In trying to explain the lapse rate difference between the last glaciation and the present day, we found that only an increase of water vapor content in the middle and upper troposphere can lead to a deepening of the lapse rate in the lower half troposphere. This was based on the assumption that the vertical structure of the average convective mass flux is not subject to change. Not surprisingly, the deepening of the lapse rate is accompanied by an increase of CAPE, which was suspected to be responsible for the increase of the water vapor content in the middle and upper troposphere. The deepening of the lapse rate during the last glaciation suggests that the water vapor content in the free troposphere is more dependent on the vertical structure of temperature than its local value (with respect to height). This result further suggests that the water vapor feedback in CO_2 induced warming may be contrary to what has been predicted by GCMs. We further estimated the feedback factor in the context of one-D radiative convective equilibrium calculations. We found that the feedback of the lapse rate has the same sign as the water vapor feedback and is as effective as water vapor feedback in reducing the tropical climate sensitivity to radiative perturbations. We stressed that results from the present analyses should be viewed cautiously since the observations about the current climate do not support the idea that the tropical tropospheric temperature can deviate considerably from a moist adiabatic profile.

Alternative efforts at explaining the mountain snow line record were discussed. When SST is assumed to have decreased by 2 K instead of the best estimate 1 K, it is also possible to explain the mountain snowline record under the moist adiabatic assumption.

Motivated by Lindzen's recent discovery of the connection between the extratropical tropopause height and the neutrality of the extratropical troposphere, we investigated the maintenance of the extratropical tropospheric temperature and wind

from the point view of the transport of PV by baroclinic eddies. We are particularly interested in whether the assumption of zero gradient of PV along isentropes in the troposphere is compatible with observations, and the implications of this assumption to the extent that it is compatible with observations. We noticed that the PV distribution of the zonal mean extratropical troposphere is well characterized by " boundary layer and interior flow " structure. We studied the zonal mean distribution of temperature and wind as a function of PV gradient along isentropic surfaces. In particular, we examined the difference and similarity between the observed troposphere and the troposphere with zero-gradient along isentropic surfaces. We further showed the implications of the efficient PV mixing along isentropic surfaces for the tropical impact on the extratropical tropospheric temperature and wind. We found that the tropical impact is significantly limited by the presence of the gradient of the planetary vorticity even in the extreme case of PV mixing. we showed that the extratropical tropospheric lapse rate will not be exactly the same as the tropical tropospheric lapse rate even when the PV in the extratropical troposphere is well mixed both vertically and horizontally. When the PV is only well mixed along isentropic surfaces, the slope of isentropes increases with height due to the increase of the planetary vorticity with latitude (equation 8.6 and Figure 8-11), and the penetration of the tropical impact is also found to be dependent on the PV distribution across isentropes originating from the extratropical ground. We also showed that the extratropical troposphere cannot be looked at in isolation from the tropics. By examing the mutual dependence between the temperature and wind distribution, we also suggested that the extratropical temperature and wind distribution can not be accurately determined without reference to the global balance of the angular momentum budget. We showed that the tropospheric wind is very sensitive to changes in the temperature distribution at the tropopause, which suggests that the stratospheric PV and PV gradient play an important role in affecting the tropospheric wind distribution. We further estimated the stratospheric influence by examining the sensitivity of the tropospheric temperature and wind distribution to changes in the cross isentrope PV distribution as well as to changes in the PV gradient along isentropic surfaces.

9.2 Outline of the future research

The strategy of this thesis is to utilize observations and simple conceptual models to give a simple interpretation to what we have observed and see what the interpretation implies. The simplicity of the models helps our understanding of the basic physical processes, but their inadequacy for addressing many details is obvious. Though we have been closely guided by observational data, there is no guarantee that the details ignored may not turn out to be important. The role of the present study is also to reveal and highlight the potentially important details.

We start from our model for the tropical tropospheric thermal structure. The parametrization of deep convection is based on the idea that convection be treated as distinguishable elements from their environment. Formulations based on this idea have intrinsical difficulties in representing adequately all the processes involved in the interaction of transient convective elements with their environment. For example, the birth and decay of the convective elements excites gravity waves, which dissipates the kinetic energy of the more turbulent flow within the convective drafts. This process is obviously more important to the parametrization of the momentum transport, but their effect on heat and moisture may not be completely negligible. The simplicity of our model precludes a close analysis of this issue, though the close agreement between the model profile and the observed profile suggests that this detail may be unimportant.

As we have seen in Chapter 2, the tropical convective boundary layer has a very detailed structure, which is not adequately represented in the present model. An immediate step to improve our model is to separate the shallow cloud layer from the dry surface boundary layer and introduce an explicit model for the shallow clouds on which we now have more observations and better theoretical understanding (Emanuel 1991). This step is also essential to understand and predict more accurately the relative humidity in the boundary layer.

There is considerable inhomogeneity in the surface level, though the tropical temperature above the boundary layer is characterized by horizontal homogeneity. An-

other immediate improvement to the present model is to introduce two surface temperatures. One is for the mean, the other represents the surface level temperature of the air participating into deep convection. This treatment will enhance the ability of moist convection in delivering heat upward, and thus the improved model may exhibit less sensitivity to radiative perturbations.

Another important feature of the tropical deep convection is that it is strongly modulated by diurnal forcing. The diurnal cycle of the tropical deep convection may has some important impact on the time mean structure of the tropical troposphere. The present model is able to produce a diurnal cycle by introducing an explicit surface heat budget and surface heat capacity. It is of interest to compare the time mean results from a transient model with a steady model like the present one. It is also of interest to compare the sensitivity of the two models to radiative perturbations.

For the treatment of water vapor, the immediate improvement is to couple it with the temperature model. Coupling would employ the assumption that the number of hydrometeors is proportional to the CAPE of the large-scale environment, which can be explicitly calculated from the temperature structure. In such a context, the cloud feedback can also be easily incorporated since the cloud amount in the upper troposphere is just the amount of hydrometeors, which may be assumed to be proportional to CAPE too.

On the issue of the maintenance of the temperature and wind in the extratropical troposphere, an immediate interest is to determine the width of the Hadley circulation in the extreme case of PV mixing by baroclinic eddies. It has been thought that the baroclinic eddies contribute to a slightly poleward shift of the edge of the Hadley circulation in its inviscid limit and to a weaker jet (Pfeffer 1981, Hoskins 1983). Our results show that a neutralized troposphere by baroclinic eddies produced a stronger jet than observed, which suggests that the much smaller jet strength than the inviscid limit may be more due to the vertical mixing by cumulus deep convection within the tropics.

The study presented in Chapter 8 highlights the importance of the boundary layer structure of a rotational baroclinic flow. A clear understanding of the dynamics

of an Ekman boundary layer subjected to surface heating or cooling will be vitally important to an understanding of the distribution of temperature and wind in the entire troposphere.

As we showed, the strength of the jet is quite sensitive to the PV gradient along isentropic surfaces. It is of interest to quantify the relationship between the gradient of PV along isentropic surfaces with the frictional parameters. It is also of interest to study how forced waves deform the tropopause and generate subsequent secondary instabilities which mix the high PV stratospheric air into the troposphere. The tropospheric temperature and wind distribution will not be understood without the understanding of the PV budget of the troposphere (Hoskins 1991). The PV budget of the troposphere appears to be somewhat dependent on the the processes which are responsible for the exchange of air between the stratosphere and the troposphere. Such a study may shed considerable light on the formation and maintenance of the storm tracks and their role in shaping the zonal mean climate.

Appendix I: A Numerical Scheme for solving equation 8.6

Equation 8.6 has the form

$$\frac{\partial \theta}{\partial y} - s(y,p)\frac{\partial \theta}{\partial p} = 0 \qquad (.1)$$

Using one-step backward difference to discrete the derivative of θ in both y and p direction, we have the difference form of equation .1

$$\theta(i,j) = \theta(i-1,j) + C(i,j)(\theta(i,j) - \theta(i,j-1)) \qquad (.2)$$

with $C(i,j) = S(i,j)\frac{\delta y}{\delta p}$

It is easy to show that the stability criterion of the above scheme is

$$\mid C(i,j) \mid_{maximum} < 1 \qquad (.3)$$

Appendix II: A Numerical Scheme for solving equation 8.12

Equation 8.12 has the form

$$A(y,z)\frac{\partial^2 U}{\partial y^2} + E(y,z)\frac{\partial U}{\partial y} + \quad S(y,z)(\tfrac{\partial u}{\partial z})^{\gamma}\tfrac{\partial^2 U}{\partial z^2} + Q(y,z)\tfrac{\partial U}{\partial z} + C(y,z) = 0 \qquad (.4)$$

The boundary conditions it is subjected to are

$$\frac{\partial U}{\partial z}\Big|_{z=z_1(y)} = T_1(y) \qquad (.5)$$

$$\frac{\partial U}{\partial z}\Big|_{z=z_2(y)} = T_2(y) \qquad (.6)$$

$$U\Big|_{y=y_1} = U_1(z) \qquad (.7)$$

$$\frac{\partial U}{\partial y}\Big|_{y=y_2} = U_{y0} \qquad (.8)$$

$z = z_1(y)$, $z = z_2(y)$, $y = y_1$ and $y = y_2$ define a closed domain. The domain and the discrete net work which we use to discretize the domain, the equation .4 and its boundary conditions are schematically shown in Figure -1.

In general $z = z_1(y)$ and $z = z_2(y)$ are not orthogonal to the two parallel line $y = y_1$ and $y = y_2$, and may not be straight lines in the y-z plane. In the rectangular

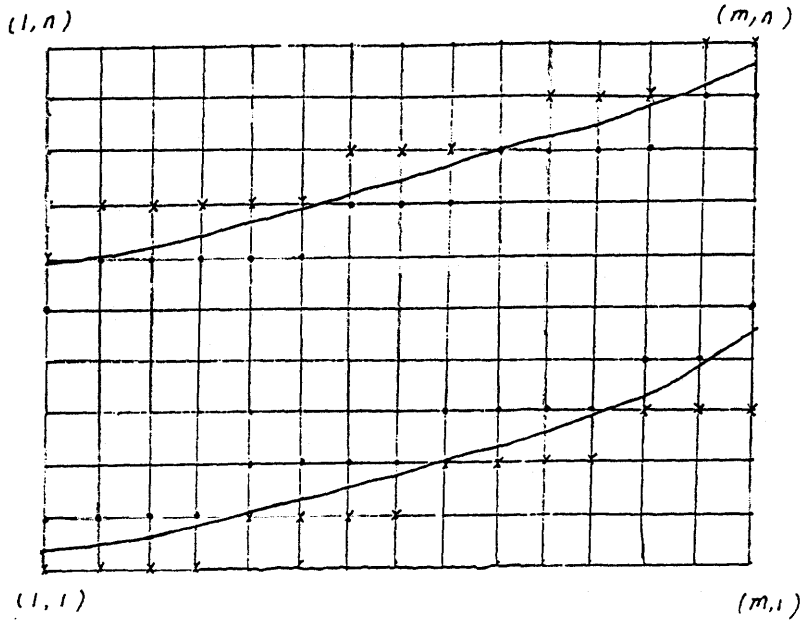

Figure -1: The net work used to discretize the elliptic equation and its boundary conditions.

.

net work, $z = z_1(y)$ and $z = z_2(y)$ may be represented by the mesh points closest to them, including the points which fall right on the boundary curves. These points are called boundary points and may be further divided into the inner boundary points and outer boundary points. The inner boundary points are those points which fall inside the domain and the outer boundary points are those fall just outside the domain. Other points within the closed domain will be called interior points. We use arrays $J_1(i)$ and $J_2(i)$(i=1,n) to denote the inner boundary points and the points which fall right on the boundary curves $z = z_1(y)$ and $z = z_2(y)$. Here we restrict ourselves to the case in which both$z_1(y)$ and $z_2(y)$ decrease monotonically with the increase of y

The equation can be solved by the over relaxation methods. Let "k" denote the step of iteration, α represent the over relaxation parameter, and the iteration start from (1,J_1(1)), column by column to the point (m, $J_2(m)$).

At the interior points (they are denoted by (i, j)), we have

$$\begin{aligned} V^k(i,j) &= [2(A(i,j)+b(i,j)(\frac{\delta y}{\delta z})^2)]^{-1} \\ &\quad [A(i,j)(U^{k-1}(i+1,j)+U^k(i-1,j))+ \end{aligned}$$

$$
\begin{aligned}
& \frac{1}{2}E(i,j)(U^{k-1}(i+1,j) - U^k(i-1,j))\delta y + \\
& B(i,j)(U^{k-1}(i,j+1) + u^k(i,j-1))(\frac{\delta y}{\delta z})^2 + \\
& \frac{1}{2}Q(i,j)(U^{k-1}(i,j+1) - U^k(i,j-1))\delta z^{-1}(\delta y)^2 + \\
& C(i,j)\delta y^2] \\
U(i,j)^k &= U(i,j)^{k-1} + \alpha V^k(i,j) \qquad (.9)
\end{aligned}
$$

$B(i,j) = S(i,j)R(i,j)$ and R(i,j) are given by

$$
\begin{aligned}
R(i,j) &= [\frac{(U^{k-1}(i,j+1) - U^k(i,j-1))}{2\delta z}]^\gamma \quad for \quad j < J_2(i-1) \\
R(i,j) &= [\frac{(U(i,j)^{k-1} + T(i)\delta z - U^k(i,j-1))}{2\delta z}]^\gamma \quad for \quad j = J_2(i) \qquad (.10)
\end{aligned}
$$

At the boundary points, we have

For $J_1(m) < j < J_2(m)$

$$
\begin{aligned}
V^k(m,j) &= [2(A(m,j) + B(m,j)(\frac{\delta y}{\delta z})^2)]^{-1} \times \\
& [A(m,j)(2U^k(m-1,j) + 2U_{y0}(j)\delta y) + \\
& E(m,j)U_{y0}(j)\delta y^2 + \\
& B(m,j)(U^k(m,j-1) + U^{k-1}(m,j+1))(\frac{\delta y}{\delta z})^2 + \\
& \frac{1}{2}Q(m,j)(U^{k-1}(m,j+1) - U^k(m,j-1))\delta y \delta y \delta z^{-1} + \\
& C(m,j)\delta y \delta y] \\
U(m,j)^k &= U(i,j)^{k-1} + \alpha V^k(i,j) \qquad (.11)
\end{aligned}
$$

For $j = J_1(m)$

$$
\begin{aligned}
V^k(m,j) &= [2A(m,j) + B(m,j)(\frac{\delta y}{\delta z})^2]^{-1} \times \\
& [A(m,j)(2U^k(m-1,j) + 2U_{y0}(j)\delta y) +
\end{aligned}
$$

$$
\begin{aligned}
& E(m,j)U_{y0}(j)\delta y^2 + \\
& B(m,j)(U^{k-1}(m,j+1) - T_1(i)\delta z)(\frac{\delta y}{\delta z})^2 + \\
& Q(m,j)T_1(i)\delta y^2 + \\
& C(m,j)\delta y^2] \\
U(m,j)^k &= U(i,j)^{k-1} + \alpha V^k(i,j) \qquad (.12)
\end{aligned}
$$

For $j = J_2(m)$

$$
\begin{aligned}
V^k(m,j) &= [2A(m,j) + B(m,j)(\frac{\delta y}{\delta z})^2]^{-1} \times \\
& [A(m,j)(2U^k(m-1,j) + 2U_{y0}(j)\delta y) + \\
& E(m,j)U_{y0}(j)\delta y^2 + \\
& B(m,j)(U^{k-1}(m,j-1) + T_2(i)\delta z)(\frac{\delta y}{\delta z})^2 + \\
& Q(m,j)T_2(i)\delta y^2 + \\
& C(m,j)\delta y^2] \\
U(m,j)^k &= U(i,j)^{k-1} + \alpha V^k(i,j) \qquad (.13)
\end{aligned}
$$

For $j = J_2(i)$ and $(J_2(i) < J_2(i+1))$,

$$
\begin{aligned}
V^k(i,j) &= [2A(i,j) + B(i,j)(\frac{\delta y}{\delta z})^2]^{-1} \times \\
& [A(i,j)(U^k(i+1, J_2(i+1)) + \\
& T_2(i+1)(J_2(i) - J_2(i+1))\delta z + U^k(i-1,j)) + \\
& \frac{1}{2}E(i,j)(U(i+1, J_2(i+1)) + \\
& T_2(i+1)(J_2(i) - J_2(i+1))
\end{aligned}
$$

$$
\begin{aligned}
& \delta z - U^k(i-1,j))\delta y + \\
& B(i,j)(U^k(i,j-1) + T_2(i)\delta z)(\frac{\delta y}{\delta z})^2 + \\
& Q(i,j) * T_2(i)(\delta y)^2 + C(i,j)(\delta y)^2] \\
U(i,j)^k &= U(i,j)^{k-1} + \alpha V^k(i,j) \qquad (.14)
\end{aligned}
$$

For $j = J_2(i)$ and $J_2(i) > J_2(i+1)$ or $J_2(i) = J_2(i+1)$,

$$\begin{aligned} V^k(i,j) &= [2A(i,j) + B(i,j)(\frac{\delta y}{\delta z})^2]^{-1} \times \\ &\quad (A(i,j)(U^{k-1}(i+1,j) + U(i-1,j)) + \\ &\quad \frac{1}{2}E(i,j)(U^{k-1}(i+1,j) - U^{k-1}(i-1,j))\delta y + \\ &\quad B(i,j)(U^k(i,j-1) + T_2(i)\delta z)(\frac{\delta y}{\delta z})^2 + \\ &\quad Q(i,j) * T_2(i)(\delta y)^2 + C(i,j)(\delta y)^2] \\ U(i,j)^k &= U(i,j)^{k-1} + \alpha V^k(i,j) \end{aligned} \tag{.15}$$

For $j = J_1(i)$ and $(J_1(i) < J_1(i-1))$,

$$\begin{aligned} V^k(i,j) &= [2A(i,j) + B(i,j)(\frac{\delta y}{\delta z})^2]^{-1} \times \\ &\quad [A(i,j)(U^k(i+1,j) - \\ &\quad T_1(i-1)(J_1(i-1) - J_1(i))\delta z + \\ &\quad U^k(i-1, J_1(i-1))) + \\ &\quad \frac{1}{2}E(i,j)(U(i+1,j) - (U^k(i-1, J_1(i-1)) - \\ &\quad T_1(i-1)(J_1(i-1) - J_2(i))\delta z)\delta y + \\ &\quad B(i,j)(U^k(i,j+1) - T_1(i)\delta z)(\frac{\delta y}{\delta z})^2 + \\ &\quad Q(i,j) * T_1(i)(\delta y)^2 + C(i,j)(\delta y)^2] \\ U(i,j)^k &= U(i,j)^{k-1} + \alpha V^k(i,j) \end{aligned} \tag{.16}$$

For $j = J_1(i)$ and $J_1(i) > J_1(i-1)$ or $J_1(i) = J_1(i-1)$,

$$\begin{aligned} V^k(i,j) &= [2A(i,j) + B(i,j)(\frac{\delta y}{\delta z})^2]^{-1} \\ &\quad (A(i,j)(U^{k-1}(i+1,j) + U(i-1,j)) + \\ &\quad \frac{1}{2}E(i,j) * (U^{k-1}(i+1,j) - U^{k-1}(i-1,j))\delta y + \\ &\quad B(i,j)(U^k(i,j+1) - T_1(i)\delta z)(\frac{\delta y}{\delta z})^2 + \\ &\quad Q(i,j) * T_1(i)\delta y^2 + C(i,j)\delta y^2] \end{aligned}$$

$$U(i,j)^k = U(i,j)^{k-1} + \alpha V^k(i,j) \qquad (.17)$$

References

Ames, W.F, 1969: *Numerical methods for partial differential equations*, Barnes & Noble, Inc., New York.

Arakawa, A. and W.H. Schubert, 1974: Interaction of a cumulus cloud ensemble with the large scale environment, Part I. *J. Atmos. Sci.*, **31**, 674-701.

Augstein,E., H. Riehl, F. Ostapoff, and V. Wagner,: 1973, Mass and energy transports in an undisturbed Atlantic Trade wind flow, *Mon. Wea. Rev.*, **101**,101-111.

Augstein, E., H. Schmidt and F. Ostapoff, 1974: The vertical structure of the atmospheric planetary boundary layer in undisturbed trade winds over the Atlantic ocean. *Bound.-Layer. Meteor.*, **6**, 129-150.

Ball, F.K., 1960: Control of inversion height by surface heating. *Quart. J. Roy. Meteor. Soc.*, **86**, 483-494.

Barton, I.J., 1983: Upper level cloud climatology from an orbiting satellite. *J. Atmos. Sci.*, **40**, 435-447.

Betts, A.K., 1991: Tropical boundary layer equilibrium in the last ice-age. Submitted to J. Geophys. Res.

Betts, A.K., 1990: Greenhouse warming and the tropical water vapor budget. *Bull. Amer. Meteor. Soc.*, **71**, 1465-1467.

Betts, A.K.,1986: An new convective scheme. Part I: Observational and theoretical basis. *Quart. J. Roy. Meteor. Soc.*, **112**, 677-691

Betts, A.K., 1982: Saturation point analysis of moist convective overturning. *J. Atmos. Sci.*, **39**, 1484-1505.

Betts, A.K., and M.J. Miller, 1986: A new-convective adjustment scheme. Part II: Single column tests using Gate wave, Boxmex, Atex and arctic air-mass data sets. *Q. J. Roy. Meteor.*, **112**, 693-709.

Betts, A.K. and M. Ridgway, 1989: Climatic equilibrium of the atmospheric convective boundary layer over a tropical ocean. *J. Atmos. Sci.*, **40**, 435-447.

Betts, A.K. and M.F. Silva Dias, 1979: Unsaturated downdraft thermodynamics in cumulonimbus. *J. Atmos. Sci.*, **36**, 1061-1071.

Blyth, A.M., W.A. Cooper and J.B. Jensen, : A study of the source of entrainment air in Montana cumuli. *J. Atmos. Sci.*, **45**, 3944-3964.

Boatman, J.F., and A.H. Auer, 1983: The role of cloud top entrainment in cumulus clouds *J. Atmos. Sci.*, **40**, 1517-1534.

Bolton, D., 1980: The computation of equivalent potential temperature. *Mon. Wea. Rev.*, **108**, 1046-1053.

Bowen, E.G., 1950: The formation of rain by coalescence. *Australian J. Sci. Res.*, **A3**, 192-213.

Braham, R. R., 1952: The water and energy budgets of the thunder storm and their relation to thunder storm development. *J. Meteor.*, 9, 227-242.

Braham R.R. and P.S. Duran, 1967: Survival of cirrus crystals in clear air. *J. Appl. Meteor.*, **6**, 1053-1061.

Bretherton R.R. 1966: Critical layer instability in baroclinic flows. *Quat. J. R. Met. Soc.*, **92**, 325-334.

Broecker, W.S. and G.H. Denton, 1989: The role of ocean-atmosphere reorganization in glacial cycles. *Geochim. Cosmochim. Acta*, **53**, 2465-2501.

Cehelsky, P., 1987: Multiple equilibria, weather regimes and non-linear equilibration in a simple baroclinic model. Ph.D thesis, MIT, 161 pp

Cehelsky, P and K.K. Tung, 1991: Nonlinear baroclinic adjustment. *J. Atmos. Sci*, **48**, 1930-1947.

Cehelsky, P and K.K. Tung, 1987: Theories of multiple equilibria and Weather regimes- critical re-examination Pat II: Baroclinic weather regimes . *J. Atmos. Sci*, **44**, 3282-3303.

Cess, R.D., 1991: Positive about water feedback. *Nature*, **349**, 462.

Cess, R.D., G.L. Potter, J.P. Blanchet, G.J. Boer, A.D. Del Genio, M.Déqué, V. Dymnikov, V. Galin, W.L. Gates, S.J. Gahn, J.T. Kiehl, A.A. Lacis, H. Le Treut, Z.-X. Li, X.-Z. Liang, B. J. McAveny, V.P. Meleshko, J.F.B. Mitchell, J.-J. Morcrette, D.A. Randall, L. Rikus, E. Roeckner, J. F. Royer, U. Schlese, D. S. Sheinin, A. Slingo, A.P. Sokolov, K.E. Taylor, W. M. Washington, R.T. Wetherald, I. Yagai, and M.-H. Zhang, 1990: Intercomparison and interpretation of climate feedback processes in 19 atmospheric general circulation models. *J. Geophys. Res.*, **95**, 16,601-16,615.

Charney, J.G. 1947: The dynamics of long waves in a baroclinic westerly current. *J. Met.*, **4** 135-162

Charney J.G. and Stern M.E. 1962: On the stability of internal baroclinic jets in a rotating atmosphere *J. Atmos. Sci.*, **19** 159-172

Charney, J.G. and Eliassen, 1964: On the growth of the Hurricane depression. *J. Atmos. Sci.*, **21**, 68-75.

Charney, J.G., 1971: Geostrophic Turbulence. *J. Atmos. Sci.* **28**, 1087-1095.

Cheng, L., T.C. Yip and H.R. Cho, 1980: Determination of mean cumulus cloud vorticity from GATE A/B scale potential vorticity budget. *J. Atmos. Sci.*, **37**, 733-753.

Chimonas, G. and R. Rossi, 1987: The relationship between tropopause potential temperature and the buoyant energy of storm air. *J. Atmos. Sci.*, **44**, 2902-2911.

Chiou, E.W., M.P. McCormick, W.P. Chu and G.K. Yue, 1990: Global distributions of cirrus determined from SAGE II occultation measurements between November 1984 and October 1988. Preprints, *Conf. Cloud Physics*, San Francisco, Amer. Meteor. Soc., 513-517.

Cho, H-R and Y. Ogura, 1974: A relationship between cloud activity and the low level convergence as observed in Reed-Recker's composite

Chou, M.D., 1986: Atmospheric solar heating rate in water vapor bands. *J. Climate Appl. Meteor.*, **25**, 1532-1542.

Chou, M.D., D.P. Krats and W. Ridgway, 1991: Infrared radiation parameterizations in numerical climate models. *J. Climate*, **4**, 424-437.

CLIMAP, 1976: The surface of the ice–age earth. *Science*, **191**, 1131-1144.

Danielsen, E.F., 1982: A dehydration mechanism for the stratosphere. *Geophys. Res. Let.*, **9**, 605-608

Dopplick, T.G., 1972: Radiative heating of the global atmosphere. *J. Atmos. Sci.*, **29**, 1278-1294.

Eady, E.T. 1949: Long waves and cyclone waves *Tellus.* **1** 33-52

Emanuel, K.A., 1991: A scheme for representing cumulus convection in Large-scale models. *J. Atmos. Sci.*, **48**, 2313-2335.

Emanuel, K.A., 1990: Personal communication.

Emanuel, K.A. and D. J. Raymond: 1991: Report from a workshop on cumulus parameterization, Key Biscayne, Florida, 3-5 May 1991. *Bul. Amer. Meteor. Soc*, **73**, 318-325.

Fairbridge, R.W., 1991: Planetary beats and geology. *New Approaches in Geomagnetism and the Earth's Rotation*, S. Flodmark, Editon. World Scientific, London, pp 222-244.

Fletcher, N.H., 1962: *The Physics of Rain Clouds*, Cambridge University Press, Cambridge, 386 pp.

Fullmer, J.W.A., 1982: Calculations of the quasi-geostrophic potential vorticity gradient from climatological data. *J. Atmos. Sci.*, **39** 1073-1877.

Gamache J.F. and R.A. Houze, 1983: Water budget of a meso-scale convective system in the tropics. *J. Atmos. Sci*, **40**, 1835-1850.

Garabedian P.R., 1964: *Partial Differential Equations.* John Wiley & Sons Inc., Newyork. 672 pp.

Garstang, M. and A.K. Betts, 1974: A review of the tropical boundary layer and cumulus convection: Structure, parameterization and Modeling. *Bull. Amer. Meteor. Soc.*,**55**, 1195-1205.

Geleyn, J.-F., C. Girard and J.-F. Louis, 1982: A simple parameterization of moist convection for large-scale atmospheric models. *Beitr. Phys. Atmosph.*, **55**, 325-334.

Gill, A.E., 1982: *Atmosphere-Ocean Dynamics*, Academic Press, New York, 622 pp.

Gray, W.M., 1974: Cumulus convection and large scale circulations, I: Broad scale and mesoscale considerations. *Mon. Wea. Rev.*,**105**, 1171-1188.

Goody, R.M. and Y.L. Yung, 1989: Atmospheric Radiation, Theoretical basis. Oxford University Press, New York, 519 pp.

Haynes, P.H. and McIntyre, M.E., 1990: On the evolution of vorticity and potential vorticity in the presence of diabatic heating and frictional or other forces, *J. Atmos. Sci.* **39**, 2021-2031

Held, I.M. 1982: On the height of the tropopause and the static stability of the troposphere *J. Atmos. Sci.,* **39** 412-417.

Held, I.M. and A.Y. Hou: Nonlinear axially symmetric circulations in anearly inviscid atmosphere. *J. Atmos. Sci.*, **37**, 515-533.

Hoskins, B.J., 1991 Towards a PV-θ view of the general circulation, *Tellus*, **43 A-B**, 27-35.

Hoskins, B.J., 1990 Theory of extratropical cyclones. Palmen Memorial Volume, (Eds. C. W. Newton, and E. O. Holopainen), Amer. Met. Soc., 63-80.

Hoskins, B.J., M.E. McIntyre and A.W. Robertson, 1985: On the use and significance of isentropic potential vorticity maps. *Quart. J. R. Met. Soc.*, **111**, 877-946

Hoskins, B.J., 1983: Modeling of the transient eddies and their feedback on the mean flow. in *Large-scale dynamic processes in the atmosphere.* Ed. B. J. Hoskins and R. Pearce. Academic Press. 399 pp.

Hoskins B.J., 1974: The geostropic momentum approximation and the semi-geotropic equations, *J. Atmos. Sci.*, **32** 233-242

Heymsfield, A. and C. M. R. Platt, 1984: A parameterization of the particle size spectrum of ice clouds in terms of the ambient temperature and the ice water content. *J. Atmos. Sci.*, **41**, 846-855.

Hou, A. Y. and R. S. Lindzen 1991: The influence of concentrated heating on the Hadley circulation. Submitted to J. Atmos. Sci.

Houghton, J.T., G.J. Jenkins and J.J. Ephraums, editors, 1990: *Climate Change. The IPCC Scientific Assessment.* Cambridge University Press, Cambridge, 365 pp.

Houze, R.A. Jr., 1989: Observed structure of meso-scale convective systems and implications for large scale heating. *Quart. J. Roy. Meteor. Soc.*, **115**, 425-461.

Houze R.A. Jr. and A.K. Betts, 1981: Convection in GATE. *Rev. Geophys. Space Phys.*, **19**, 541-576.

Jensen, J.B., P.H. Austin, M.B. Baker and A. M. Blyth, 1985: Turbulent mixing, spectral evolution, and dynamics in a warmer cumulus cloud. *J. Atmos. Sci.*, **42**, 173-192.

Johnson, R.H., 1980: Diagnosis of convective and meso-scale motions during phase III of GATE. *J. Atmos. Sci.* **37**, 733-753.

Johnson, R.H. and G.S. Young, 1983: Heat and moisture budgets of tropical mesoscale anvil clouds. *J. Atmos. Sci*, **40**, 2138-2147.

Kley, D., A. L. Scemeltkopf, K. Kelly, R. H. Winkler, T. L. Thompson and M. McFarland, 1983: The U-2 Lyman Alpha hygrometer: results from the 1980 Panama experiment in the 1980 stratospheric-tropospheric exchange experiment. A. P. Margozzi, NASA Tech Memo 842297, 85-125.

Kelly K., K.R. Chan, M. Loewenstein, J.R. Podolske, S.E. Strahan, J.C. Wilson and D. Kley, 1991: Water vapor and cloud water measurements over Darwin during the STEP 1987 tropical mission. Submitted to *J. Geophys. Res.*

Krishnamurti, T.N., Ramanathan, Hua-lu Pan, Pasch J. R. and Molinari. J., 1980, **101**, 465-472.

Krishnamuti, T.N.,and J.W. Moxim, 1971 : On parameterization of convective and non-convective latent heat release. *J. Appl. Meteor.*, **10**,3-13.

Landau, L.D. and E.M. Lifshitz, 1981: *Fluid Mechanics.* Pergamon Press, New York, 536 pp.

Lindzen, R.S., 1988: Some remarks on cumulus parameterization. *PAGEOPH*, **126**, 123-135.

Lindzen, R.S., 1992: Baroclinic neutrality and the tropopause. Submitted to *J. Atmos. Sci.*

Lindzen, R.S., 1990a: Some coolness concerning global warming. *Bull. Amer. Meteor. Soc.*, **71**, 288-299.

Lindzen, R.S., 1990b: Response. *Bull. Amer. Meteor. Soc.*, **71**, 1465-1467.

Lindzen, R.S., 1981: Some remarks on cumulus parameterization. Report on NASA-GISS Workshop: *Clouds in climate-modelling and satellite observational studies*, 42-51. (N.B. The contents of this paper are largely to be found in Lindzen (1988)).

Lindzen, R.S. and B. Farrel: The role of polar regions in global climate and a new parameterization of global heat transport. *Mon. Wea. Rew.*, **108**, 2064-2079.

Lindzen, R.S., A.Y. Hou, and B.F. Farrell, 1982: The role of convective model choice in calculating the climate impact of doubling CO_2. *J. Atmos. Sci.*, **39**, 1189-1205.

Lindzen, R.S. and S. Nigam, 1987: On the role of sea surface temperature gradients in forcing low level winds and convergence in the tropics. *J. Atmos. Sci.*, **45**, 2440-2448.

Liou, K.N., 1986: Influence of cirrus clouds on weather and climate processes: a global perspective. *Mon. Wea. Rev.*, **114**, 1167-1199.

Liou, K.N., 1980: An Introduction to Atmospheric Radiation. Academic Press Inc, 111 Fifth Avenue, Newyork.

Lord, S.J., 1978: Development and observational verification of a cumulus cloud parameterization. PH.D Thesis. UCLA.

Lorenz, E.N., 1967: The nature and theory of the general circulation of the atmosphere. World Meteorological Organization. Geneva, Switzerland, 161 pp

Malkus, J.S., 1954: Some results of a trade cumulus cloud investigation. *J. Meteor.*, **11**, 220-237.

Manabe, S. and R.F. Strickler, 1964: Thermal equilibrium of the atmosphere with a convective adjustment. *J. Atmos. Sci.*, **21**, 361-385.

Manabe, S., J. Smagorinsky and R. F. Strickler, 1965: Simulated climatology of a general circulation model with a hydrologic cycle. *Mon. Wea. Rev.*, **93**, 769-798.

Marshall, J.S. and W.M. Palmer, 1948: The distribution of rain drops with size. *J. Meteor.*, **5**, 165-166.

Mason, B.J., 1971: *The Physics of Clouds.* Clarendon Press, Oxford, 671 pp.

Mastenbrook, H.J., 1968: Water vapor in the stratosphere and high troposphere. *J. Atmos. Sci.*, **25**, 299-311.

McClatchey, R.A., R.W. Fenn, J.E.A. Selby, F.E. Volz and J.S. Garing, 1972: *Optical properties of the atmosphere*, third ed. AFCRL-72-0497, 108 pp. [NTIS N7318412.]

Newell, R.E., J.W. Kidson, D.G. Vincent and G.J. Boer, 1972: *The General Circulation of the Tropical Atmosphere and Interactions with Extratropical Latitudes, Vol. 1*, MIT Press, Cambridge, 258pp.

Nitta T. 1975: Observational determination of cloud mass flux distribution. *J. Atmos. Sci.*, **32**, 73-91.

Ogura, Y. and H.R. Cho 1973: Diagnostic determination of cumulus cloud population from the observed large-scale variables. *J. Atmos. Sci.*, **30**, 1276-1286.

Oort, A.H., 1983: *Global atmospheric circulation statistics, 1958-1973.* NOAA Professional Paper 14, Rockville, MD., NOAA, U.S. Department of Commerce. 180pp.

Ooyama, K., 1971: A theory on parameterization of cumulus convection. *J. Meteor. Soc. Japan*, **49**, 744-756.

Paluch, I. R., 1979: The entrainment mechanism in Colorado cumuli. *J. Atmos. Sci.*, **36**, 2462-2478.

Pedlosky, J. 1979: *Geophysical Fluid Dynamics.* Springer-Verlag. 624 pp.

Peixoto, J.P. and Crisi, A.R., 1965: Hemispheric humidity conditions during the IGY. Sci. Report No. 6, Contract AF 19(628)-2408, Dept. of Meteorology. Mass. Inst. of Technology, 39-85.

Petterssen S.and S. Smebye 1971: On the development of extratropical cyclones. *Quart. J. Roy. Meteor. Soc.*, **97**, 457-482.

Pfeffer R.L., 1981: Wave-mean flow interactions in the atmosphere, it J. Atmos. Sci., **38** 1341-1359

Phillips, N.A., 1954: Energy transformations and meridional circulations associated with simple baroclinic waves in a two-level quasi-geostropic model. *Tellus*, **6**, 273-286.

Pocinki, L., 1955: Stability of a simple baroclinic flow with horizontal shear. A.F. Cambridge Research Center, Res. Pap. NO. 38, 78pp.

Raga, G.B., J.B. Jensen and M.B. Baker, 1990: Characteristics of cumulus cloud bands off the coast of Hawaii. *Q. J. Atmos. Sci.*, **47**, 338-355.

Ramanathan V. and W. Collins, 1991: Thermodynamic regulation of ocean warming by cirrus clouds deduced from observations of the 1987 El Nino. *Nature*, **351**, 27-32.

Rasch, P.J. and D.L. Williamson, 1990: Computational aspects of moisture transport in global models of the atmosphere. *Q. J. Roy. Met. Soc.*, **116**, 1071-1090.

Raymond, D.J., 1979: A two-scale model model of moist, nonprecipitating convection. *J. Atmos. Sci.*, **47**, 338-355. -

Raval, A. and V. Ramanathan, 1989: Observational determination of the greenhouse effect. *Nature*, **342**, 758-761.

Reed, R.J. and E. E. Recker, 1971: Structure and properties of synoptic -scale wave disturbances in the equatorial western Pacific. *J. Atmos. Sci.*, **28**, 1117-1133.

Renno, N. O., 1992:*Cumulus convection parameterization and numerical modelling of moist atmospheres.* PH.D Thesis, Mass. Inst. of Tech., 297 pp.

Riehl, H., 1979: *Climate and Weather in the Tropics.* Academic Press, New York, 611 pp.

Riehl, H. and J.S. Malkus, 1979: The heat balance of the equatorial trough zone, revisited. *Contributions to Atmospheric Physics*, **52**, 287-305.

Riehl, H. and J. S. Malkus, 1958: On the heat balance in the equatorial trough zone. *Geophysica* (Helsinki), **6**, 503-538.

Riehl, H., T.C. Yeh, J.S. Malkus and N.E. Laseur, 1951: The north east trade wind of the Pacific Ocean. *Quart. J. Roy. Meteor. Soc.*, **77**, 598-526.

Rind, D. 1990: Puzzles from the tropics. *Nature*, **346**, 317-318.

Rind, D. and D. Peteet, 1985: Terrestrial conditions at the last glacial maximum and CLIMAP sea-surface temperature estimates: Are they consistent? *Quaternary Research*, **24**, 1-22

Rind, D., E.W. Chiou, W. Chu, J. Larsen, S. Oltmans, J. Lerner, M.P. McCormick and L. McMaster, 1991: Positive water vapor feedback in climate models confirmed by satellite data. *Nature*, **349**, 500-503

Rogers, R.R. and M.K. Yau, 1989: *A Short Course in Cloud Physics.* Pergamon Press, London, 293 pp.

Salmon, R., 1980: Baroclinic instability and geostropic turbulence. *Geophys. Astrophys. Fluid. Dyn.*,**15**, 167-211.

Salmon, R., 1978: Two layer quasi-geostropic turbulence in a simple special case. *Geophys. Astrophys. Fluid. Dyn.*,**10**, 25-53

Sander, F. 1988: Life history of mobile troughs in the upper westlies. *Mon. Wea. Rew..* **116**, 2629-2648

Sander, F. 1986: Explosive cyclongenesis over the west-central north atlantic ocean 1981-1984 Part I: Composite structure and mean behavior. *Mon. Wea. Rew.*, **114** 1781-1794

Sarachik, E.S., 1978: Tropical sea surface temperature: an interactive one-dimensional atmosphere-ocean model. *Dyn. Atmos. Oceans*, **2**, 455-469.

Sarachik, E.S., 1985: A simple theory for the vertical structure of the tropical atmosphere.*PAGEOPH*, **123**, 261-271.

Schneider, E.K., 1977: Axially symmetric steady-state models of the basic state for instability and climate studies. Part II: Nonlinear calculations. *J. Atmos. Sci.*, **34**, 280-296.

Schlesinger, M.E, 1988: *Physically-based modelling and simulation of climate and climate change.* Part 2. Kluwer Academic Publishers.

Shapiro M.A., 1980: Turbulent mixing within tropopause folds as a mechanism for the exchange of chemical constituents between the stratosphere and troposphere. *J. Atmos. Sci.*, **37**, 994-1004

Shoeberl, M.R., and Lindzen, R. S., 1984: A numerical simulation of barotropic instability. Part I: Wave-mean flow interaction. *J. Atmos. Sci.*, **41**, 1368-1379.

Squires, P., 1958: Penetrative downdrafts in cumuli. *Tellus*, **10**, 382-389.

Starr, D.O'C. and S.H. Melfi, 1991: *The Role of Water Vapor in Climate. NASA Conference Publication 3120*, NASA Goddard Space Flight Center. p. 49.

Stommel, H., 1947: Entrainment of air into a cumulus cloud. *J. Meteor.*, **4**, 91-94.

Stone, P. H., 1978: Baroclinic adjustment. *J. Atmos. Sci.*, 37, 1708-1721.

Taylor, G. R. and M. B. Baker, 1991: Entrainment and detrainment in cumulus clouds. ıJ. Atmos. Sci., **48**, 112-121.

Telford, J. W., 1975: Turbulence, entrainment, and mixing in cloud dynamics. *Pure Appl. Geophys.*, **113**, 1067-1084.

Tennekes, H.,1973: A model for the dynamics of the inversion above a convective boundary layer. *J. Atmos. Sci.*, **32**, 558-567.

Thompson, M. R. ,J. Steven, W. Ppayne, E. E. Recker and R. J. Reed, 1978: Structure and properties of synoptical- scale waves disturbances in the inter-tropical convergence zone of Eastern Atlantic. *J. Atmos. Sci.*, **36**, 53-72.

Thompson, P.D., 1960: *Numerical Weather Analysis and Prediction*, Macmillan, New York.

Turner, J.R., 1979: *Buoyancy Effects in Fluids.* Cambridge University Press, Cambridge, 368 pp.

Turner, J.R., 1962: The starting plume in neutral surroundings. *J. Fluid Mech.*, **13**, 356-368.

Williams, E.R., S.A. Rutledge, S.G. Geotis, N. Renno, E. Rasmussen, and T. Rickenbach, 1992: A radar and electrical study of tropical "hot towers". *J. Atmos. Sci.*, in press.

Vallis G. K. and J. O. Roads, 1984: Large-scale stationary and turbulent flow over topography. *J. Atmos. Sci.*, 41, 3255-3271

Vallis, G. K. 1988: Numerical studies of eddy transport properties in eddy resolving and parameterized models. *Quart. J. Roy. Metteor. Soc.*, **114**, 183-204

Warner, J. and P. Squires, 1958: Liquid water content and the adiabatic model of cumulus development. *Tellus*, **10**, 390-394.

Warner, J. 1970: On steady state one-dimensional models of cumulus convection. *J. Atmos. Sci.*, **10**, 1035-1040.

Xu K. and K.A. Emanuel 1988: Is the tropical atmosphere conditionally unstable? *Mon. Wea. Rev.*, **117**, 1471-1479.

Yanai, M., and J.H.,Cho, 1973: Determination of bulk properties of tropical cloud clusters from large scale heat and moisture budgets. *J. Atmos. Sci.*, **30**, 611-627.

Yau, M.K., 1991: Personal communication.